MOLECULAR DYNAMICS STUDY OF DIFFUSION OF ARGON IN WATER AT DIFFERENT TEMPERATURES

A Dissertation

submitted to the Central Department of Physics,
University Campus, in the Partial Fulfillment for the Requirement of
Master's Degree of Science in Physics

By

Anup Pandey
Central Department of Physics
University Campus, Tribhuvan University
Kirtipur, Kathmandu
Nepal
September 03, 2010

ACKNOWLEDGEMENTS

The work presented in this thesis owes much to the inspiration and guidance of Dr. Narayan Prasad Adhikari, who as a supervisor influenced me throughout this work.

I would also like to express my gratitude to honorable Prof. Dr. Devendra Raj Mishra for his generous support and suggestion in pursuing the dissertation work.

My deep appreciation goes to Prof. Dr. Lok Narayan Jha (Head, Central Department of Physics) for his valuable co-operation throughout this work. Also my deepest gratitude goes to all the teachers of CDP for their valuable suggestion and encouragement throughout the work.

It would be unfair from my part if i do not recognize the contribution of my senior and friend Mr. Sunil Kumar Thapa, who has started the work on this field. His constant support and encouragement is undoubtedly praise worthy.

My sincere thanks goes to my lab partners Mr. Hem Bahadur Moktan and Mr. Udaya Raj Dahal who were with me on every part of the work. Their support on every aspect as well as company motivated me to bring this work at this stage.

I must, of course, express my heartiest thank to the Abdus Salam International Centre for Theoretical Physics (ICTP), office of external activities, NET-56, for providing me the fellowship for this work. Similarly, i would like to thank Nepal Academy of Science And Technology, NAST for providing financial support.

Finally, I am thankful to my respected parents for upbringing me to this state of knowledge. I am also grateful to all my family members and friends for their tremendous love and support.

This thesis is dedicated to all of you.

Anup Pandey
Date:September 03, 2010

Recommendation

It is certified that Mr. Anup Pandey has carried out the dissertation work entitled **Molecular Dynamics Study of Diffusion of Gaseous Argon in Water at Different Temperatures** under my supervision and guidance.
I recommend the dissertation in the partial fulfillment for the requirement of Master's Degree of Science in Physics.

.....
(Supervisor)
Dr. Narayan Prasad Adhikari
Central Department of Physics
Tribhuwan University, Kirtipur
Kathmandu, Nepal

Date: .....

EVALUATION

We certify that we have read this dissertation and in our opinion, it is satisfactory in the scope and quality as a dissertation in the partial fulfillment for the requirement of Master's Degree of Science in Physics.

Evaluation Committee:

Dr. Narayan Prasad Adhikari
(Supervisor)

Prof. Dr. Lok Narayan Jha
(Head)
Central Department of Physics
Tribhuvan University
Kirtipur, Kathmandu
Nepal

(External Examiner)

(Internal Examiner)

Date:

ABSTRACT

Molecular dynamics study of a binary mixture of argon and SPC/E water, with argon as solute and water as solvent, at argon mole fraction of 0.023 have been accomplished at temperatures 293 K, 298 K, 303 K, 308 K and 313 K. The solvent-solvent, solute-solute and solute-solvent radial distribution functions (RDFs) have been estimated. The water-water radial distribution function has been found to agree with the experimental values within 5%. Self-diffusion coefficients of both solvent and solute have been determined by means of mean-squared displacement (MSD)curves using Einstein's relation. The evaluated self-diffusion coefficient at temperature 298 K has been found to agree with the experimental value within 4%. Also the values of self-diffusion coefficient of water have been found to agree with the available experimental values within 8% at maximum. Then, the Darken's relation has been invoked in order to determine the mutual/binary diffusion coefficients at the respective temperatures. The temperature dependence of the diffusion coefficients has also been analyzed. The estimated values of self-diffusion coefficients of water and argon as well as the mutual diffusion coefficients of argon in water have given the linear Arrhenius plot, which indicates that the self-diffusion coefficients have an Arrhenius dependence on temperature. Moreover, the temperature dependence of the diffusion coefficients has been found to be consistent with the nature of RDF's at the respective temperatures.

Contents

Chapter 1

Introduction

1.1 General Considerations

The experimental methods and theoretical techniques have been complementing each other yielding an accelerated progress in the understanding of material at atomistic level. The question that frequently arises in numerous context is the relation between the bulk properties of matter and the interactions among the constituent atoms and molecules. The experimental method of studying the microscopic properties is ambiguous and cumbersome. Rather the constructive approach is molecular dynamics method that tries to reproduce the behavior using model system [1, 2]. The success of classical MD is based on the fact that a large contribution to the molecular motion can be treated using classical mechanics. With the computer power available nowadays, the equations of motion can be solved for systems of the order of 10^6 atoms. In our study, the system consists of argon in water. Argon is an inert gas and water is the vital element for the survival of the organisms on the earth. Here, the time evolution of the system in the molecular level is studied using molecular dynamics in order to determine the equilibrium dynamic properties of the system. It is important to review the basic characteristic features of argon and water before going into the details of the study [3].

1.1.1 Argon

Argon is a monoatomic, colorless, odorless, tasteless and nontoxic gas, present in the atmosphere at a concentration of just under 1% (0.934%) by volume. After nitrogen and oxygen, argon is the most abundant element in air. It is a member of inert or noble gases which signifies that argon is chemically inactive. Argon was first discovered by Lord Rayleigh and Sir William Ramsay in 1894. Its normal boiling point is -185.9^{o}C. The gas is approximately 1.4 times as heavy as air and is slightly soluble in water. Its freezing point is only a few degrees lower than its normal boiling point, -199.3^{o}C. Argon has approximately the same solubility as oxygen and it is 2.5 times as soluble in water as nitrogen. It is not found in any compounds. Seawater contains 0.45 ppm argon. Argon being a noble gas does not react with water even at high temperatures or under any other special conditions [4].

Argon is valued for its total inertness. It is used where a completely non-reactive gas is

needed. It is the most abundant, and least expensive, truly inert gas. Argon is used with methane as a filler gas, and as a high purity inert shield gas in the manufacture of silicon and germanium crystals used in the semiconductor industry. Argon is used in winemaking to displace oxygen in barrels and thus prevent the formation of vinegar. Similarly, it is used to prevent open bottles of wine from oxidizing and to top off wine barrels, so the wine doesn't turn into vinegar during the aging process. Also they are filled in light bulbs and incandescent lamps to protect the filament. The argon method or potassium-argon method is applied in geology to date solidification time of volcanic materials [5]. In atomic research argon is applied to protect other elements from unwanted effects. It is applied in tyres of luxury cars to protect rubber and prevent noise emissions at high speed. Another popular application are argon laser for eye correction, arteries welding and tumor removal. Argon does not have any biological use and is non-water hazardous as well. It is physiologically ineffective. All these make the study of argon more interesting [6].

1.1.2 Diffusion of Argon

Most of the uses of argon mentioned above includes the diffusion of argon in one way or the other. Diffusion is the transport of matter from one region to another region in space without any application of external forces other than the concentration difference (see chapter 2). Whether the case of filling argon along with the nitrogen in the bulbs or protecting wine from turning out into venegar, it is the diffusion process that occurs directly or indirectly. So, the diffusion of argon in liquid is of utmost importance.

The study of diffusion of argon in olive oil provides the basis to measure fat space within the body [5]. The diffusion coefficient of argon in water helps to study the excretion of argon from the human skin [4]. The atmospheric argon diffuse in rain water and along with it enters the earth surface. The quantity of argon is calculated to evaluate the age of rock. This is the important geological use of argon. As the breathing air contains argon, diffusion of argon occurs in lungs as well. The high percentage of argon in breathing air leads to oxygen deprivation and asphyxiation. Also the mass diffusion rate can be used to separate the stable isotopes of argon from a mixture.

Although argon is inert, its diffusion effect has remarkable effects on geological, health as well as industrial sector. All these provided us the means to study about the diffusion of argon in water.

In an attempt to contribute in the above mentioned fields which are relatively confined but of much importance, a simple study of mutual diffusion of argon in water is done. A few pertinent studies have been done on this subject. Experimentally, some of the famous techniques used for the study of diffusion are, Electron-Spin Resonance (ESR), Dynamic Light Scattering (DLS) and Nuclear magnetic resonance (NMR) [7]. The mass spectrometry method is also used in some cases [4]. These methods are expensive and difficult to handle. An alternative method free from experimental cumbersome is molecular dynamics simulation which has beed adopted in our study.

1.1.3 Scope of the Present Work

In this study, the molecular dynamics technique has been used to study the diffusion of argon in water. The entire work has been described in five major chapters.

The theoretical description of diffusion is presented in chapter 2. The expression for self-diffusion, which is the famous Einstein's relation, is derived using Fick's law and equation of continuity. Then comes the binary diffusion with an empirical Darken's relation. A short introduction of radial distributed function is also provided in a simplified manner. Also, in this chapter a basic idea on several aspects of molecular dynamics is explained along with its limitations. A brief introduction on the available molecular dynamics software is included as well. Finally, the chapter ends with the description of GROMACS (Groningen Machine for Chemical Simulations), the molecular dynamics package used in the current study.

The details of the simulation procedure carried out in this work is explained in chapter 3. This chapter basically helps the newcomers to use molecular dynamics and GROMACS. It contains a fine detail of every step in molecular dynamics from modelling of a system to its dynamics. Also provided is the various commands in GROMACS along with their use. The outcome of simulation is entirely based on the steps taken in this chapter.

The results of present study is presented in chapter 4. The results thus obtained are the discussed and analyzed. Initially, the structural analysis is done by estimating the pair distribution function for the argon-water system. Then the self-diffusion coefficient at various temperatures for each component (water and argon) are analysed on the basis of mean square displacement plot. Then, on the basis of self-diffusion coefficients, the mutual diffusion coefficient of argon in water at different temperatures is calculated by invoking Darken's relation. Also, the temperature variation of the diffusion coefficients are presented. Finally, in chapter 5, the study is concluded with its future scope.

Chapter 2

Theory

2.1 Diffusion Theory

2.1.1 Diffusion: The Definition

In a thermodynamic system, different physical quantities such as mass or matter, momentum and energy are transferred from one region of a system to another by various transport phenomena. The mass or matter alone can be transported by several processes. Diffusion is one of the processes by which matter is transported from one part of a system to another as a result of random molecular motions without requiring bulk motion. Other processes include convection or dispersion which use bulk motion and thus are quite different from diffusion. Diffusion is a time-dependent process, constituted by random motion of given entities and causing the statistical distribution of these entities to spread in space. Thus the concept of diffusion is tied to notion of mass transfer, driven by a concentration gradient [7].

A simple classical experiment can be taken to illustrate a diffusion phenomenon. A tall cylindrical vessel with its lower part filled with iodine solution is taken and a column of clear water is poured on top carefully and slowly so that no convection currents are set up. At first,a well-defined boundary separates the colored part from the clear part.In time it is found that the upper part becomes colored, the color getting fainter towards the top, while the lower part becomes correspondingly less intensely colored. After sufficient time, the whole solution appears uniformly colored. There is evidently a transfer of iodine molecules from the lower to the upper part of the vessel taking place in the absence of convection currents. Therefore, the iodine is said to have diffused into the water [7]. Similarly if a few crystals of colored material like copper sulphate are placed at the bottom of a tall bottle filled with water, the color will slowly spread through the bottle. At first the color will be concentrated in the bottom of the bottle.After a day it will penetrate upward a few centimeters. After several years the solution will appear homogeneous [8].

In the above example, if it were possible to watch individual molecules of iodine or copper sulphate it would be found that the motion of each molecule is a random. In a dilute solution, each molecule behaves independently of the others, which it seldom meets, and each is constantly undergoing collision with solvent molecules. As a result of collisions it

moves sometimes towards a region of higher concentration and sometimes that of lower concentration having no preferred direction of motion towards one or the other. The motion of a single molecule can be described in terms of the random molecular walk picture. For such motion, although it is possible to calculate the mean-squared distance travelled in a given interval of time, it is not possible to say in which direction a given molecule will move in that time.

In the random molecular motions, where no molecule has a preferred direction of motion, has to be reconciled with the fact that a transfer of molecules from the region of higher to that of lower concentration is nevertheless observed. Let us consider any horizontal section in the solution and two thin and equal volume elements, one just below and one just above the section. Though it is not possible to say which way any particular molecule will move in a given interval of time, it can be said that on the average a definite fraction of the molecules in the lower volume element will cross the section from below; and the same fraction of molecules in the upper volume element will cross the section from above in a given time. Thus, because there are more molecules in the lower element than in the upper one, there is a net transfer from the lower to the upper side of the section as a result of random molecular motions [7]. Thus, diffusion is caused by random molecular motion of the particles in the fluid.

2.1.2 Mathematical Treatment: Einstein's Relation

Transport coefficients describe the material properties of a fluid within the framework of continuum fluid dynamics. The most familiar of the transport coefficients are those applicable to simple fluids; these are the diffusion coefficient, the shear and bulk viscosities and the thermal conductivity. In a continuous system the diffusion coefficient D is defined by Fick's law relating mass flow to density gradient [17]. The Fick's law states that the rate of transfer of diffusing substance through unit area of a section, which is defined as particle flux **J**, is proportional to the concentration gradient measured normal to the section, i.e.,

$$\mathbf{J} = -D\nabla C(r,t), \tag{2.1}$$

where C(r,t) is concentration of the diffusing substance which is function of position and time, and D, the proportionality constant, is referred to as the self or mutual diffusion coefficient. The diffusion coefficient measures the rate of diffusion of the substance. The negative sign indicates that the diffusion occurs in the direction opposite to that of increasing concentration. The flux **J** and the concentration C(r,t) are both expressed in terms of the same unit of quantity, e.g. gram or gram molecules. Then from equation (2.1), it is clear that D is independent of this unit and has dimensions $(length)^2(time)^{-1}$ [7].

It must be noted that the statement expressed mathematically by equation (2.1) is in general valid only for an isotropic medium, whose structure and diffusion properties in the neighborhood of any point are the same relative to all directions. Because of this symmetry, **J** is along the normal to the surface of constant concentration through the point [7].

To determine the diffusion coefficient of the substance it is necessary to compute the concentration profile of the diffusing substance. This is done under the assumption that at time t=0, the substance was concentrated at the origin of our coordinate frame, i.e., $C(r,0) = \delta(r)$. However, to compute the time evolution of the concentration profile, equation (2.1) must be combined with the equation of continuity given below, which expresses conservation of the mass of the substance, i.e.,

$$\frac{\partial C(r,t)}{\partial t} + \nabla.\mathbf{J}(r,t) = 0. \tag{2.2}$$

Using equation 2.1, we get

$$\frac{\partial C(r,t)}{\partial t} - \nabla.(\nabla C(r,t)) = 0 \tag{2.3}$$

or

$$\frac{\partial C(r,t)}{\partial t} - \nabla^2 C(r,t)) = 0. \tag{2.4}$$

As stated earlier, equation (2.4) is solved using the boundary condition

$$C(r,0) = \delta(r) \tag{2.5}$$

where $\delta(r)$ is the Dirac delta function. This will yield [16]

$$C(r,t) = \frac{1}{(4\pi Dt)^{d/2}} \exp(-\frac{r^2}{4Dt}) \tag{2.6}$$

where d represents the dimensionality of the system. For a three-dimensional system as general is the case, it carries a value of 3.

The time dependence of second moment of C(r,t) is defined as

$$< r^2(t) > \equiv \int d\mathbf{r} C(r,t) r^2 \tag{2.7}$$

where C(r,t) satisfies the normalization condition

$$\int d\mathbf{r} C(r,t) = 1. \tag{2.8}$$

The second moment is also known as mean-squared displacement (MSD) of the diffusing particles.

The time evolution of $< r^2(t) >$ can be obtained by multiplying equation (2.3) by r^2 and integrating over all space. Then,

$$\int d\mathbf{r}\ r^2 \frac{\partial C(r,t)}{\partial t} = \int d\mathbf{r}\ r^2 D\nabla.(\nabla C(r,t)). \tag{2.9}$$

Changing the order of integration and derivative, we get

$$\frac{\partial}{\partial t}\int d\mathbf{r}\ r^2 C(r,t) = D\int d\mathbf{r}\ r^2\nabla.(\nabla C(r,t)). \tag{2.10}$$

From equation (2.7), equation (2.10) can be written as

$$\frac{\partial}{\partial t} < r^2(t) >= D\int d\mathbf{r}\ r^2\nabla.(\nabla C(r,t)). \tag{2.11}$$

Since

$$\nabla.(\phi\nabla\psi) = \nabla\phi.\nabla\psi + \phi\nabla^2\psi, \tag{2.12}$$

equation (2.11) can be written as

$$\frac{\partial}{\partial t} < r^2(t) >= D\int d\mathbf{r}\nabla.(r^2\nabla C(r,t)) - D\int d\mathbf{r}\nabla r^2.\nabla C(r,t). \tag{2.13}$$

Using the Gauss divergence theorem

$$\int_V d\mathbf{r}(\nabla.\mathbf{A}) = \int_S d\mathbf{S}.\mathbf{A} \tag{2.14}$$

in the first part and taking derivative in the second part we get,

$$\frac{\partial}{\partial t} < r^2(t) >= D\int d\mathbf{S}.(r^2\nabla C(r,t)) - 2D\int d\mathbf{r}\ \mathbf{r}.\nabla C(r,t). \tag{2.15}$$

The surface integral is zero over the surface enclosing the entire space under consideration. Thus, the first term vanishes. Using equation (2.12) in the second integral, it is seen that

$$\frac{\partial}{\partial t} < r^2(t) >= -2D\int d\mathbf{r}\ \nabla.(\mathbf{r}C(r,t)) + 2D\int d\mathbf{r}\nabla.\mathbf{r}C(r,t). \tag{2.16}$$

Again, the first integral vanishes by divergence theorem and $\nabla.\mathbf{r}$=3. Using these, (2.16) becomes

$$\frac{\partial}{\partial t} < r^2(t) >= 6D\int d\mathbf{r}C(r,t). \tag{2.17}$$

Now, using the normalization condition (2.8), an expression for diffusion coefficient can be obtained as

$$D = \frac{\partial < r^2(t) >}{6\partial t}. \tag{2.18}$$

Equation (2.18) is the famous Einstein relation which relates the diffusion coefficient with the mean-squared displacement (MSD). In this equation D is a macroscopic transport coefficient, the mean square displacement has a microscopic interpretation [16]. As expressed in equation (2.18), the instantaneous diffusion coefficient is given by the slope of a curve of MSD of the diffusive particles versus time. For an MSD that behaves as a straight line after a prolonged period of time, equation (2.18) reduces to

$$D = \lim_{t\to\infty}\frac{< r^2(t) >}{6t}. \tag{2.19}$$

2.1.2.1 Self Diffusion

The self diffusion occurs in a homogeneous system where no chemical concentration gradient exists. In a homogeneous system, the constituent particles are in rapid translational motion due to various interactions with other particles and thermal agitation. The motion can also be termed as "random walk". The molecular displacements are characterized by the corresponding diffusion coefficient which is called the *self-diffusion coefficient*. In three dimensional space diffusion coefficient is related to mean square displacement after certain time t via Einstein relation given by equation (2.19). Thus the diffusion coefficient given by Einstein relation is self diffusion coefficient [30].
The self diffusion is a simple form of diffusion where the molecules of the diffusing species are identical to the other molecules in every aspect. The only difference is that the diffusing species is labelled and that too does not affect the interaction of the labelled molecules with the others. For instance, the diffusion of similar species having a particular polarization of the nuclear spin or having a modified isotopic composition [16]. This term is used for the diffusion not only in a pure system of single component but also in a homogeneous multi-component system. Following the general of looking for a molecular description of the properties of matter, the self diffusion coefficient has become a key quantity for interpreting and modelling transports in liquids, because among all transport coefficients the self diffusion coefficient is certainly the most simple to interpret. For example, the extraction of self-diffusion coefficients from molecular dynamics simulation is straightforward by evaluation of the mean-squared displacement from the simulated trajectories of the particles. Microscopically, it is characterized by the noncooperative random-walk motion of the individual molecules [30].

2.1.2.2 Binary Diffusion

The diffusion of two different species in a binary mixture is called binary diffusion and the corresponding diffusion coefficient is called *binary diffusion coefficient*. If, as an external perturbation, a concentration inhomogeneity is set up for one of the components, the system responds with another diffusion process called binary diffusion. This is because a concentration gradient of any component results in mass fluxes of all other components. In this case the species diffuse cooperatively, so as to smear out the concentration inhomogeneity [30]. This process is also termed as mutual diffusion in work on fluid mixtures, in other fields the term inter diffusion, mass diffusion, chemical diffusion, or transport diffusion are also in use. The cooperativity of the mass flows distinguishes mutual diffusion from the stochastic motion of individual molecules reflected by the self diffusion process. For example, the mass flows of the two components in binary systems are coupled and a single quantity, called mutual diffusion coefficient, is sufficient to characterize the diffusion process, regardless of which of the mass flows is observed [30].
The simplest self diffusion-mutual diffusion relationship for the binary system is the Darken's relation sometimes called Hartley-Crank relation [31, 32].

$$D_{12} = N_2 D_1 + N_1 D_2. \tag{2.20}$$

D_{12} is the binary diffusion coefficient. D_1 and D_2 are the self diffusion coefficients of species 1 and 2, respectively. N_1 and N_2 are the corresponding mole fractions. For a binary system

under infinite dilution, the binary diffusion coefficient becomes equal to the self-diffusion coefficient of one of the components. From the applications' point of view, mutual diffusion is more important than self-diffusion and plays a major role in many physical and chemical processes. It is characterized by the cooperative motion of the molecules and therefore its theoretical description is more complex than that of the self diffusion. Experimentally, the use of nuclear magnetic resonance spin-echo experiments provides an elegant and convenient method for monitoring self diffusion in liquids. The methods such as dynamic light scattering and Taylor dispersion methods are frequently adopted for measuring mutual diffusion [30].

2.2 Radial Distribution Function: An idea

The fluid state is characterized by the absence of any permanent structure. There are, nevertheless, well-defined structural correlations that can be measured experimentally to provide important details about the average molecular organization. The treatment of the structural correlation begins with the general pair distribution function $g(\mathbf{r}_1,\mathbf{r}_2)$[17]. If the system is isotropic, the pair distribution is a function of only the separation r_{12}=|$\mathbf{r}_1$-$\mathbf{r}_2$|; it is then usually called the *radial distribution function* and written as *g(r)*. The probability of observing a second molecule in dr given that there is a molecule at the origin of r is given by ρg(r)dr, where ρ=N/V is the overall number density of the system. This probability is not normalized to unity. Instead, the definition of *g(r)* implies that on average the number of particles lying within the range r to r+dr from a reference particle is $4\pi r^2\rho$g(r)dr. Then

$$\int_0^\infty \rho g(r) 4\pi r^2 dr \approx N \tag{2.21}$$

Since the influence of particles at the reference particle diminishes as r becomes large, g(r) tends to unity at large r, and g(r) vanishes as r tends to zero as a consequence of the strongly repulsive forces that act at a small particle separation. The form of g(r) provides considerable insight into the study of the structure of liquids mainly of two reasons. Firstly, if we assume that the potential energy of the N-body system is pair-wise additive, then all the thermodynamic functions of the system can be written in terms of g(r). Secondly, g(r) is measurable by radiation scattering experiments. It shows a pattern of peaks and troughs. The peaks in g(r) represent *shells* of neighbors around the reference particle. Integration of $4\pi r^2\rho$g(r) upto the position of first minimum therefore provides an estimate of the nearest neighbor co-ordination number [28, 29]. The RDF primarily addresses the local structure, but gives little direct information as to whether long-range crystalline order exists[17]. In a solid, the RDF has an infinite number of sharp peaks whose separations and heights are characteristic of the lattice structure. The RDF of liquid has a small number of peaks at short distances, superimposed on a steady decay to a constant value at longer distances. Figure 2.1 and 2.2 illustrate the structure of RDF.
As seen from the figure, at short range up to a finite distance, *RDF* has a zero value, indicating that there is a zero probability of finding the particles within this distance. Mathematically, it is due to r^{-12} term of Lennard-Jones interaction and repulsive Coulomb interaction

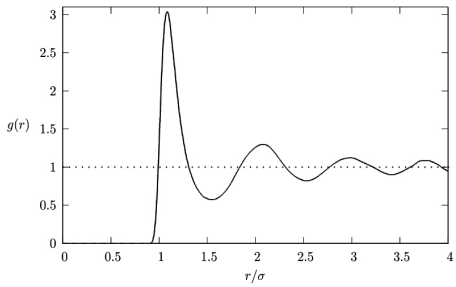

Figure 2.1: Radial Distribution Function of simple LJ liquid

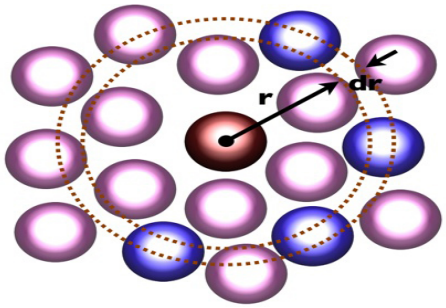

Figure 2.2: Simple model of system illustrating 'shells'in rdf

incorporated in the model of the system. Physically, it signifies the presence of a hard core in the interatomic interaction which gives rise to an excluded volume in the spatial distribution of particles. In other words, particles, either argon atoms or solvent molecules, repel each other at this short range. This repulsion is a characteristics of the density of the system. The distance of separation is less than the van der Waal's radius of the molecule under consideration. Beyond this distance, *g(r)* starts to rise and becomes oscillatory gaining some peaks and at long ranges approaches unity. The oscillatory nature of *g(r)* has a very simple physical meaning. It shows that with reference to a given particle, other particles in the system are not distributed uniformly. Rather, they are arranged in discrete spherical shell-like structures having certain radius with the center at reference particle. Therefore, the first peak in *g(r)* signifies position of the first nearest-neighbors contained in the first shell. The second peak indicates the position of second nearest-neighbors contained in the second shell and so on. However, the peaks are seen to damp out fairly quickly approaching unity at long range. This implies that there is only local order in the system and no long-range order which is a characteristic feature of the liquid state. This is because in liquid, particles are uncorrelated when they are far apart[14].

2.3 Molecular Dynamics: An Introduction

Molecular dynamics simulations is the modern realization of an old, essentially old-fashioned, idea in science; namely, the behavior of a system can be computed if we have, for the systems parts, a set of initial conditions plus forces of interaction. From the time of Newton to the present day, this deterministic mechanical interpretation of Nature has dominated science [9]. The impressive static images of inorganic molecules and biological macromolecules with atomic resolution is provided by crystallography. However, these pictures convey no information on dynamic features like conformational variation, ligand binding or protein folding, diffusion, etc. A dynamic picture fundamentally relies on spectroscopical observations that contain little or no information about the molecular geometry. Moreover, at present there is no technique that provides high resolution in time and space at the same time. Besides, the experimental measurement of the different transport properties of a system such as diffusion coefficient is difficult and time consuming as well as expensive.

One of the best ways to address this problem is computer simulation of classical molecular dynamics (MD). MD simulations permit the study of complex dynamic processes that occur in biological systems like protein stability, protein folding, conformational changes etc. and to watch a molecule at atomic resolution while it performs its function. The first crude MD simulations were carried out in the late fifties by Alder and Wainwright [1957, 1959] with a system of hard spheres moving with constant velocity between elastic collisions. In 1964, Rahman modelled the first Lennard-Jones system, and in 1971 Rahman and Stillinger made a simulation on a liquid water [15]. In the seventies, numerous techniques were developed that allowed simulations of complex molecules and transient systems. The first simulation of a protein, the bovine pancreatic trypsin inhibitor (BPTI), was performed in 1977. Simulations at that time were performed *in vacuo*, but the availability of vast computer power nowadays allows for simulations of much larger systems, e.g. proteins in their native environment like water or membrane [14]. In the last decade, people have begun simulating simple systems such as the diffusion of gases into solids, interfaces between different liquids, or rarefied gases. Also the MD techniques have evolved in the application to macroscopic or "real" systems. While molecular level phenomena will always be of interest, large scale use of microscopic methods will produce macroscopic effects. The field of gas dynamics has for years recognized the relationship between microscopic interaction of atoms and macroscopic properties such as temperature, pressure and viscosity [10].

In classical molecular dynamics Newton's equations of motion are solved for a system of N atoms interacting according to a potential energy U. It is a function of space ($\mathbf{r}$) with which Newton's equation of motion for i^{th} atom can be stated as

$$m_i \frac{\partial^2 \mathbf{r}_i}{\partial t^2} = -\nabla_i U(r) = \mathbf{F}_i. \tag{2.22}$$

Here m_i is the mass and $\boldsymbol{r}_i$ is the position of the i^{th} atom. The right-hand side is negative gradient of the potential which is equal to the force F_i acting on the atom. This equation relates the derivative of the potential energy to the changes in the position as a function of time. Thus, provided a model of the potential energy U of the system under study which is

known as force field, integration of equation (2.22) yields the trajectory of the system that describes the positions, velocities and accelerations of the particles as they vary with time. The trajectory provides insight into the system's conformational flexibility as the system explores different accessible parts of the phase space. Thus the method is deterministic; once the positions and velocities of each atom are known, the state of the system can be predicted for any time. Moreover, the equilibrium and transport properties of the system can be calculated using the trajectory [14].
Molecular dynamics simulations can be considered as a simple program which are designed taken into consideration that they are in many respects very similar to real experiments [16]. The overall process can be summarized into four major steps as follows:

- Modelling a System,
- Initialization,
- Force Calculation,
- Integration of Equation of Motion.

2.3.1 Modelling a System

Modelling a system means preparing a system model under study. A computer simulation is applied to a precisely defined model for the material of interest. A model is actually a composite of two: one for interactions among the molecules making up the system and another for interactions between the molecules and their environment [9]. The model for molecular interactions is contained in an intermolecular potential energy function. This potential function implicitly describes the geometric shapes of individual molecules or, more precisely, their electron clouds. Thus when we specify the potential function, we establish the symmetry of the molecules,whether they are rigid or flexible, how many interaction sites occupy each molecule, and so on. The second part of the simulated model encompasses boundary conditions, which describe how the molecules interact with their surroundings. So setting boundary conditions completes the definition of the model system to be simulated [9]. This indicates that the model comprises of the force field and system topology. A force field is constituted by the functional form of the empirical potential describing the interactions between the atoms and/or molecules along with the parameters used in that function. These parameters may be well depths of energies, spring constants for bonds, etc. The topology of the system consists of lists of atoms that are connected to each other [14].

The choice of force fields depends upon the nature of the system. There are numerous force fields for different applications. The most popular force fields for biomolecular simulations are GROMOS96, OPLS-AA, CHARMM and AMBER. They show considerable differences in the strategy of parameter specification and the resulting parameters. Nevertheless, the functional forms of these force fields are very similar [14].

In conventional MD simulations, the particles moving in the simulation cell, obey the laws of classical mechanics. The instantaneous forces acting on the particles are calculated from potential energy functions i.e. force fields, expressed normally as simple analytical continuous functions. These potential functions are derived empirically. Atoms are treated as spherically symmetric particles connected through covalent bonds forming molecules. Interactions between atoms of molecules are represented by effective pair-wise additive potentials. This empirical approach splits the total potential energy of the system into a bonded(inter molecule) and non-bonded(intra molecular) part [3]. The bonded interaction encompasses terms for bond stretching U_{bond}, bond angle bending U_{angle}, dihedral angle potential U_{dihed}, and out-of-plane distortions alias improper U_{impr}. They are not exclusively pair interactions, but include 3-body and 4-body interactions as well. Non-bonded interactions are represented by the Van der Waals potential U_{vdW} and the Coulomb potential $U_{Coulomb}$. Therefore, the total potential energy function of a system can be stated as

$$U_{total} = U_{bond} + U_{angle} + U_{dihed} + U_{impr} + U_{vdW} + U_{Coulomb}. \tag{2.23}$$

In classical MD studies, the bond stretching, bond angle vibration, and improper dihedral potential energy contributions are approximated in terms of harmonic potentials. However, the potential function for proper bond dihedral is characterized by periodic potentials [11]. The potential energy functions are defined below.

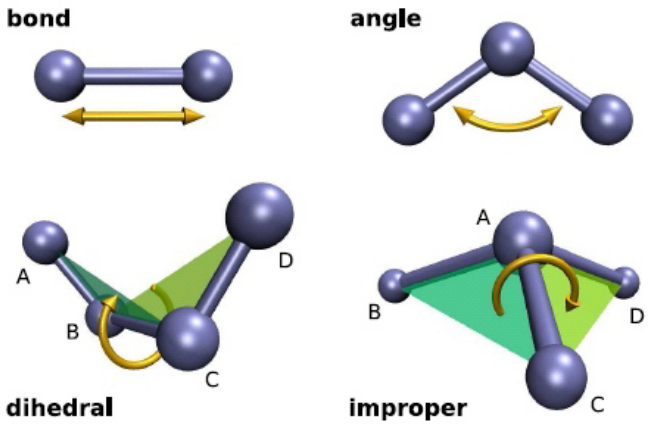

Figure 2.3: Different types of bonds in a molecule [14] .

2.3.1.1 Bond Stretching

The bond stretching potential between two covalently bonded i^{th} and j^{th} atoms in a molecule is defined as

$$U_{bond} = \frac{1}{2} k_{ij}^{r} (r_{ij} - b_{ij})^2. \tag{2.24}$$

Here b_{ij} represents the bond length and k_{ij}^{r} represents force constant. Figure 2.3 (upper-left) represents the principle and figure 2.4 represents the potential [12].

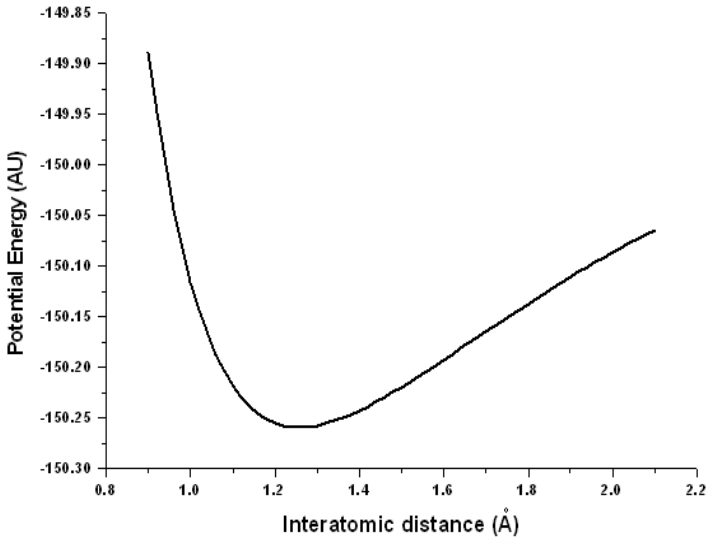

Figure 2.4: Harmonic potential for bond stretching for a typical system [14].

2.3.1.2 Bond-angle Vibration

The bond angle vibration formed by triplet of atoms *(i,j,k)* in a molecule is defined as

$$U_{angle} = \frac{1}{2} k^{\Theta}_{ijk} (\Theta_{ijk} - \Theta^{0}_{ijk})^2. \tag{2.25}$$

Here k^{Θ}_{ijk} is the force constant and Θ^{0}_{ijk} is the equilibrium bond angle. Figure 2.3 (upper-right) represents the principle. Atom $j$is in the middle and atoms i and k are at the ends. Figure 2.5 represents the potential [12].

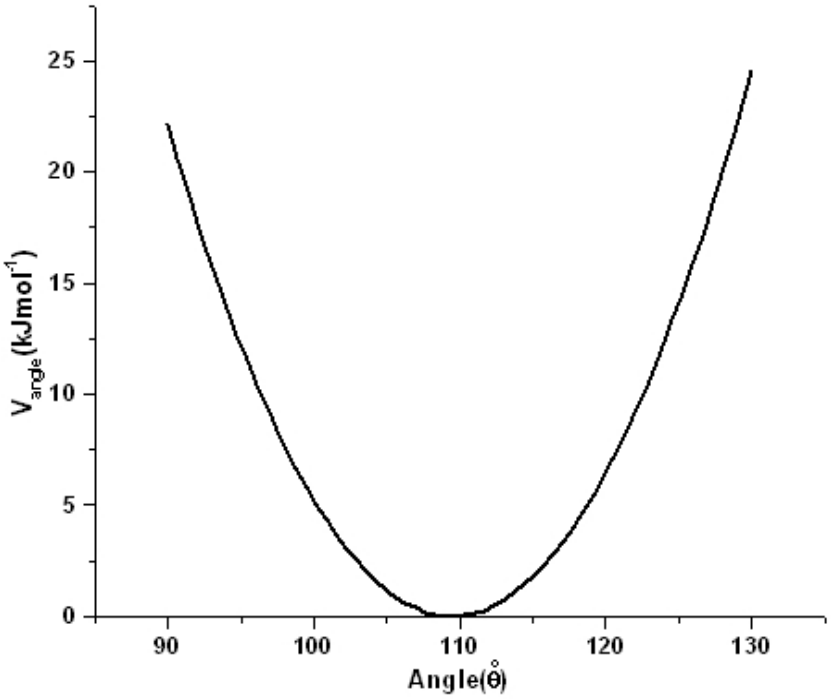

Figure 2.5: Harmonic potential for bond angle vibration for a typical system [14].

2.3.1.3 Proper Dihedrals

The dihedral is defined by the angle between the two planes determined by atoms *A-B-C* and *B-C-D*. It measures torsion around bonds as shown in figure 2.3 (lower-left). The periodic potential is defined as

$$U_{dihed} = \frac{k_i^{\Phi}}{2}(1 + \cos(n\Phi_i + \delta_i)). \tag{2.26}$$

Here Φ_i is dihedral angle, k_i^{Φ} is the barrier height, and δ_i is a reference angle at which the potential is maximum. The periodicity n_i counts the number of minima for a full rotation of 360°. The potential is represented by figure 2.6 [12].

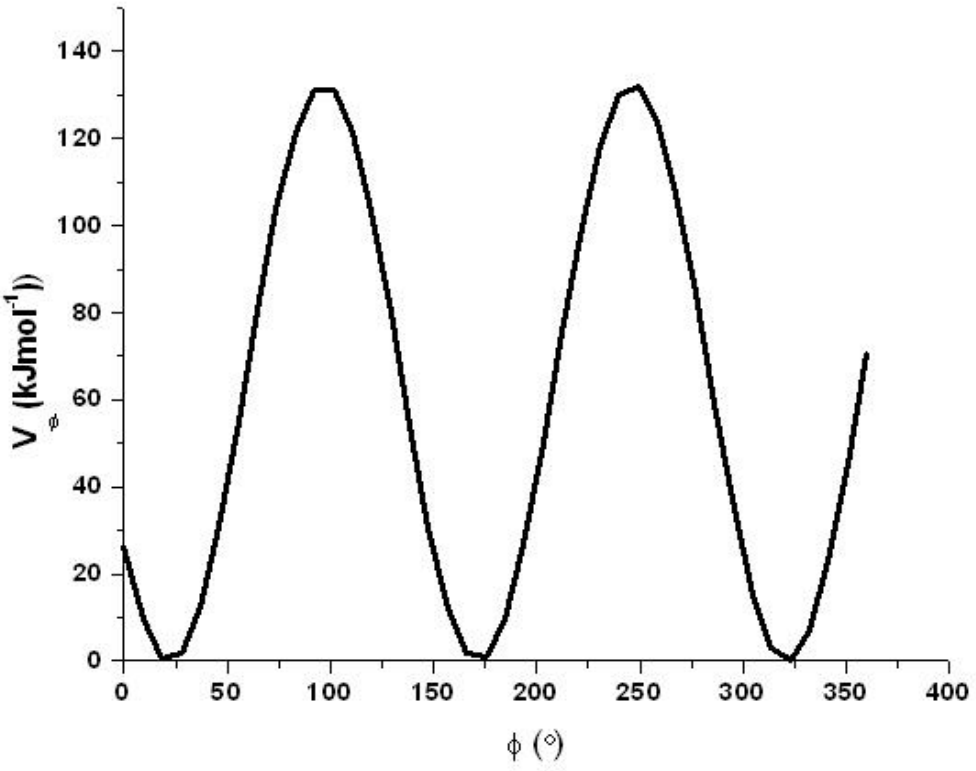

Figure 2.6: Harmonic potential for proper dihedral of a typical system [14].

2.3.1.4 Improper Dihedrals

The improper dihedrals keep planar groups planar or prevent molecules from flipping over to their mirror images. The principle has been shown in figure 2.3 (lower-right). The potential is defined as

$$U_{impr} = \frac{1}{2}k^{\omega}(\omega_{ijkl} - \omega_0)^2, \tag{2.27}$$

where the parameters ω_0 and k_ω mark the equilibrium improper dihedral angle and force constant, respectively. Figure 2.7 represents the potential [12].

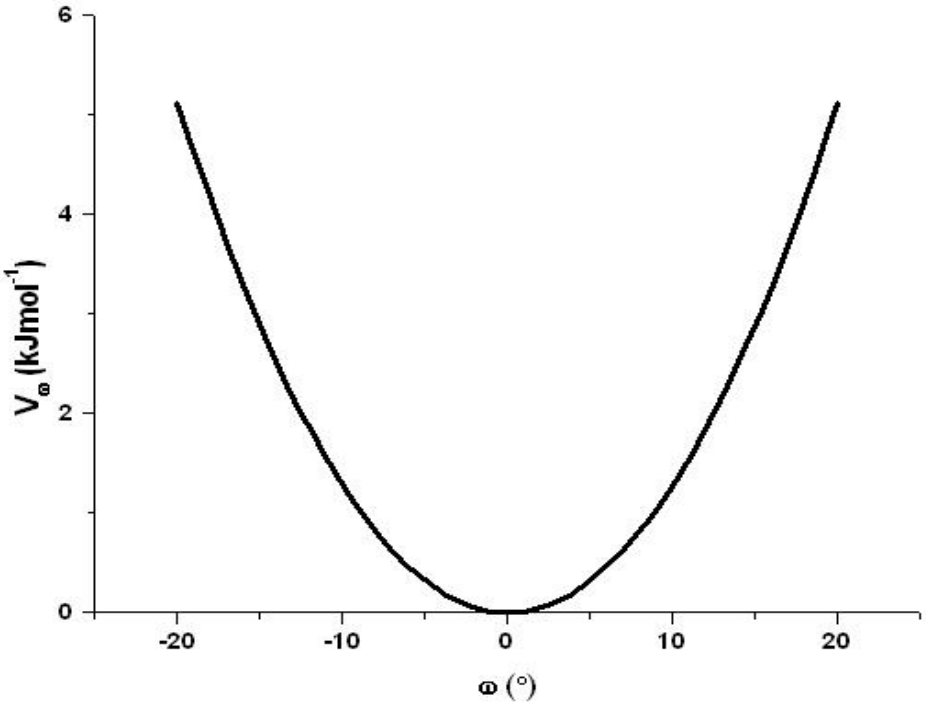

Figure 2.7: Harmonic potential for improper dihedral for a typical system [14].

2.3.1.5 Lennard-Jones's Interaction

It is a non-bonded interaction. The potential energy function is composed of the attractive dispersion energy due to induced dipole interactions and a repulsive term due to overlapping electron clouds in interacting atoms which are well explained by two terms in the Lennard-Jones potential. The LJ potential is defined as

$$U_{LJ} = 4\epsilon_{ij}[(\frac{\sigma_{ij}}{r_{ij}})^{12} - (\frac{\sigma_{ij}}{r_{ij}})^{6}]. \tag{2.28}$$

The r_{ij}^{-6} term describes attraction at long ranges (van der Waals force, or dispersion force)and the r_{ij}^{-12} term describes Pauli repulsion at short ranges due to overlapping electron orbitals. In the above relation $2^{1/6}\sigma_{ij}$ is the equilibrium distance called van der Waals radius at which the inter-particle potential is zero and ϵ_{ij} represents the minimum energy depth, that is , the depth of the potential well [13]. Also it clearly indicates that the potential energy function depends on inter atomic or intermolecular distance r_{ij}. Figure 2.8 represents the potential.

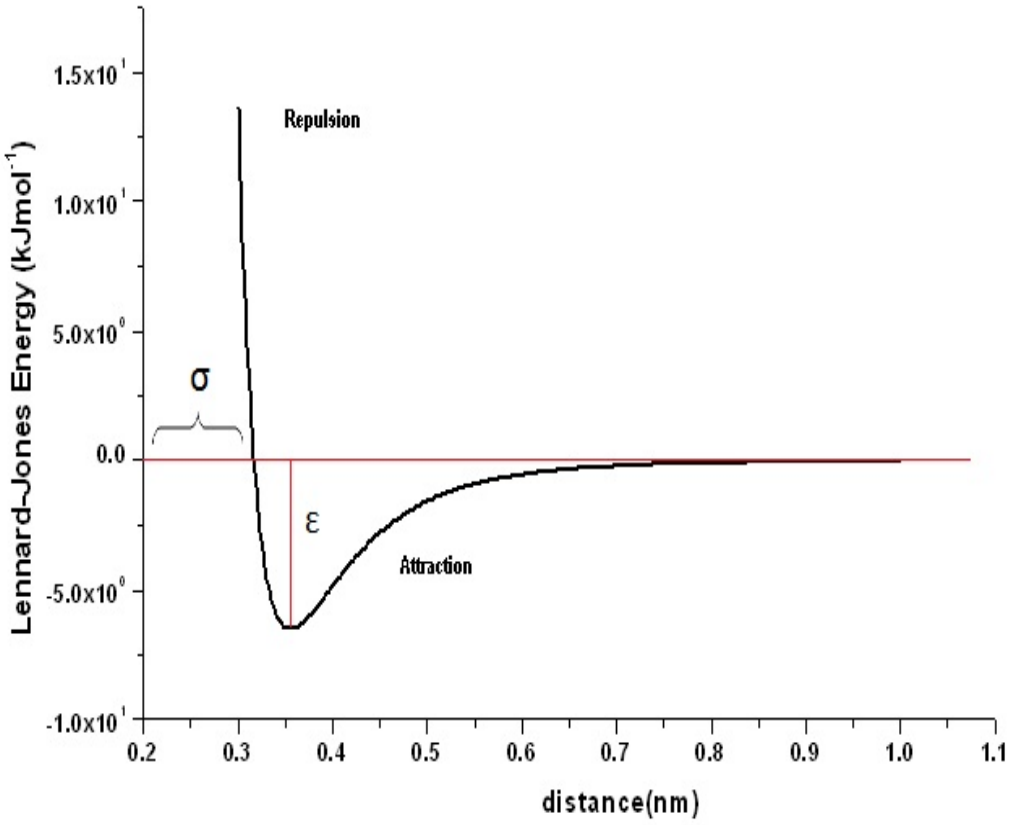

Figure 2.8: Lennard-Jones potential for a typical system.

2.3.1.6 Coulomb Interaction

It is a non-bonded interaction that arises due to the presence of some partial charge in the atoms or molecules. This type of interaction, commonly called electrostatic interaction, may occur between atoms of same or different molecules. The interaction is defined by Coulomb potential, approximated by the interaction between two point charge q_i and q_j as given below [14].

$$U_{Coulomb} = \frac{q_i q_j}{4\pi\epsilon\epsilon_0 r_{ij}}. \tag{2.29}$$

Here ϵ denotes the dielectric constant, ϵ_0 is the permittivity of free space and r_{ij} is the distance between the charges. In molecules, the atoms share their valence electrons and the electron density may be shifted due to different electronegativity of the atoms. These different charge densities can be mapped into partial point charges which are represented by q_i and q_j in the expression above.But atoms are not charged unless they are ions,so the atomic charges in this expression are an artificial construct [14]. The potential is represented by figure 2.9.

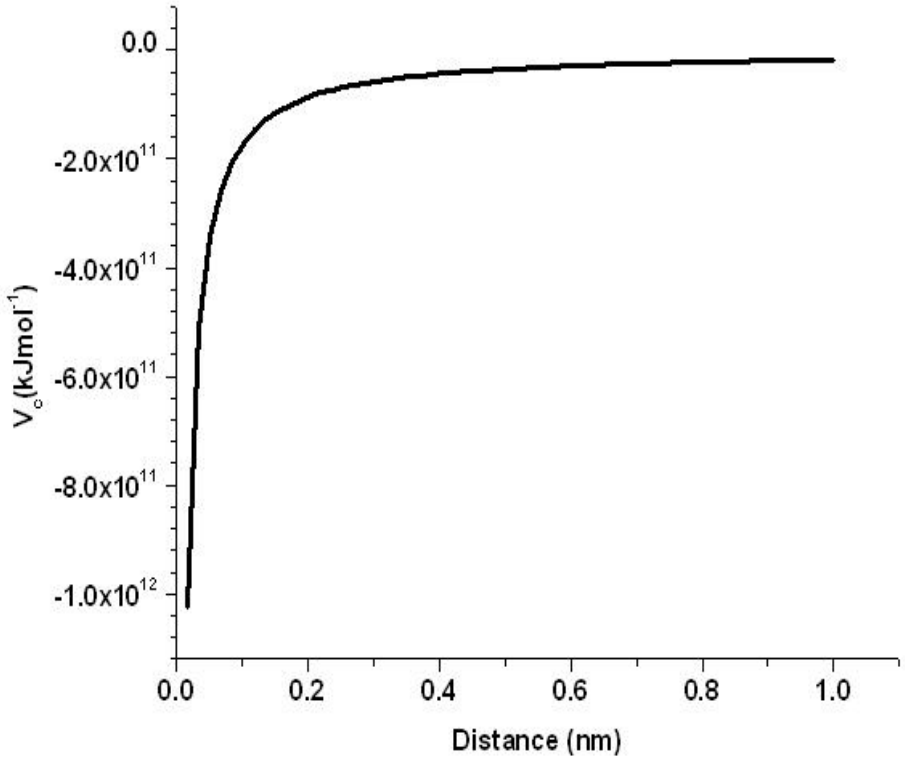

Figure 2.9: Coulomb potential (Attractive) for a typical system [14].

2.3.2 Simulation Box and Periodic Boundary Conditions

One of the most important tasks of modelling a system is to construct a simulation box and tackle various effects thereby. As the computer simulations are usually performed on small number of molecules, $10 \leq N \leq 10{,}000$, the simulation box is generally taken to be cubic which contains all the molecules of the system under study. In other words, all the molecules are kept inside this simulation box. A major obstacle on choosing such simulation box is that the large fraction of molecules lie on the surface of the cube. As an example, for 1000 molecules arranged in a cube of side 10, more than 488 molecules appear on the cube faces. The molecules on the surface experience quite different forces from molecules in the bulk [15].

A system that is bounded but free of physical walls can be constructed by resorting to periodic boundary conditions. Molecular dynamics simulations of any system aims to provide information about the properties of a macroscopic sample. Therefore, in order to simulate bulk phases by overcoming surface effects, it is necessary to implement periodic boundary conditions [16]. The introduction of periodic boundaries is equivalent to considering an infinite, space-filling array of identical copies of the simulation region. In the course of simulation, as a molecule moves in the original box, its periodic image in each of the neighboring

boxes moves in exactly the same way. Thus, a molecule that leaves the simulation region through a particular bounding face immediately reenters the region through the opposite face. This conserves the number density of the system [15, 16]. Figure 2.10 represents the application of periodic boundary conditions.

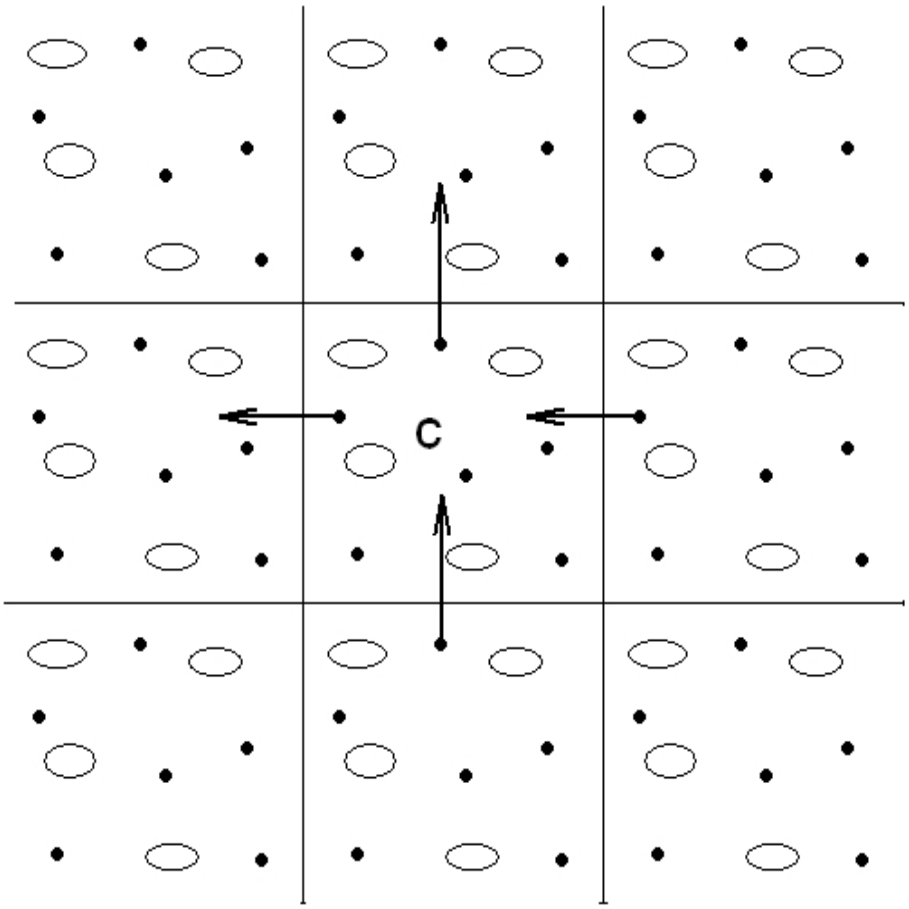

Figure 2.10: Schematic representation of periodic boundary condition. A primitive cell is represented by box C other boxes are its replica [14].

2.3.3 Initialization

The next step to follow is assign initial positions and velocities to all particles in the system. The particles positions should be chosen compatible with the structure that we are aiming to simulate, taking into consideration that the atomic or molecular cores do not overlap. This can be often achieved by initially placing the particles on a cubic lattice. The density and initial temperature are chosen such that the simple cubic lattice is mechanically unstable and melts rapidly. First, each particle is put on its position and lattice site and then to each velocity component of every particle a value is attributed using Maxwell-Boltzmann distribution. Subsequently, all velocities are shifted such that the total momentum is zero. The resulting velocities are then scaled to adjust the mean kinetic energy to the desired value. The relation given below holds in thermal equilibrium.

$$< v_\alpha^2 >= \frac{k_B T}{m}. \tag{2.30}$$

Here v_α is the α component of the velocity, m is mass of a given particle, T is temerature and k_B is Boltzman's constant [16, 14].

2.3.4 Force Calculation

This part includes the calculation of force acting on every particle. If we consider a model system with pairwise additive interactions, we have to consider the contributions to the force on particle $\boldsymbol{i}$ due to all its neighbors. The formula is given as;

$$\mathbf{F}_i = -\nabla_i U(\mathbf{r}_i). \tag{2.31}$$

Initially, the current distance in the x, y, and z directions between each pair of particles i and j is calculated. Then taking a periodic boundary conditions,a cutoff at a distance r_c is used in the explicit calculation of intermolecular interactions, where r_c is chosen to be less than half the length of the cubic simulation box [16]. It is because if the intermolecular interaction is long-ranged such as Coulomb interaction, there will be a substantial interaction between a particle and its own images in the neighboring boxes. Consequently the symmetry of the cell structure is imposed on the system which is in reality isotropic [15]. Using cutoff distance, the evaluation of intermolecular interactions between particles i and j to the interaction between i and the nearest periodic image of j is limited. This is called nearest-image convention and can be reliably employed on a system in which dispersion forces dominate Coulomb or dipolar interactions [16]. An example is Lennard-Jones fluid which is also the system under study. The near-image convention has been illustrated in the figure 2.11.

When the interaction beyond r_c is significant, long range correction should be done. This correction is usually based on the concept in which the field beyond r_c is constant (mean field approximation). In the case of Lennard-Jones interaction the long-range correction term is given as:

$$U_{LR} = 2\pi N \rho \int_{r_c}^{\infty} dr \;\; r^2 U_{L-J} \tag{2.32}$$

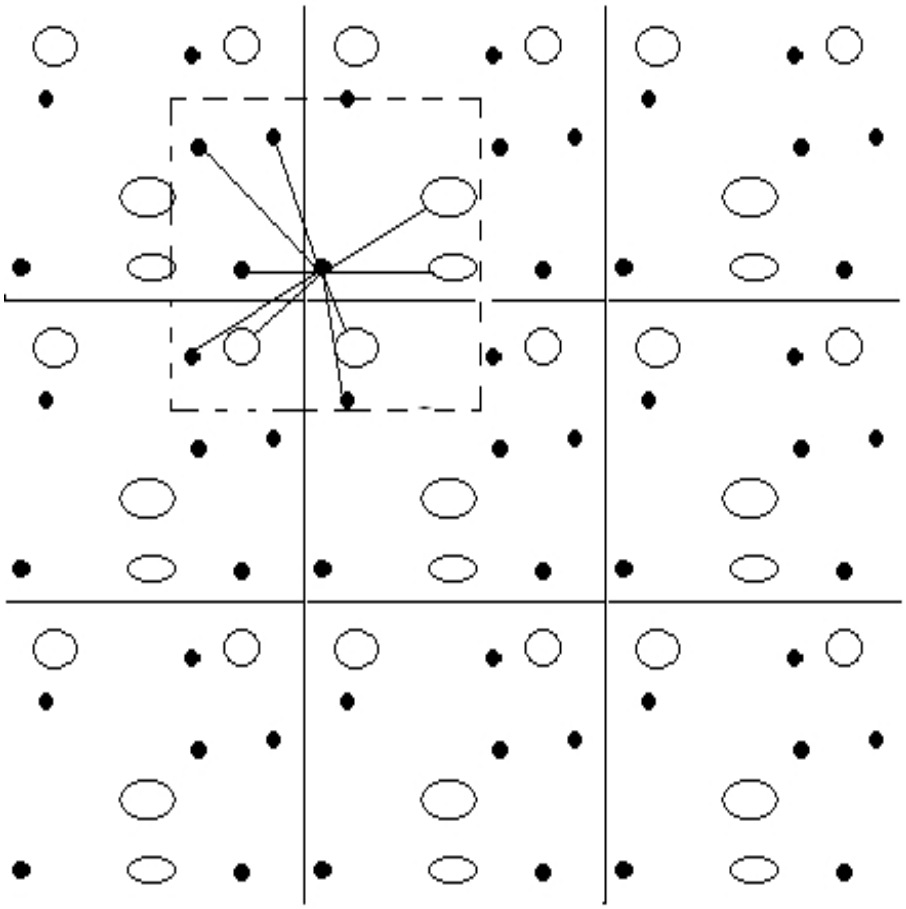

Figure 2.11: Use of cutoff and near-image convention for periodic boundary condition [16].

or,

$$U_{LR} = \frac{8}{3}[\frac{1}{3}(\frac{\sigma_{ij}}{r_c})^9 - (\frac{\sigma_{ij}}{r_c})^3]. \tag{2.33}$$

2.3.5 Integration of Equation of Motion

The first objective of molecular dynamics simulation is to compute the phase space trajectories which is obtained by solving Newton's equation. To obtain the phase space trajectories both the time-dependent positions r_i and time- dependent momentum p_i are desirable and are obtained by the integration of equation of motion. Both the position coordinates and velocity components are calculated with the help of known initial position coordinates and the velocity components. This calculation is done after all forces between the particles have been calculated. A variety of different numerical methods is available for this task.

2.3.5.1 Verlet Algorithm

The Verlet algorithm [Verlet 1967] is one of the simplest algorithms that uses positions and accelerations at time t and the positions from time $t - dt$ to calculate new positions at time $t + dt$. The Verlet algorithm uses no explicit velocities. It is a famous, the simplest, and usually the best algorithm. To derive it, let us consider a particle with the position $\mathbf{r}$ and velocity $\mathbf{v}$. Then a Taylor expansion of the position coordinate $\mathbf{r}$ about time t is

$$\mathbf{r}(t+\delta t) = \mathbf{r}(t) + \mathbf{v}(t)\delta t + \frac{\mathbf{F}(t)}{2m}\delta t^2 + \frac{\delta t^3}{3!}\frac{d^3\mathbf{r}}{dt^3} + O(\delta t^4). \tag{2.34}$$

Here δt is the time step in the molecular dynamics simulation, m is the mass, and $\mathbf{F}$ is the force on the particle. Similarly,

$$\mathbf{r}(t-\delta t) = \mathbf{r}(t) - \mathbf{v}(t)\delta t + \frac{\mathbf{F}(t)}{2m}\delta t^2 - \frac{\delta t^3}{3!}\frac{d^3\mathbf{r}}{dt^3} + O(\delta t^4). \tag{2.35}$$

Adding equation (2.34) and equation (2.35), it is seen that

$$\mathbf{r}(t+\delta t) + \mathbf{r}(t-\delta t) = 2\mathbf{r}(t) + \frac{\mathbf{F}(t)}{m}\delta t^2 + O(\delta t^4) \tag{2.36}$$

or,

$$\mathbf{r}(t+\delta t) \approx 2\mathbf{r}(t) - \mathbf{r}(t-\delta t) + \frac{\mathbf{F}(t)}{m}\delta t^2 + O(\delta t^4). \tag{2.37}$$

Thus, there is an error of order δt^4 in the estimate of the new position. It is also seen that the Verlet algorithm does not use the velocity to compute the new position.
To derive velocity subtracting (2.35) from equation (2.34), we obtain

$$\mathbf{r}(t+\delta t) - \mathbf{r}(t-\delta t) = 2\mathbf{v}(t)\delta t + O(\delta t^3) \tag{2.38}$$

or,

$$\mathbf{v}(t) = \frac{\mathbf{r}(t+\delta t) - \mathbf{r}(t-\delta t)}{2\delta t} + O(\delta t^2). \tag{2.39}$$

This expression for velocity is accurate to order of δt^2. Since the new positions have been computed, the positions at time $t - \delta t$ can be discarded. The current positions become the old positions and the new positions become the current positions [16].

2.3.5.2 Leapfrog Algorithm

In Leapfrog algorithm [Hockney 1970], the velocities are first calculated at time t+$\delta t/2$, these are used to calculate the positions, r, at time t+δt. In this way, the velocities leap over the positions, then the positions leap over the velocities. There are several algorithms which are equivalent to the Verlet algorithm. The Leap Frog algorithm can be derived as follows.
To derive the Leapfrog algorithm from Verlet scheme, it is started by defining velocities at the half-integer steps as

$$\mathbf{v}(t - \delta t/2) \equiv \frac{\mathbf{r}(t) - \mathbf{r}(t - \delta t)}{\delta t} \tag{2.40}$$

and

$$\mathbf{v}(t + \delta t/2) \equiv \frac{\mathbf{r}(t) + \mathbf{r}(t + \delta t)}{\delta t}. \tag{2.41}$$

From equation (2.41) an expression for the new positions based on the old positions and velocities can immediately be obtained as

$$\mathbf{r}(t + \delta t) = \mathbf{r}(t) + \mathbf{v}(t + \delta t/2)\delta t. \tag{2.42}$$

Using Taylor series expansion on velocity about t , we get

$$\mathbf{v}(t + \delta t/2) = \mathbf{v}(t) + \delta t\frac{\mathbf{F}(t)}{2m}. \tag{2.43}$$

Again,

$$\mathbf{v}(t - \delta t/2) = \mathbf{v}(t) - \delta t\frac{\mathbf{F}(t)}{2m} \tag{2.44}$$

Subtracting equation (2.43) from equation (2.44) it is seen that

$$\mathbf{v}(t + \delta t/2) = \mathbf{v}(t - \delta t/2) + \delta t\frac{\mathbf{F}(t)}{m}. \tag{2.45}$$

Equation equation (2.45) gives the update of velocity based on new old velocity and force on the particle.

As the leapfrog algorithm is derived from the Verlet algorithm, it gives rise to identical trajectories. However, the velocities are not defined at the same time as the positions. As a consequence, kinetic and potential energy are also not defined at the same time, and hence total energy cannot be computed directly in the Leapfrog algorithm [16]. Figure 2.12 gives a schematic representation of the algorithm.

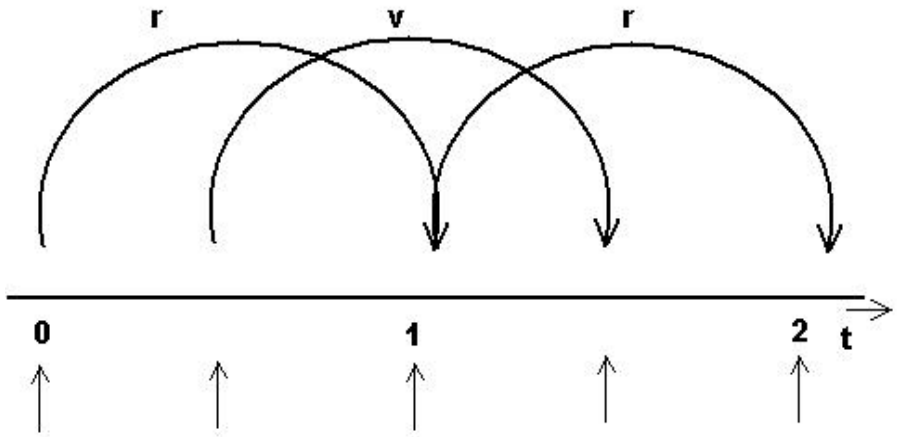

Figure 2.12: Schematic representation of Leapfrog algorithm. It is so called as **r** and **v** are leaping like frogs over back of each other [12].

2.3.6 Constraint Algorithm

The famous constraint algorithm used in MD is **SHAKE** algorithm. The internal constraints such as interatomic bonds, bond angles, proper dihedrals, improper dihedrals etc., are to be taken into account in polyatomic systems. That is, the equilibrium bond lengths, bond angles should remain unchanged throughout the simulation. For such systems, the standard Leap Frog method of calculation of new positions and velocities then may not be sufficient. Therefore, a set of independent generalized coordinates must be constructed to obey the constraint-free equations of motion. In these equations the constraints appear implicitly. In other words, **SHAKE** is a method that deals with Leapfrog algorithm with internal constraints [14].

SHAKE uses Cartesian coordinates for each of the atoms to describe the configuration of molecules with internal constraints. It is a procedure that approaches internal constraints by going through the constraints one by one, cyclically, adjusting the coordinates to satisfy each constraints in turn. The procedure is repeated until all constraints are satisfied to within a specified tolerance level [14].

Operationally, SHAKE algorithm changes a set of unconstrained coordinates $\mathbf{r}'$ to a set of coordinates $\mathbf{r}''$ that fulfill a list of distance constraints using a set $\mathbf{r}$ as reference. i.e.,

$$SHAKE(\mathbf{r}' \hookrightarrow \mathbf{r}''; \mathbf{r}). \tag{2.46}$$

This action is consistent with solving a set of Lagrange multipliers in the constrained equations of motion.

Let us assume that the equations of motion must fulfill N_c holonomic constraints expressed as

$$\sigma_k(\mathbf{r}_1.....\mathbf{r}_N) = 0; \qquad k = 1.....N_c \tag{2.47}$$

(e.g.$(\mathbf{r}_1 - \mathbf{r}_2)^2 - b^2 = 0$). Then the forces are defined as

$$-\frac{\partial}{\partial \mathbf{r}_i}(U + \sum_{k=1}^{N_c} \lambda_k \sigma_k) \tag{2.48}$$

where λ_k are Lagrange multipliers which must be solved to fulfill the constraint equations. The second part of this sum determines the constraint forces G_i which are defined as

$$G_i = -\sum_{k=1}^{N_c} \lambda_k \frac{\partial \sigma_k}{\partial \mathbf{r}_i}. \tag{2.49}$$

The displacement due to the constraint forces in the Leapfrog algorithm is equal to (G_i/m_i) $(\delta t)^2$. The solutions of a set of coupled equations of the second degree is required in solving the Lagrange multipliers and hence the displacements. These are solved iteratively by SHAKE within a specified tolerance level [12, 14].

2.3.7 Various Ensembles in Molecular Dynamics

Conventional MD differs from most experimental studies in that it is the energy and volume that are fixed, rather than temperature and pressure. In statistical mechanical terms, MD produces microcanonical (NVE) ensemble averages, whereas constant-temperature experiments correspond to the canonical (NVT) ensemble; if constant pressure is imposed as well, as is generally the case in the laboratory, it is the isothermalisobaric (NPT) ensemble that is the relevant one. It is assumed that by averaging over a sufficient number of time steps these time averages become approximate measures of the corresponding NVE ensemble averages (Ergodic hypothesis). While the choice of ensemble is usually one of convenience at the macroscopic level since (away from the critical point) thermal fluctuations are small, for the microscopic systems studied by MD the fluctuations of nonregulated quantities can be sufficiently large to make precise measurement difficult [17, 3]. A short description regarding constant temperature and constant pressure is presented in the next sections.

2.3.8 Temperature Calculation and Control

Temperature is defined in molecular dynamics simulations in the microcanonical ensemble (constant NVE) by making use of the equipartition principle which states that the average kinetic energy per degree of freedom is $k_B T/2$. Therefore, the instantaneous temperature of the system is defined as

$$T(t) = \frac{2}{(3N - Nc)k_B} \sum_{i}^{N} \frac{1}{2} m_i v_i^2(t). \tag{2.50}$$

Here N and N_c represent the number of particles and number of constraints on the system, respectively. m_i and k_B represent mass of the ith particle and Boltzmann's constant, respectively. The average temperature of the system is given by the time or ensemble average of the instantaneous temperature,i.e.,

$$T =< T(t) >=< \frac{2}{(3N - Nc)k_B} \sum_{i}^{N} \frac{1}{2} m_i v_i^2(t) > . \tag{2.51}$$

The initial velocities are generated according to the Maxwell-Boltzmann distribution at the desired temperature as mentioned in initialization. However, the velocity distribution does not remain constant as the simulation continues. The computed velocities need to be adjusted in order to maintain the correct temperature. Beside getting the temperature to the right target, it is also necessary to produce the correct statistical ensembles. So the temperature-control mechanism should be employed. The several methods have been developed for temperature control [16, 17].

2.3.8.1 Direct Velocity Rescaling

Any temperature drift is corrected periodically by velocity rescaling. This method involves rescaling of the velocities of each particle at each time step by a factor of $(T_{tar}/T_{cur})^{1/2}$ where T_{tar} is the desired thermodynamic temperature and T_{cur} is the current kinetic temperature. Even though this method transfers energy to or from the system very efficiently, ultimately the speed of this method depends on the potential energy expression, the parameters, the nature of the coupling between the vibrational, rotational, and translational modes, and the system size. It is because the fundamental limitation to achieving equilibrium is how rapidly energy can be transferred to or from among the various internal degrees of freedoms of the molecule [14].

2.3.8.2 Berendsen Scheme

Berendsen method is refined approach to velocity rescaling. In this method the deviation of the current temperature of the system, T_{cur} from the target thermodynamic temperature T_{tar} is slowly corrected according to

$$\frac{dT_{cur}}{dt} = \frac{T_{tar} - T_{cur}}{\tau}. \tag{2.52}$$

This indicates that a temperature deviation decays exponentially with a time constant τ . That is this method forces the system towards the desired temperature at a rate determined by τ, while only slightly perturbing the forces on each molecule [14, 12].

In this method each velocity is multiplied by a factor χ at each time step δt

$$\chi = [1 + \frac{\delta t}{\tau_c}[\frac{T_{tar}}{T_{cur} - 1}]]^{1/2} \tag{2.53}$$

where τ_c is the current time constant. It is close, but not exactly equal, to τ, i.e,

$$\tau = \frac{2C_v\tau_c}{N_{df}k_B} \tag{2.54}$$

where C_v is the total heat capacity of the system, k_B is Boltzmann constant, and $N_{df} = (3N - N_c)$ is the total number of degrees of freedom. The reason that $\tau \neq \tau_c$ is that the kinetic energy change caused by scaling the velocities is partly redistributed between kinetic and potential energy and hence the change in temperature is less than the scaling energy. In practice, the ratio τ/τ_c ranges from 1 (gas) to 2 (harmonic solid) to 3 (water). When the term temperature coupling time constant is used , it refers to the parameter τ_c. It should be noted that Berendsen method is stable up to $\tau_c \approx \delta t$ [12, 14].

2.3.8.3 Extended Ensemble Method: Nosé-Hoover Scheme

The Berendsen method is extremely efficient for relaxing a system to the target temperature T_{tar}. However, once the system has reached equilibrium it might be more important to probe a correct canonical ensemble. This is not the case for Berendsen method although the difference is usually negligible [12].

To enable canonical ensemble simulations, the extended-ensemble approach was first proposed by Nosé and later modified by Hoover . In this method the system Hamiltonian is extended by introducing a thermal reservoir, often called heat bath, and a friction term in the equations of motion. The friction force is proportional to the product of each particle's velocity and a friction parameter ξ. This friction parameter (or heat bath variable) is a fully dynamic quantity with its own equation of motion; the time derivative is calculated from the difference between the current kinetic energy and the kinetic energy associated with the target temperature [12, 14].

In Hoover's formulation, the particle's equations of motion equation (2.22) are replaced by

$$\frac{d^2 r_i}{dt^2} = \frac{F_i}{m_i} - \xi \frac{dr_i}{dt}, \tag{2.55}$$

where the equation of motion for the heat bath parameter ξ is

$$\frac{d\xi}{dt} = \frac{1}{Q}(T_{cur} - T_{tar}). \tag{2.56}$$

The strength of the coupling is determined by the constant Q, usually called the mass parameter of the reservoir, in combination with the target temperature. To maintain the coupling strength, Q would have to be changed in proportion to the change in reference temperature. For this reason, it is preferable to use τ_c which is the period of the oscillations of kinetic energy between the system and the reservoir. It is directly related to Q and T_{tar} via

$$Q = \frac{\tau_c^2 T_{tar}}{4\pi^2}. \tag{2.57}$$

A much more intuitive way of selecting the Nosé-Hoover coupling strength similar to the Berendsen method is provided by this relation. Moreover, τ_c is independent of system size and reference temperature [12].

2.3.9 Pressure Calculation and Control

Most experiments are performed at constant pressure instead of constant volume. If one is interested in simulating the effect of, for example, the composition of the solvent on the properties of a system one has to ensure that the pressure remains constant. For that the volume of the system is adjusted. Thus, for such a system it is much more convenient to simulate at constant pressure [16]. Pressure is a tensor which can be defined by means of a 3×3 square matrix as

$$P = \begin{bmatrix} P_{xx} & P_{xy} & P_{xz} \\ P_{yx} & P_{yy} & P_{yz} \\ P_{zx} & P_{zy} & P_{zz} \end{bmatrix}. \tag{2.58}$$

Each element of the pressure tensor is the force acting on the surface of an infinitesimal cubic volume that has edges parallel to the x, y, and z axes. The first subscript denotes the normal direction to the plane on which the force acts, and the second one denotes the direction of that force [14].

Pressure is contributed by two components. They are

- the momentum carried by the particles as they cross the surface area and
- the momentum transferred as a result of forces between interacting particles that lie on different sides of the surface.

Hence P can be expressed as

$$P = \frac{1}{V}[\sum_{i}^{N} m_i \mathbf{v}_i.\mathbf{v}_i + \sum_{i}^{N} \mathbf{r}_i.\mathbf{f}_i] \tag{2.59}$$

where $\mathbf{r}_i$, $\mathbf{v}_i$ and $\mathbf{f}_i$ indicate the x, y, or z components of position, velocity, and force vector of the i^th particle, respectively. In an isotropic situation, the pressure tensor is diagonal with P_{xx}, P_{yy} and P_{zz} equal. The instantaneous pressure is calculated as [14]

$$P = \frac{1}{3}[P_{xx} + P_{yy} + P_{zz}]. \tag{2.60}$$

There are several different but equivalent ways to measure the pressure of a classical N-body system. The most common among these is based on the virial equation for the pressure. The scalar virial equation for pressure for pairwise additive interactions at constant temperature T is

$$P = \rho k_B T + \frac{1}{3V} < \sum_{i<j} \mathbf{f}(\mathbf{r}_{ij}).\mathbf{r}_{ij} > . \tag{2.61}$$

Here $\mathbf{f}(\mathbf{r}_{ij})$ is the force between particles i and j at a distance $\mathbf{r}_{ij}$ [17].

If the isothermal-isobaric system is desired for simulation, the pressure of the system must remain constant at some value. This can be achieved by coupling the system to a pressure bath or barostat [12, 14]. There are several methods for this purpose.

2.3.9.1 Berendsen Scheme

The Berendsen Scheme corrects the deviation of the current pressure $\mathbf{P}_{cur}$ of the system from the target pressure $\mathbf{P}_{tar}$ according to

$$\frac{d\mathbf{P}_{cur}}{dt} = \frac{\mathbf{P}_{tar} - \mathbf{P}_{cur}}{\tau_p}. \tag{2.62}$$

This indicates that a pressure deviation decays exponentially with a time constant τ_p.

The Berendsen scheme rescales the coordinates and box vectors every step with a matrix μ, which has the effect of a first-order kinetic relaxation of the pressure towards a given reference pressure or target pressure. This scaling matrix μ is given by:

$$\mu_{ij} = \delta_{ij} - \frac{\Delta t}{3\tau_p}\beta_{ij}[(P_{tar})_{ij} - (P_{cur})_{ij}(t)]. \tag{2.63}$$

Here β is the isothermal compressibility of the system. In most cases, μ will be a diagonal matrix, with equal elements on the diagonal, the value of which is generally not known. It suffices to take a rough estimate because the value of β only influences the non-critical time constant of the pressure relaxation without affecting the average pressure itself [12].

2.3.9.2 Parrinello-Rahman Scheme

In cases where the fluctuations in pressure or volume are important (e.g. to calculate thermodynamic properties) it might be a problem that the exact ensemble is not well defined for the weak coupling scheme of Berendsen [12]. The Parrinello-Rahman method of pressure coupling is an extended-ensemble approach, which is similar to the Nosé-Hoover temperature coupling. With the Parrinello-Rahman barostat, the box vectors are represented by the matrix $\mathbf{b}$, and they obey the matrix equation of motion

$$\frac{d\mathbf{b}^2}{dt^2} = V\mathbf{W}^{-1}\mathbf{b}'^{-1}(\mathbf{P}_{cur} - \mathbf{P}_{tar}). \tag{2.64}$$

Here V denotes the volume of the box, and $\mathbf{W}$ is a matrix parameter that determines the strength of the coupling. The matrices $\mathbf{P}_{cur}$ and $\mathbf{P}_{tar}$ are the current and the target pressures respectively.

The equations of motion for the particles are also changed, just as for the Nosé-Hoover coupling. In most cases one would combine the Parrinello-Rahman barostat with the Nosé-Hoover thermostat. The equations of motion are

$$\frac{d^2\mathbf{r}_i}{dt^2} = \frac{\mathbf{F}_i}{m_i} - \mathbf{M}\frac{\mathbf{r}_i}{dt} \tag{2.65}$$

with

$$\mathbf{M} = \mathbf{b}^{-1}[\mathbf{b}\frac{d\mathbf{b}'}{dt} + \frac{d\mathbf{b}}{dt}\mathbf{b}']\mathbf{b}'^{-1}. \tag{2.66}$$

The inverse matrix $\mathbf{W}^{-1}$ is related to the τ_p as

$$(W_{ij})^{-1} = \frac{4\pi^2 \beta_{ij}}{3\tau_p^2 L}. \tag{2.67}$$

Just as for the Nosé-Hoover thermostat, the Parrinello-Rahman time constant is not equivalent to the relaxation time used in the Berendsen pressure coupling algorithm. In most cases it is needed to use a 4-5 times larger time constant with Parrinello-Rahman coupling. If the current pressure is very far from equilibrium, the Parrinello-Rahman coupling may result in very large box oscillations that could even crash the simulation run. In that case, one would have to increase the time constant, or better use the weak coupling scheme to reach the target pressure, and then switch to Parrinello-Rahman coupling once the system is in equilibrium [12].

2.3.10 Different Software Packages for Molecular Dynamics

There are different packages for the MD simulations and all of them have their own features, merits and demerits. These features may not be sufficient to fulfill all the needs of the simulation problem. Here is a brief introduction to three of the most popular molecular dynamics packages:

- GROMACS (Groningen Machine for Chemical Simulations),
- AMBER (Assisted Model Building and Energy Refinement system),
- CHARMM (Chemistry at Harvard Macromolecular Mechanics).

2.3.11 GROMACS

GROMACS (Groningen Machine for Chemical Simulation) was originally developed by Department of Biophysical Chemistry at Groningen University in the Netherlands. It is a versatile package that performs molecular dynamics simulations and energy minimization [12]. It is primarily designed for biochemical molecules like proteins and lipids that have many complicated bonded interactions, but since it is extremely fast at calculating the non-bonded interactions (that usually dominate simulations)many groups are also using it for research on non-biological systems, for example polymers, gases, liquids and so on.

GROMACS contains a script to convert molecular coordinates from a PDB file into the formats it uses internally. Once a configuration file for the simulation has been created, the actual simulation run produce a trajectory file, describing the movements of the atoms over time. The trajectory file can then be analyzed or visualized with a number of supplied tools [12]. The main features of GROMACS are as described below.

1. **User-Friendly**: GROMACS is user-friendly, with topologies, parameter files, and error messages written in clear text format. There is a lot of consistency checking, but no scripting language; all programs use a simple interface with command line options for input and output files. Help files can be accessed through GROMACS directly or via the extensive user manual available for free. When simulations are running, GROMACS can output its progress, giving details of the time and date it expects to finish [14].

2. **High Compatibility**: GROMACS does not have a force field of its own, but it is compatible with GROMOS, OPLS, AMBER, and ENCAD force fields. Interfaces with popular quantum-chemical packages such as MOPAC, GAMESUK, and GAUSSIAN are provided to perform mixed MM/QM simulations [14].

3. **Versatility**: The aim of GROMACS is to provide a versatile and efficient MD program with source code, especially directed towards the simulation of biological macromolecules in aqueous and membrane environments. It is able to run on single processors as well as on parallel using standard message passing interface (MPI) communication. It provides not only microcanonical Hamiltonian mechanics, but also stochastic dynamics (SD) including Langevin and Brownian dynamics and energy minimization(EM) [14].

4. **Fastest and Flexible Software**: The highly optimized code makes GROMACS the fastest software for molecular simulations to date. It is faster in calculating the non-bonded interactions which is dominant in any simulation. Besides, the support of different force fields and the open source (GPL) character make GROMACS very flexible [14].

5. **Freeware**: Unlike AMBER and CHARMM, GROMACS is freely available and can be downloaded from the Internet easily and compiled on any linux-based operating system. It is available from http://www.gromacs.org for free under the Groningen University General Public Licence [14].

It is due to these features that GROMACS has been widely used throughout the world including us for this study.

2.3.12 Limitations of Molecular Dynamics

Molecular dynamics simulations have certain limitations and it is essential to know these limitations so that the simulation is performed accurately. Because of those limitations it is advised to perform checks on known experimental properties to assess the accuracy of the simulation[12]. These limitations are described below.

- The simulations are classical. This implies that the motion of atoms are described by classical mechanics. This scheme is acceptable at normal temperatures. However, there are exceptions like motion of light hydrogen atoms, tunnelling of proton,Helium liquid at low temperature,the high frequency vibrations of covalent bonds etc where the classical mechanics fails and requires quantum mechanical treatment.

- MD approximates that electrons are in the ground state. This is another limitation of Molecular dynamics because electron transfer processes and electronically excited states can not be treated. Actually, MD use a conservative force field that is the function of positions of atoms only. This means that the electronic motions are not considered: the electrons are supposed to adjust their dynamics instantly when the atomic positions change (the Born-Oppenheimer approximation), and remain in their ground state.

- Another limitation of MD simulations is that the force fields that are used to provide the forces are approximate. As knowledge improves these parameters can be modified to improve accuracy.

- As a final limitation, the boundary conditions in MD are unnatural. To simulate a bulk system, the unwanted boundary created by a cluster of particles of a small size system with its environment must be avoided.

Although these limitations are encountered time and again during simulations, different simulation softwares like GROMACS have been improved to solve the problems tactfully. Molecular dynamics, therefore, will be an eminent revolutionary aspect of research and development of molecular science [12].

Chapter 3

Details of Simulation

3.1 Details of Simulation

This section comprises of the detail explanation of the simulation of the system under study. The generalized description of all the steps, previously discussed in chapter 2 in the section of theory of molecular dynamics, is strictly followed in this section. Besides, the description of modelling of an argon atom and the method to specify the force fields have been presented. Also explained is the way a water molecule is modelled and the process of creation of multiple number of water molecules. The queries regarding the creation of simulation box and the application of the periodic boundary conditions is well resolved in this section. As our system consists of argon atoms in water, the details regarding the mixing of argon atoms in water is also illustrated. The process of energy minimization, its necessity and how is it accomplished in simulation is sorted out in this section. We also describe the methods used to equilibrate the system under study at a particular temperature and pressure. Moreover, we explain how we prepared the final system for the production simulation that yield the phase space trajectory which is essential to derive the diffusion coefficient of argon in water. As indicated in the previous chapters, it is by far quite obvious why we preferred Groningen Machine for Chemical Simulations (GROMACS) for our study. Thus, in this chapter our explanation of different steps of molecular dynamics simulation is very much pertinent with GROMACS.

3.1.1 Modelling Argon

Argon is monoatomic, so the contributions from bond, bond angle, dihedral angle and improper dihedral angle are all zero and we do not need to consider them in our model. In other words, it is quite obvious to ignore the bonded interactions in case of monoatomic elements. But, it is of utmost importance to include the interactions between argon atoms if a system contains more than one argon atom. These interactions are non-bonded and in our model, the non-bonded interaction between two argon atoms have been approximated by Lennard-Jones potential

$$U_{AR-AR}(r_{ij}) = 4\epsilon_1[(\frac{\sigma_1}{r_{ij}})^{12} - (\frac{\sigma_1}{r_{ij}})^6]. \tag{3.1}$$

In equation (3.1), r_{ij} is the distance between two argon atoms i and j, $2^{1/6}\sigma_1$ is the equilibrium distance between two argon atoms also called van der Waal's radius, and ϵ_1 is the minimum energy depth which measures the strength of the interaction [12].

As argon atoms do not have any partial charge, the Coulomb interaction between argon atoms does not occur. Thus, the Coulomb interaction is excluded in our model of argon.

The argon model is prepared by using the GROMACS file architecture. A model is designed by adding an atom and its relevant parameters to an atomic parameter file named $ffG43a1.atp$. Here $ffG43a1$ represents the force field we have chosen for our system, which will be explained in the following sections. The extension *.atp* stands for *atom type parameter*. In the file $ffG43a1.atp$ the type of atom and its mass is listed as

AR 39.94800.

Here AR stands for the name of the argon atom, and 39.94800 is its mass in atomic mass unit (a.m.u.). After listing all the information in *.atp* file, the next step is to enter the information regarding argon atom in the file named $ffG43a1.rtp$ where the extension *.rtp* stands for *residue type parameter*. The atom is taken as residue in GROMACS and the parameters for an argon atom residue are entered in the following way.

[**AR**]

[**atoms**]

Name	Type	Charge	Chargegroup
AR	AR	0	0

where [AR] stands for the residue name for argon atom. The section [atoms] contains information about the atoms in the residue. So, in this section AR stand for argon atom type. The argon being neutral have zero charge and belong to zero charge group. For the non-bonded interaction between two argon atoms, GROMACS does not take the values of σ and ϵ directly for the Lennard-Jones interaction stated in (3.1). Rather, it takes the modified form of equation (3.2) defined as

$$U_{AR-AR}(r_{ij}) = \frac{C_{12}^1}{r_{ij}^{12}} - \frac{C_6^1}{r_{ij}^6}, \tag{3.2}$$

where the parameter C_{12}^1=$4\epsilon_1\sigma_1^{12}$ and the parameter C_6^1=$4\epsilon_1\sigma_1^6$ [12]. The values of these parameters for argon are specified in the topology of GROMACS software and are given in table 3.1 . The parameters for the non bonded interactions , C_{12}^1 and C_6^1, is to be entered in the file *ffG43a1nb.itp* as follows:

[**atomtypes**]

name	mass	charge	ptype	C_6	C_{12}
AR	39.94800	0.000	A	0.0062647225	9.8470440E-06

Parameters	Values
C_{12}^1	9.847044×10^{-6} kJmol^{-1}nm^{12}
C_6^1	6.2647225×10^{-3} kJmol^{-1}nm^6

Table 3.1: L-J Parameters for *AR*

where *name* represents the name of the atom entered in ffG43a1.atp file. The mass of AR is 39.94800 a.m.u. and charge is zero. It is a particle of type A as understood by GROMACS. C_6 and C_{12} are the parameters defined in (3.3).

[**nonbond-params**]

i	j	func	C_6	C_{12}
AR	AR	1	0.0062647225	9.847044E-06

where i and j stands for the argon atoms of the system. The parameter *func* defines the interaction potential. In our case, the force field *ffG43a1* uses numeral 1 for the specification of Lennard-Jones potential. The Lennard-Jones curve for the argon-argon (AR-AR) interaction with the above mentioned parameters is shown in the figure 3.1 below.

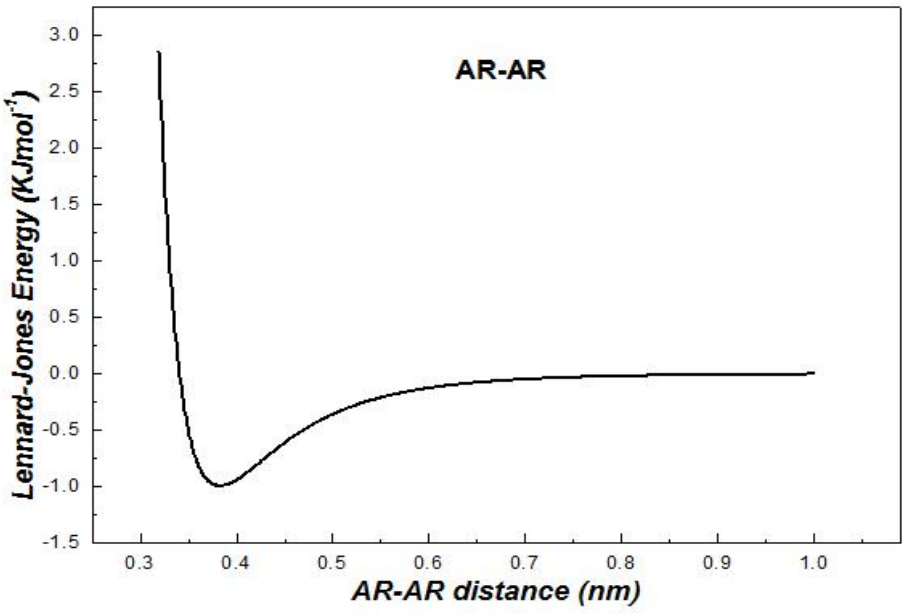

Figure 3.1: Lennard-Jones interaction energy between two argon atoms as a function of their separation. The equilibrium distance is 0.3833nm.

After defining the non-bonded pair interactions parameters in the topology of the GROMACS , the next step in the modelling of argon atom is to create basic files needed for

the simulation. The first file that we need to create is the initial structure file of the argon atoms. This file is created in the Protein Data Bank (PDB) format. The sample entries in the file *ar.pdb* for a single argon atom are stated below [18].

```
MODEL        1
ATOM      1      AR      AR      1      8.750   0.000   0.000   1.00   0.00

ENDMDL
```

The *MODEL* in the first row and first column stands for the model of given argon atom. The number 1 in the first row and second column indicates the model sequence number. The keyword *ATOM* in the second row and first column represents the record which presents atomic coordinates, occupancy, and temperature factor for each atom. The numbers 1 in the second column is atom serial number. The keyword in the third column represents the name of the argon atom that has been defined in the *ffG43a1.atp* file. The keyword *AR* in the fourth column is the name of the residue (atom) followed by the number 1 in the fifth column called the residue sequence number. The real numbers in the sixth, seventh, and eighth column represent x, y, and z coordinates for each atom in Angstrom (Å). The number 1 in the ninth column represents occupancy, and the number in the tenth column represents temperature factor which is by default zero [14].

GROMACS accepts initial structure file **.pdb*, and can convert them to the GROMACS native format, with the use of the ***pdb2gmx*** command. ***pdb2gmx*** takes the .pdb file, and outputs two files. The x-y-z co-ordinates of the atoms are stored in a *.gro* file, and the atomic masses, charges, and bonds are stored in a *.top* file. In our model, this program took *ar.pdb* as input and produced GROMACS structure file *ar.gro* and GROMACS topology file *ar.top*. In this case *ar.top* is self designed. Contents of the file *ar.gro* are as presented below.

```
5
1AR      AR      1      0.875      0.000      0
2AR      AR      2      0.124      0.000      0
.....................................................................................
```

There is a change in the contents of the file *ar.gro* and *ar.pdb*. The number 5 in the first line denotes the number of atoms in system. The values of coordinates is changed from Angstrom (Å) to nanometer (nm).

The contents of the file *ar.top* is shown below.

```
Include force-field parameters
#include ffG43a1.itp
Include water topology file
#include spce.itp

[moleculetype]
molname       nrexcl
AR

[atoms]
nr      type      resnr      residue      atom      cgnr      charge      mass
1       AR         1         AR       AR        0         0         39.94800

[system]
Argon in water

[molecules]
AR        1
SOL         212
```

The term *nrexcl* represents the number of exclusions for the argon atoms. The exclusions are the atoms **i+1**, **i+2**, etc, that do not have non-bonded interaction such as Lennard-Jones with the atom **i** [12].
In this way argon is modelled in the GROMACS package which constitute a vital part of our system.

3.1.2 Modelling Water

There are different molecular models for water which have been developed in order to help discover the structure of water. If the model can successfully predict the physical properties of liquid water such as self diffusion coefficient, viscosity etc. then the structure of liquid water is determined. Various parameters required for modelling are geometry, electric charge, and Lennard-Jones parameters. A recent review listed 46 distinct models, so indirectly indicating their lack of success in quantitatively reproducing the properties of real water. They may, however, offer useful insight into water's behavior [19]. Some of the frequently used models are; Simple Point Charge(SPC)[20], SPC/E (Simple Point Charge-Extended)[21], TIP3P (Transferable Intermolecular Potential 3P)[**?**], TIP4P (Transferable Intermolecular Potential 4P) [23], and TIP5P (Transferable Intermolecular Potential 5P)[24]. A number of these models use water molecules with a wider (more tetrahedral) H-O-H angle and longer H-O bond length than those expected of gaseous or liquid water and indicative of the importance of including parameters giving strong hydrogen bonding. Water molecules in liquid water are all non-equivalent (differing in their molecular orbital, their precise geometry and molecular vibrations) due to their hydrogen bonding status, which is influenced by the arrangement of the surrounding water molecules. Some models are polarizable to make some

allowance for this whereas other simpler models try to reproduce 'average' structures [25].

We have used SPC/E model in our study. This model is an extension to SPC model developed in 1987 [21]. The specific force field for this model is GROMOS and can be adopted to other force fields as well. It is a planar model which consists of a three point charge on each atomic site. Two out of three are located at hydrogen atom sites and one in oxygen atom. Each hydrogen atom carries a partial charge of +0.4238e, and the oxygen atom carries a charge of -0.8476e where e is the elementary charge having magnitude 1.6022×10^{-19} Coulomb. The values for σ and ε are $3.166(\mathrm{A}^o)$ and $0.650 KJmol^{-1}$ respectively same as that of SPC model [25].

3.1.2.1 Intramolecular Potential Parameters

The intramolecular potential parameters of the water model depends on the geometry of the model. From the perspective of geometry, there are three types of models:

1. rigid models,
2. flexible models,and
3. polarizable models.

In the rigid models, the geometry of the water molecule is fixed which means the distance between hydrogen atom and oxygen atom and bond angle HOH don't change in time. Therefore, the configurational parameters are positions and velocities of each atomic site only. Flexible water models include bond stretching and angle bending. Polarizable water models includes an explicit polarization term, which should enhance the ability to reproduce water in different phases and the interaction between them[26]. In flexible SPC/E model the intramolecular potential consists of harmonic bond and angle vibration terms defined as

$$U_{OH}(r) = \frac{1}{2}\sum K_{OH}(r - b_{0H})^2 \tag{3.3}$$

and

$$U_{OH}(\Theta) = \frac{1}{2}\sum K_{HOH}(\Theta - \Theta_0)^2. \tag{3.4}$$

Here K_{OH} is spring constant which measures the strength of interatomic bond between oxygen and hydrogen atom; b_{0H} is the bond length between oxygen and hydrogen atoms. Similarly K_{HOH} is spring constant for bond-angle vibration with Θ_0 as the equilibrium HOH bond angle. The parameters that are used for our study are listed in table 3.2 [12].
These parameters are present in the file name spce.itp inherent in GROMACS.

3.1.2.2 Intermolecular Potential Parameters

The intermolecular interaction indicates the non bonded interaction between water molecules. In this section we discuss different types of interactions that take place among the water molecules and the parameters thus involved. The intermolecular interaction potential between two SPC/E water molecules can be discussed in following two headings [14].

Parameters	Values
K_{OH}	3.45× 10^5 kJmol^{-1}nm^{-2}
b_{OH}	0.1 nm
K_{HOH}	3.83× 10^2 kJmol^{-1}rad^{-2}
Θ_0	109.47 deg

Table 3.2: Intramolecular potential parameters for flexible SPC/E water.

1. Lennard-Jones Potential and
2. Coulomb interaction.

The Lennard-Jones potential between the two SPC/E water molecules can be expressed as:

$$U_{WW}(r_{ij}) = 4\epsilon_2[(\frac{\sigma_2}{r_{ij}})^{12} - (\frac{\sigma_2}{r_{ij}})^6], \tag{3.5}$$

where r_{ij} is the distance between two oxygen atoms i and j of two different water molecules, $2^{1/6}\sigma_2$ is the equilibrium distance between the two oxygen atoms also called van der Waal's radius and ϵ_2 is the minimum energy depth which measures the strength of the interaction.

As stated in chapter 2, GROMACS takes the modified form of equation (3.5) given as:

$$U_{WW}(r_{ij}) = \frac{C_{12}^2}{r_{ij}^{12}} - \frac{C_6^2}{r_{ij}^6}, \tag{3.6}$$

where the parameter C_{12}^2=$4\epsilon_2\sigma_2^{12}$ and the parameter C_6^2=$4\epsilon_2\sigma_2^6$. In this work, the values of these parameters are taken as follows [12]: These L-J parameters are entered in the file

Parameters	Values
σ_2	0.316565 nm
ϵ_2	78.197 k_B
C_{12}^2	2.634129e-06 kJmol^{-1}nm^{12}
C_6^2	2.6173456e-03 kJmol^{-1}nm^6

Table 3.3: L-J Parameters for SPC/E water.

ffG43a1nb.itp as the case of argon atom.

[**atomtypes**]

name	mass	charge	ptype	C6	C12
OW	15.99940	-0.82e	A	0.26171e-02	0.26331e-05
HW	1.00800	+0.41e	A	0.00000e+00	0.00000e+00

[**nonbonded-params**]

i	j	func	C6	C12
OW	OW	1	0.26171e-02	0.26331e-05

OW HW 1 0.00000e+00 0.00E+00

Here, OW stands for water oxygen and HW for water hydrogen. Particle type A indicates that both of these are treated as atomic particles by GROMACS [12]. Function 1 stands for Lennard-Jones interaction. A graph of L-J interaction energy as a function of intermolecular distance of water is shown in figure 3.2.

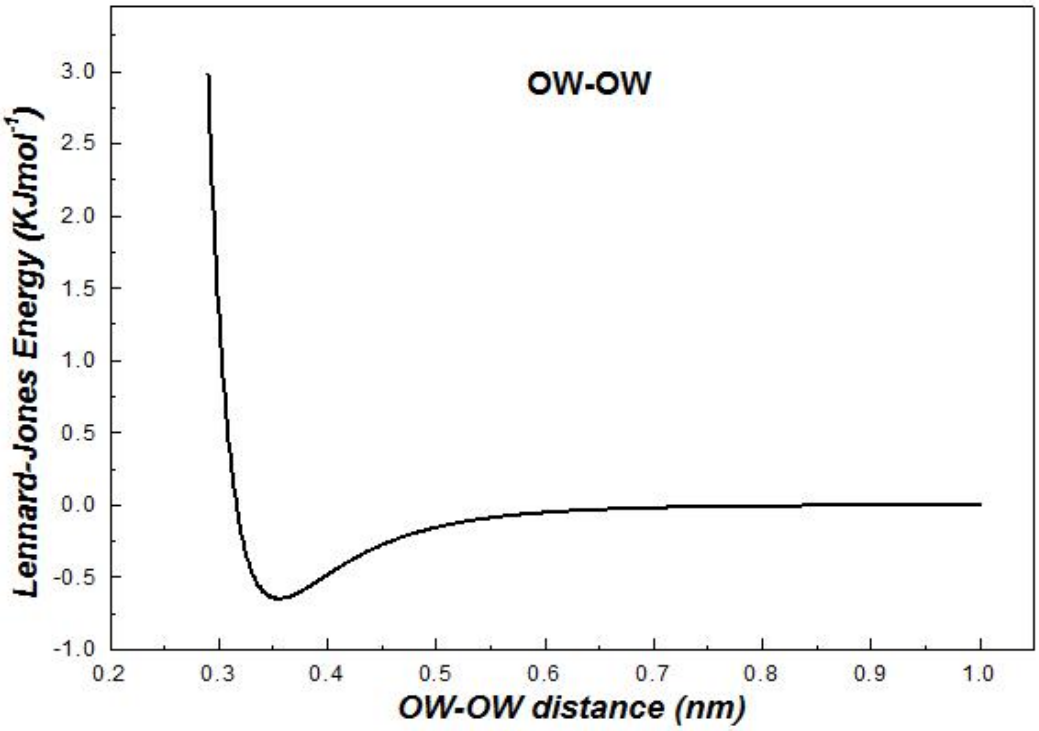

Figure 3.2: Lennard-Jones interaction energy between two oxygen atoms of SPC/E water as a function of their separation. The equilibrium distance is 0.355 nm.

The non-bonded interaction comprises of Coulomb interaction between oxygen and hydrogen atoms of two different water molecules as well. This is because there is a partial charge -0.8476+e in oxygen and 0.4238 in hydrogen atoms. The Coulomb interaction is expressed as

$$U_C = \sum_{\alpha=1}^{3}\sum_{\beta=1}^{3} \frac{q_i^\alpha q_j^\beta}{4\pi\epsilon_0 r_{ij}^{\alpha\beta}}. \tag{3.7}$$

Here, q_i^α and q_i^β are the charges at sites α and β in the molecule i, respectively; $r_{ij}^{\alpha\beta}$ is the distance between site α in molecule i and site β in molecule j; ϵ_0 is the permittivity of vacuum.

As our system contains argon in water,the inter-molecular interaction also consists of the interaction between argon atoms and water molecules. This interaction occurs due to the interaction between the argon atom and oxygen of water. We have not considered any form of interaction with hydrogen of water because hydrogen has very low values for sigma and epsilon and its partial charge is also zero. Also the interaction between argon and oxygen of water cannot be Coulomb interaction because the argon atom is neutral with no partial charge eventhough the water oxygen atom contains a partial charge of -0.8476e. The only interaction occuring is Lennard-Jones interaction which can be stated as

$$U_{AR-W}(r_{ij}) = 4\epsilon[(\frac{\sigma}{r_{ij}})^{12} - (\frac{\sigma}{r_{ij}})^{6}], \tag{3.8}$$

where

$$\epsilon = (\epsilon_1\epsilon_2)^{1/2} \tag{3.9}$$

and

$$\sigma = \frac{1}{2}(\sigma_1 + \sigma_2) \tag{3.10}$$

according to Lorentz-Berthelot combining rule [12, 14]. As usual for GROMACS equation (3.8) gets modified to

$$U_{AR-W}(r_{ij}) = \frac{C_{12}}{r_{ij}^{12}} - \frac{C_6}{r_{ij}^{6}} \tag{3.11}$$

where the parameter C_{12}=$4\epsilon\sigma^{12}$ and the parameter C_6=$4\epsilon\sigma^6$. The values of these parameters for this case in enlisted in the file *ffG43a1nb.itp* of GROMACS software. For simplicity these values are shown in the table 3.4.

Parameters	Values
C_{12}	$4.84507\times10^{-6}\ kJmol^{-1}nm^{12}$
C_6	$4.0493\times10^{-3}\ kJmol^{-1}nm^{6}$

Table 3.4: L-J parameters for argon and SPC/E water interaction.

A sample of how these parameters are entered in the file *ffG43a1nb.itp* is shown below.

[nonbonded-params]

i	j	func	C6	C12
AR	OW	1	4.4049314e-03	9.847E-06
OW	HW	1	0.000000e+00	0.000000e+00.

The L-J interaction curve with the above mentioned parameters is shown in figure 3.3.

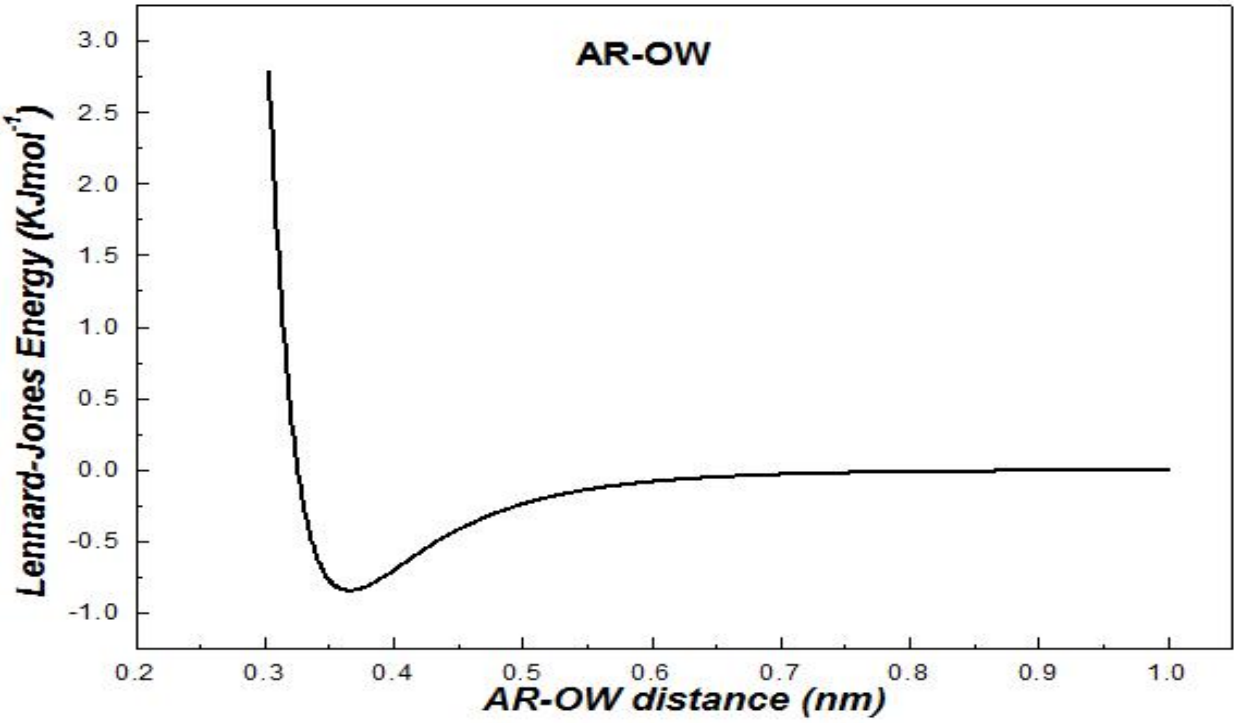

Figure 3.3: Lennard-Jones interaction energy between argon and water-oxygen as a function of distance between them. The equilibrium distance is 0.365 nm

This concludes the task of modelling of the system under study. The details of remaining parts of the simulation is presented in the following sections.

3.1.3 Simulation Cell and Periodic Boundary Conditions

In GROMACS simulation cell or the box was created using the program ***editconf***. The *editconf* converts generic structure format to *.gro* or *.pdb*. The box can be modified with options $-box$,$-d$ and $-angles$. Option -bt determines the box type: triclinic is a triclinic box, cubic is a rectangular box with all sides equal and so on. Option -box requires only one value for a cubic box [man editconf.

We selected a cubical simulation box for our system with all the specifications as given below in Table 3.5.

Box type	Box vectors			Box vector angles			Box volume
	a	**b**	**c**	∠**ab**	∠**bc**	∠**ca**	
Cubic	1.86206 nm	1.86206 nm	1.86206 nm	90°	90°	90°	6.45626 nm^3

Table 3.5: Parameters for cubical simulation box

In the table, ∠**ab** means angle between the box vectors **a** and **b** and so on. The file ar.gro was provided as input and a structure file *b4em.gro* is obtained as an output. The contents of *b4em.gro* are as follows.

```
5
1AR      AR      1      1.456      1.061      0.796
2AR      AR      2      0.581      1.061      1.133
..... .....
1.86206      1.86206      1.86206
```

The contents of this file are modified than that of *ar.gro*. It is that the values of x, y, and z coordinates have changed, and the last line shows the dimensions of the simulation box. All the other information remain unchanged. Moreover, ***editconf*** applies the periodic boundary conditions by default. With these boundary conditions only one, the nearest, image of each particle is considered for short-range non-bonded interaction terms [12].

3.1.4 Solvation of Argon

By far a simulation box is created which contains 5 argon atoms. The we have to add water molecules in the box or in other words solvate the solute configuration. This solvation process is carried out by the program ***genbox*** inherent in GROMACS [see man genbox] [12].

The default solvent is Simple Point Charge water (SPC), with coordinates from *spc*216.*gro*. The program ***genbox*** takes the files *b4em.gro*, which is the output file of the program ***editconf***, and *spc*216.*gro* as input and produces $afgen.gro$ as the output file. File *spc*216.*gro* is a coordinate file for SPC water molecules (also can be considered as a coordinate file of SPC/E because there is no difference in the structure of SPC AND SPC/E), which is present in the GROMACS package. This structure file contains 216 water molecules. But, it should be noted that some solvent molecules are removed from the box where the distance between any atom of the solute and any atom of the solvent molecule is less than the sum of the van

der Waals radii of both atoms. So in the system under study the output structure file contains 212 water molecules with 5 argon atoms [man genbox] [12]. The output file $afgen.gro$ is also a structure file in GROMACS format. The contents of a section of this output file are presented as follows:

```
641
1AR      AR      1      1.456      1.061      0.796
2AR      AR      2      0.581      1.061      1.133
.....................................................................
.....................................................................
6SOL       OW      6      0.230      0.628      0.113
7SOL      HW1      7      0.137      0.626      0.150
8SOL      HW2      8      0.231      0.589      0.021
.....................................................................
.....................................................................
217SOL     OW     639      0.875      1.646      0.337
217SOL     HW1    640      0.798      1.611      0.283
217SOL     HW2    641      0.843      1.717      0.399
1.86206     1.86206     1.86206
```

It is clearly observed that the contents are similar to that of the $b4em.gro$. Here 641 indicates the total number of atoms including that of argon and water molecules. Each atom associated with the water molecule is assigned respective x, y, and z coordinates in nanometer scale [12].

3.1.5 Energy Minimization

Macroscopic properties are always ensemble averages over a representative statistical ensemble (either equilibrium or non-equilibrium) of molecular system. Eventhough MD can generate equilibrium as well as non- equilibrium ensemble, the initial configuration can't be far from equilibrium as this leads to the failure of entire MD. The starting non-equilibrium configuration may arise due to bad van der Waals contacts between atoms when the are too close. To bring system into equilibrium, energy minimization is required. Another reason to perform an energy minimization is the removal of all kinetic energy from the system [12]. Thus energy minimization brings the system in a stable potential energy condition.
In a large number of dimensions the potential energy function of a (macro)molecular system is a very complex landscape. It has large number of points where all derivatives of the potential energy function with respect to the coordinates are zero and all second derivatives are nonnegative. These points are the minimum energy points. The deepest point among them is called *global minimum* while others are called *local minima*. In GROMACS, the energy minimization can bring the system only to its one of these nearest local minima and cannot reach the global minimum. In GROMACS energy minimization is done using following two algorithms [12].

1. Steepest-descent algorithm,

2. Conjugate gradient algorithm.

We have used steepest descent algorithm for our system. Therefore, it is described in detail in the following subsection.

3.1.5.1 Steepest-Descent Algorithm

Steepest descent algorithm for minimization takes a step in the direction of the negative gradient (hence in the direction of the force), without any consideration of the history built up in previous steps. The step size is adjusted such that the search is fast but the motion is always downhill. This is not the most efficient algorithm as its convergence can be quite slow, especially in the vicinity of the local minimum. However, it is robust and easy to implement [12].

Here, a vector **r** representing all *3N* coordinates is defined. Initially a maximum displacement h_0 must be provided. The forces **F**and potential energy are calculated first. The new positions are calculated using

$$\mathbf{r}_{n+1} = \mathbf{r}_n + \frac{\mathbf{F}_n}{\max(F_n)} h_n \tag{3.12}$$

where h_n is the maximum displacement, $\mathbf{F}_n$ is the force or the negative gradient of the potential energy function V, and $\max(F_n)$is the largest of the absolute values of the force components. The forces and energies are again calculated for the new positions with the conditions
If($V_{n+1} < V_n$),then the new positions are accepted and $h_{n+1} = 1.2h_n$.
If($\mathrm{V}_{n+1} \geq \mathrm{V}_n$), then the new positions ar rejected and $h_n = 0.2h_n$.
This algorithm stops when either a user-specified number of force evaluations have been performed or when $\max(F_n)$ is smaller than a specified value ϵ [12].

GROMACS uses two programs namely ***grompp*** and ***mdrun*** for energy minimization. The gromacs preprocessor, ***grompp***, reads a molecular topology file, checks the validity of the file, expands the topology from a molecular description to an atomic description. Then a coordinate file, $afgen.gro$, is read and velocities can be generated from a Maxwellian distribution if requested. It also reads parameters for the mdrun (eg. number of MD steps, time step, cut-off), and others such as NEMD parameters, which are corrected so that the net acceleration is zero. Eventually a binary file, $afem.tpr$, is produced that can serve as the sole input file for the MD program. Also a structure file $afgen.gro$, is obtained as output file. *em.mdp* is a grompp input with MD parameters. Its contents are presented below.
These parameters indicate that GROMACS uses flexible SPC/E water for energy minimization and the system is not coupled with any thermostat or barostat.

The input topology file used by *grompp* is *ar.top*. It contains directives which include the force field parameters, molecule topology file, and SPC/E water topology. Also, it contains information about the system and the number and types of molecules in the system which is already described in modelling argon.

```
;       Input file
;
cpp                =  /lib/cpp      ; c preprocessor
define             =  -DFLEX_SPCE   ; flexible SPC/E water model used
constraints        =  none          ; constraints are not applied
integrator         =  steep         ; steepest descent algorithm
nsteps             =  1000          ; number of steps
;
;       Energy minimizing stuff
;
emtol              =  50            ; tolerence level
emstep             =  0.001         ; time step 1 fs
nstcomm            =  1             ; frequency for centre of mass motion removal
ns_type            =  grid          ; neighbour search type
rlist              =  0.9           ; distance of neighbours
rcoulomb           =  0.9           ; coulomb cut-off distance
rvdw               =  0.9           ; L-J cut-off distance
Tcoupl             =  no            ; temperature coupling is not applied
Pcoupl             =  no            ; pressure coupling is not applied
gen_vel            =  no            ; no generation of velocity
```

Figure 3.4: Parameters for energy minimization

The ***mdrun*** program is the main computational chemistry engine within GROMACS. Obviously, it performs Molecular Dynamics simulations and energy minimization. The mdrun program reads the run input file (-s) $afem.tpr$ and produces at least four output files. The output files are the log file (-g) *md.log*, the trajectory file (-o) $afem.trr$, the structure file (-c)$afem.gro$ and the energy file (-e) *ener.edr*. The trajectory file contains coordinates, velocities and optionally forces. The structure file contains the coordinates and velocities of the last step. The energy file contains energies, the temperature, pressure, etc, a lot of these things are also present in the log file [12].

By far it is quite obvious that the structure of the system changes after energy minimization. The structure of the system before and after energy minimization is shown in figure 3.5. The ball and stick represent water molecules while argon atoms are enclosed in the circles.

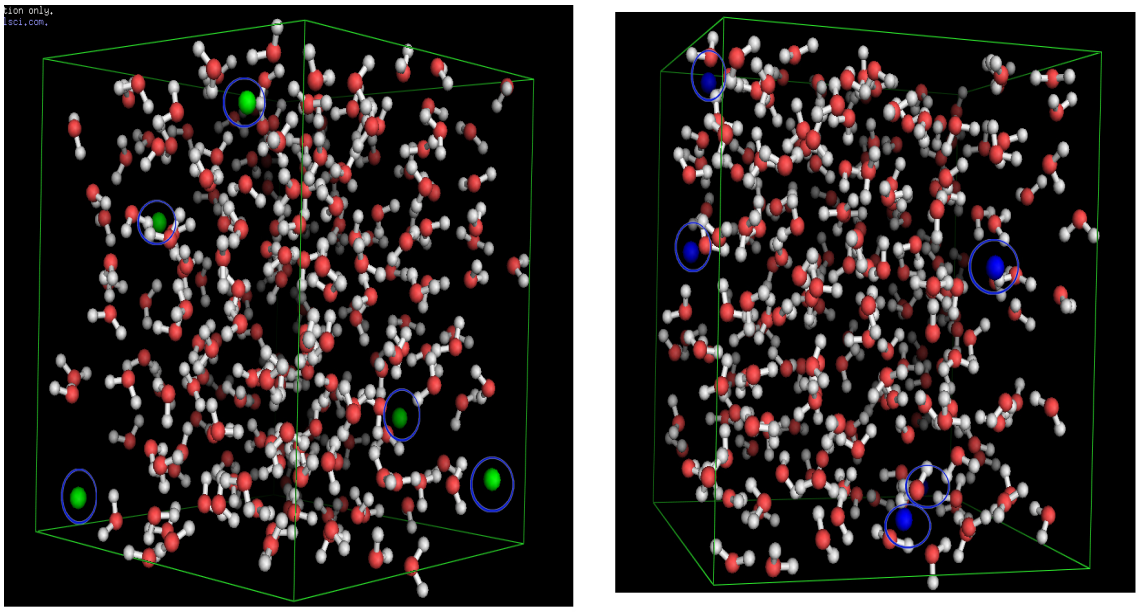

Figure 3.5: System structure before and after energy minimization. Enclosed in the circles are the argon atoms (figure generated by pyMol).

After energy minimization the system reaches its local minimum (energy). The local minimum state is reached after certain steps (in the present system it is 80) provided in *em.mdp*. Figure 3.6 shows the variation of potential energy of the system with time steps. It is clearly observed that after certain steps energy reaches to its almost constant negative value which is -11549.8379 kJmol^{-1}. This constant value of energy indicates the local minimum.

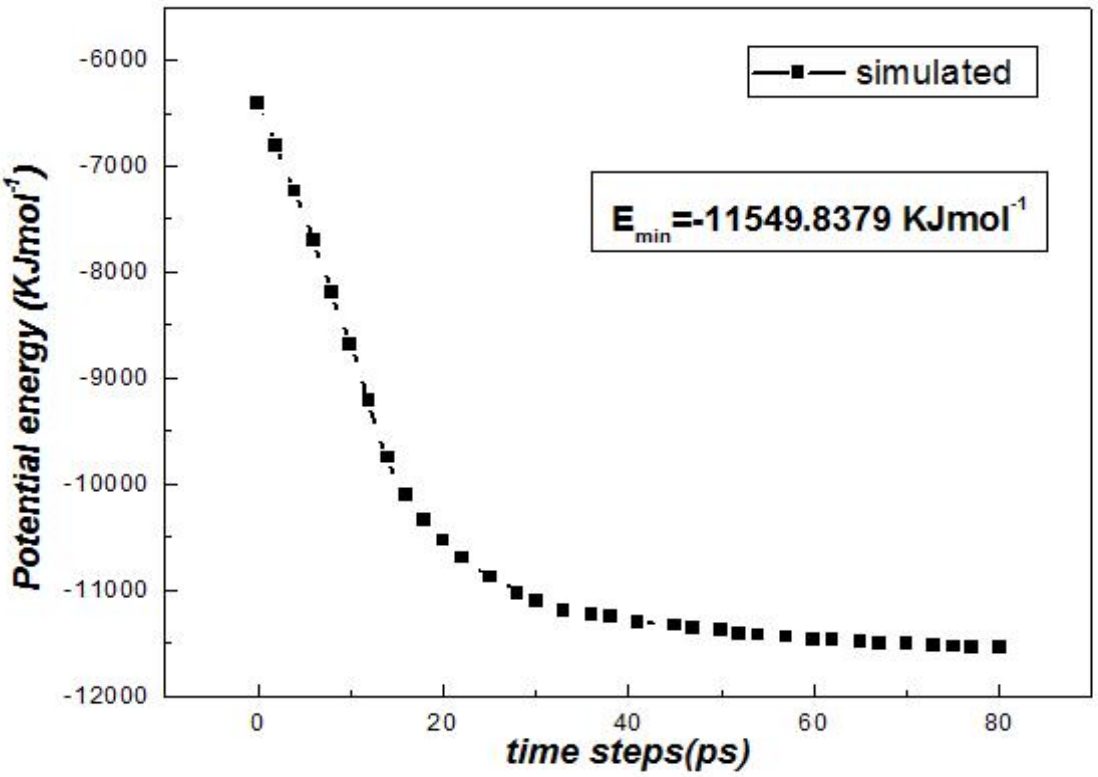

Figure 3.6: **Potential Energy of the system after energy minimization.**

3.1.6 Equilibration

The simulation itself can run after the energy minimization is accomplished. Over the first few hundred time-steps the system relaxes from the arbitrarily assigned initial conditions and approaches equilibrium; this relaxation phase is called equilibration [9]. The major purpose of the present simulation is to determine the dynamic property, diffusion coefficient, of the system under study. The dynamical variables, however, are very sensitive to the parameters such as temperature, pressure, density, etc. An isolated system at equilibrium satisfies, firstly the total number of molecules and total energy should be constants and independent of time. Secondly, thermodynamic properties such as the temperature and pressure should be fluctuating about stable average values. Therefore, before the production run, the equilibration is done in the present system mainly to get the constant average density and temperature of the system. The system is coupled to a suitable thermostat. GROMACS uses the term *Temperature Coupling* for this process. Similarly, a constant pressure is subjected to the system by coupling the system with a suitable barostat. GROMACS understands this process as *Pressure Coupling* [9, 12].

In GROMACS equilibration is also carried out using the programs ***grompp*** and ***mdrun*** same as in case of energy minimization. So for ***grompp*** the input files needed are the structure file $afem.gro$, the topology file $ar.top$, and the run input parameter file $feq.mdp$. These files are preprossed by ***grompp*** which then generates the run input file $afeq.tpr$ as output. The program ***mdrun*** uses this file as input and produces the trajectory file $afeq.trr$, energy file $afeq.edr$ as well as structure file $afeq.gro$. From the file $afeq.edr$, the system pressure and temperature can be derived using the program ***g_energy*** inherent in GROMACS [12].

The structure file $afem.gro$ is obtained as an output of the energy minimization. The contents of run input parameters file $feq.mdp$ for equilibration is significantly different from that for the energy minimization. This file uses Leap-frog algorithm for integrating Newton's equation of motion. Temperature coupling is accomplished with a Berendsen-thermostat to a bath with temperature ***ref_t*** and time constant ***tau_t*** of 0.01 ps. The reference temperatures taken for this system are 293K , 298 K , 303 K , 308 K and 313 K. The pressure coupling used is Berendsen with the time constant, ***tau_t***, of 0.1 ps. This implies that the box size is not fixed and is scaled every timestep. The reference pressure for coupling ***ref_p*** is 1 bar. The velocities are generated using Maxwell-Boltzmann distribution function at temperature ***gen_temp*** which is specified for the system under study. An isothermal compressibility taken is 4.60×10^{-5} bar^{-1}. All the bonds are converted into constraints and the constraint algorithm used is SHAKE. Also constraints are applied to the starting configuration [12].

Table 3.5 lists the temperatures and the densities of the system after five equilibration processes at different temperatures carried out for the system structure obtained after energy minimization.

S.N.	Temperature (K)	Density (kgm^{-3})
1	293	1021.558±0.056
2	298	1018.452±0.057
3	303	1014.928±0.057
4	308	1011.380±0.058
5	313	1008.070±0.058

Table 3.5: Equilibrium densities at different temperature and pressure 1 bar using Berendsen algorithm.

```
title                =  MDP FOR ARGON
cpp                  =  /lib/cpp         ; C preprocessor
integrator           =  md               ; Leap-Frog Algorithm
dt                   =  0.002            ; Time step = 2 fs
nsteps               =  25000000         ; Total time = 50 ns
nstcomm              =  1
nstxout              =  250              ; Output control parameters
nstvout              =  1000
nstfout              =  0
nstlog               =  100
nstenergy            =  100
energygrps           =  system
nstlist              =  10               ; NEIGHBOUR SEARCHING parameters
ns_type              =  grid
rlist                =  0.9
rcoulomb             =  0.9              ; ELECTROSTATIC and VdW parameters.
rvdw                 =  0.9
epsilon-r            =  1
Tcoupl               =  berendsen        ; TEMPERATURE COUPLING is on
tc-grps              =  system
tau_t                =  0.01
ref_t                =  298
Pcoupl               =  berendsen        ; PRESSURE COUPLING is on
tau_p                =  0.1
compressibility      =  4.6e-5
ref_p                =  1.0
gen_vel              =  yes              ; generate initially
gen_temp             =  298
gen_seed             =  173529           ; give different values for different trials.
constraints          =  all-bonds        ; BONDS parameters
constraint-algorithm = shake
unconstrained-start  = no
```

Figure 3.7: Run input parameters for equilibration at temperature 298 K and pressure 1 bar.

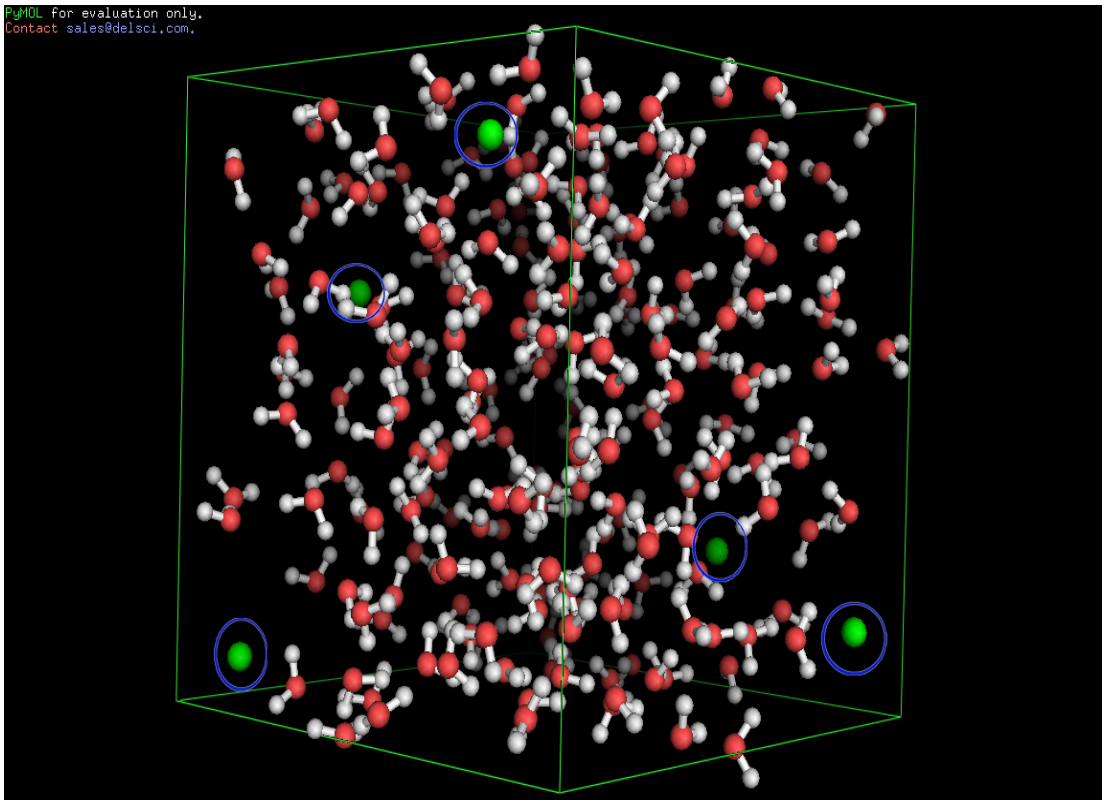

Figure 3.8: System structure at temperature 293 K and density 1021.558 kg m^{-3}.

Figure 3.8 shows the system structure structure at temperature 293 K and density 1021.558 kg m^3. In the figure, argon atoms are represented by encircled balls and water molecules by ball and stick. The figure is generated by using PYMOL.

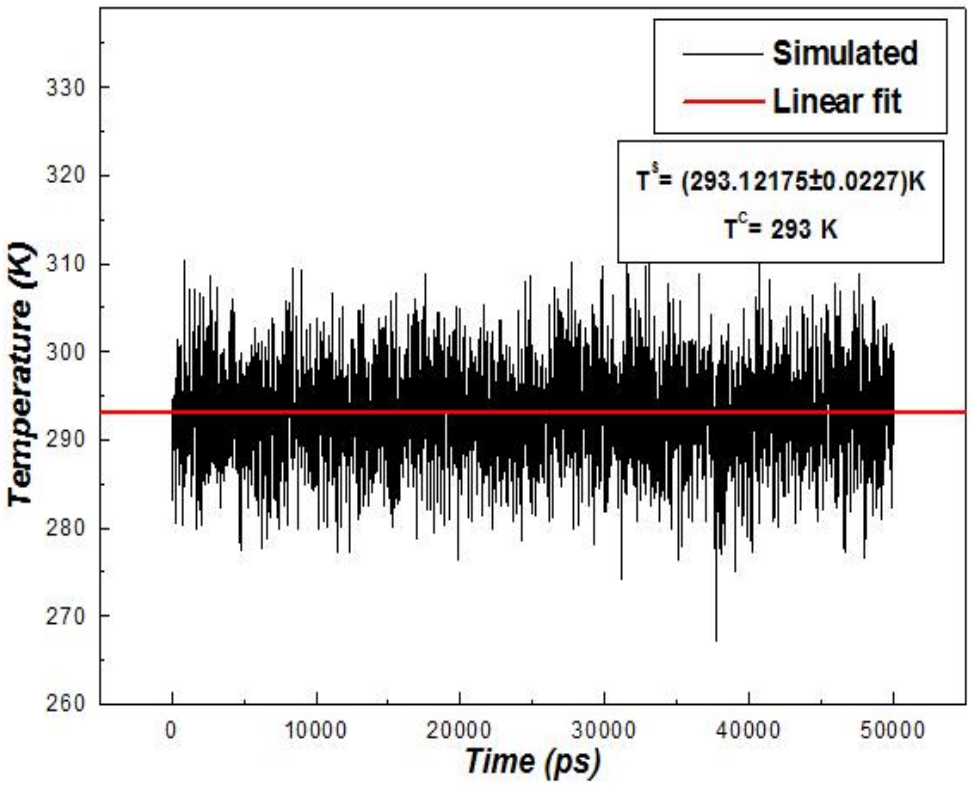

Figure 3.9: System temperature profile after equilibration period of 50 ns at 293 K using Berendsen thermostat.

Figure 3.9 shows that the variation of system temperature with time during the equilibration. After the equilibration of 50 ns using NPT ensemble, the system's temperature fluctuates around the average value of 293.12175 K which very closely approximates our coupled temperature 293 K.

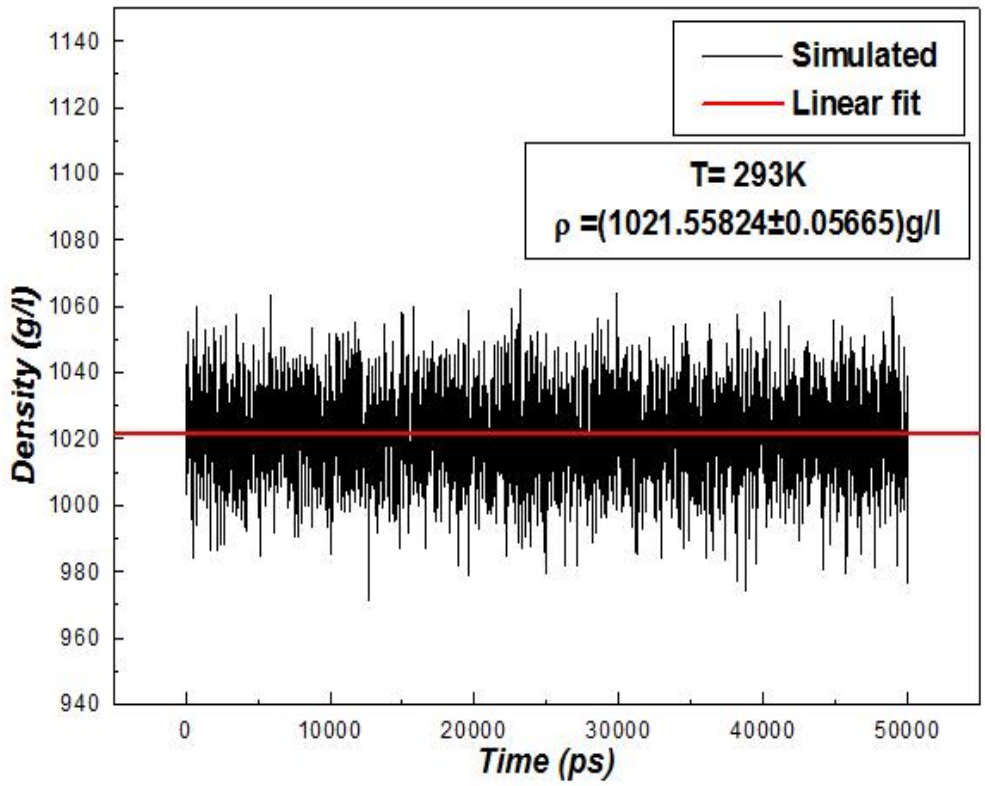

Figure 3.10: System density profile after equilibration period of 50 ns at 293 K using Berendsen thermostat and barostat.

Figure 3.10 shows the variation of system density with time during equilibration at temperature 293 K. As the dynamic properties such as diffusion coefficient are very sensitive to the density of the system, it is very important to attain the correct system density before production run. Thus, the purpose of equilibration is to attain the correct system density as well. In the equilibration of 50 ns, the simulated density of the system is obtained to as 1021.558 kg m^{-3}. The experimental water density is 998.200 kg m^{-3} [27]. Thus the system density at this temperature is close to the water density, supporting the fact that our system contains more water molecules compared to the argon atoms.

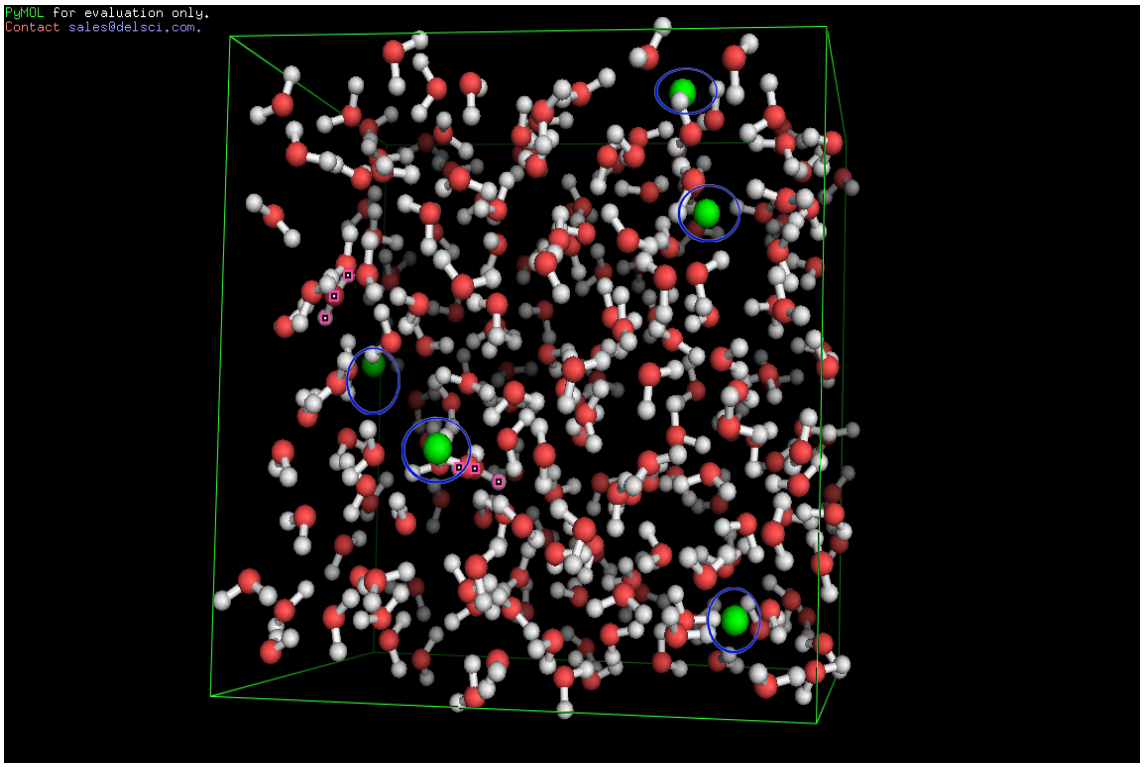

Figure 3.11: System structure at temperature 298 K and density 1018.452 kg m^{-3}.

Figure 3.11 shows system structure at temperature 298 K and density 1018.452 kg m^{-3}. The argon atoms are represented by encircled balls and the water molecules by ball and stick. The figure is generated by using PYMOL.

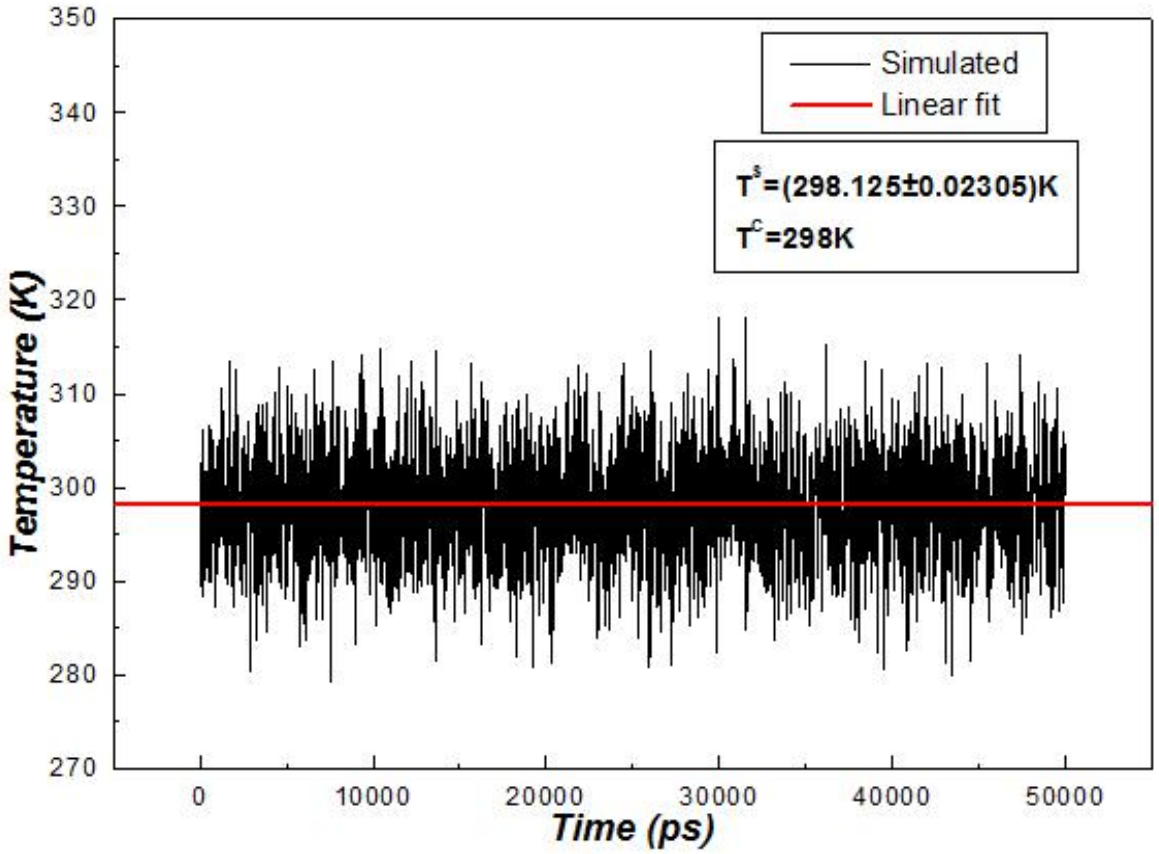

Figure 3.12: System temperature after equilibration period of 50 ns at 298 K using Berendsen thermostat.

Figure 3.12 shows the fluctuations in the system temperature with time during equilibration. The equilibration is done for 50 ns using NPT ensemble and the average simulated temperature is obtained as 298.125 K. The coupled temperature is 298 K. This shows that the temperature of the system, after simulation, is very close to the coupled temperature.

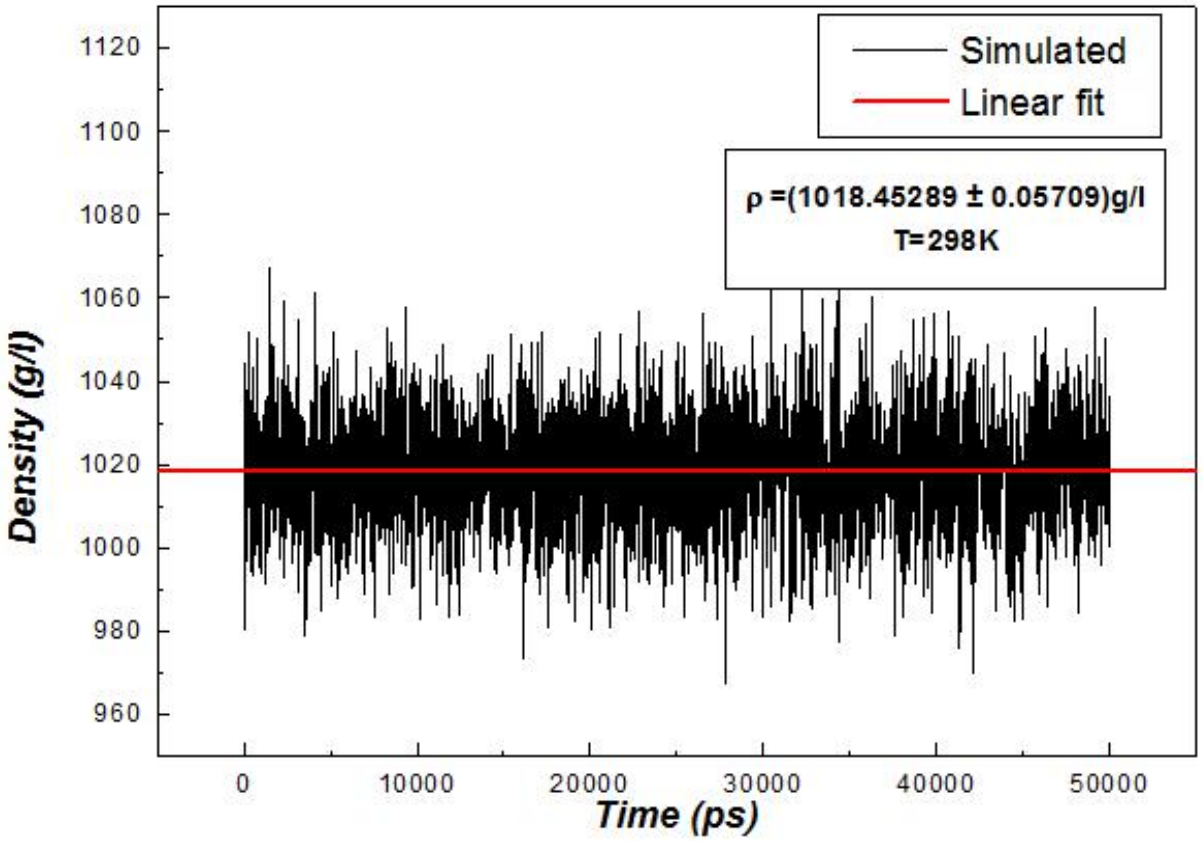

Figure 3.13: System density after equilibration period of 50 ns at 298 K using Berendsen thermostat.

Figure 3.13 shows the variation of system density with time during equilibration. The system density fluctuates to the constant average value of 1018.452±0.057 kg m^{-3} after equilibration of 50 ns. The experimental water density at this temperature is 997.048±0.01 kg m^{-3} which is again close to the system density as required [27].

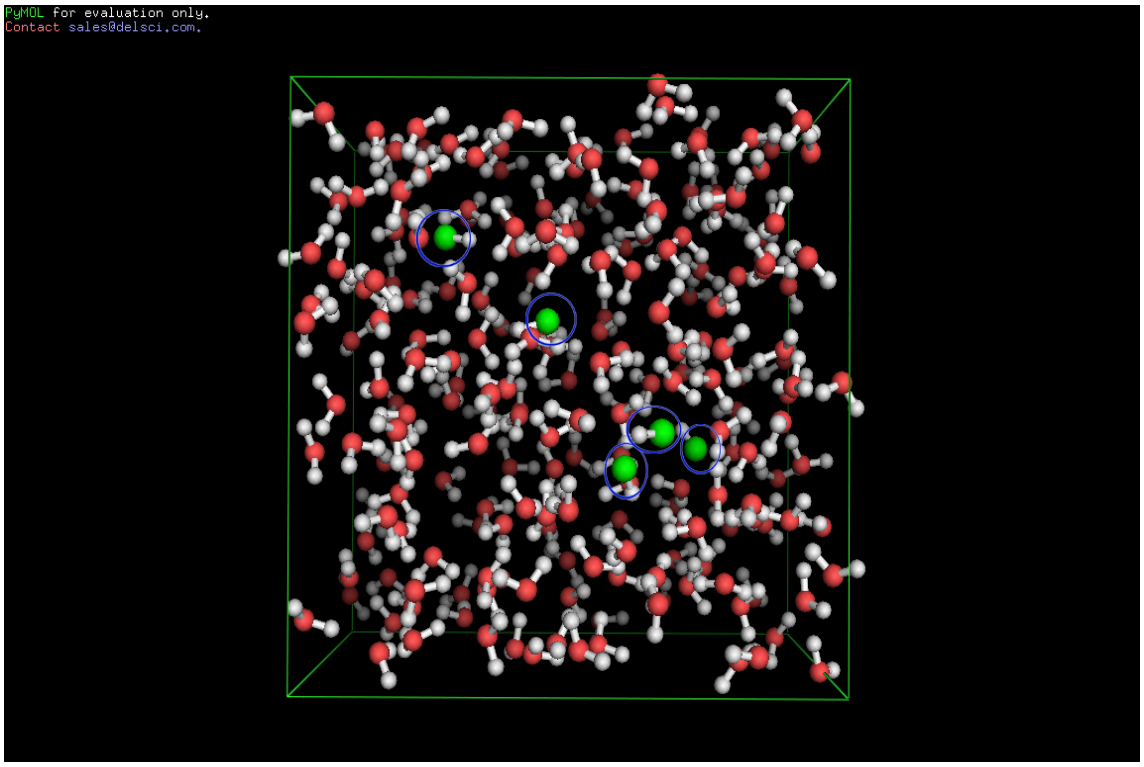

Figure 3.14: System structure at temperature 303 K and density 1014.928 kg m^{-3}.

Figure 3.14 shows the system structure at temperature 303 K and density 1014.928 kg m^{-3}. The water molecules are represented as ball and sticks and the argon atoms are encircled balls. The figure is generated by using PYMOL.

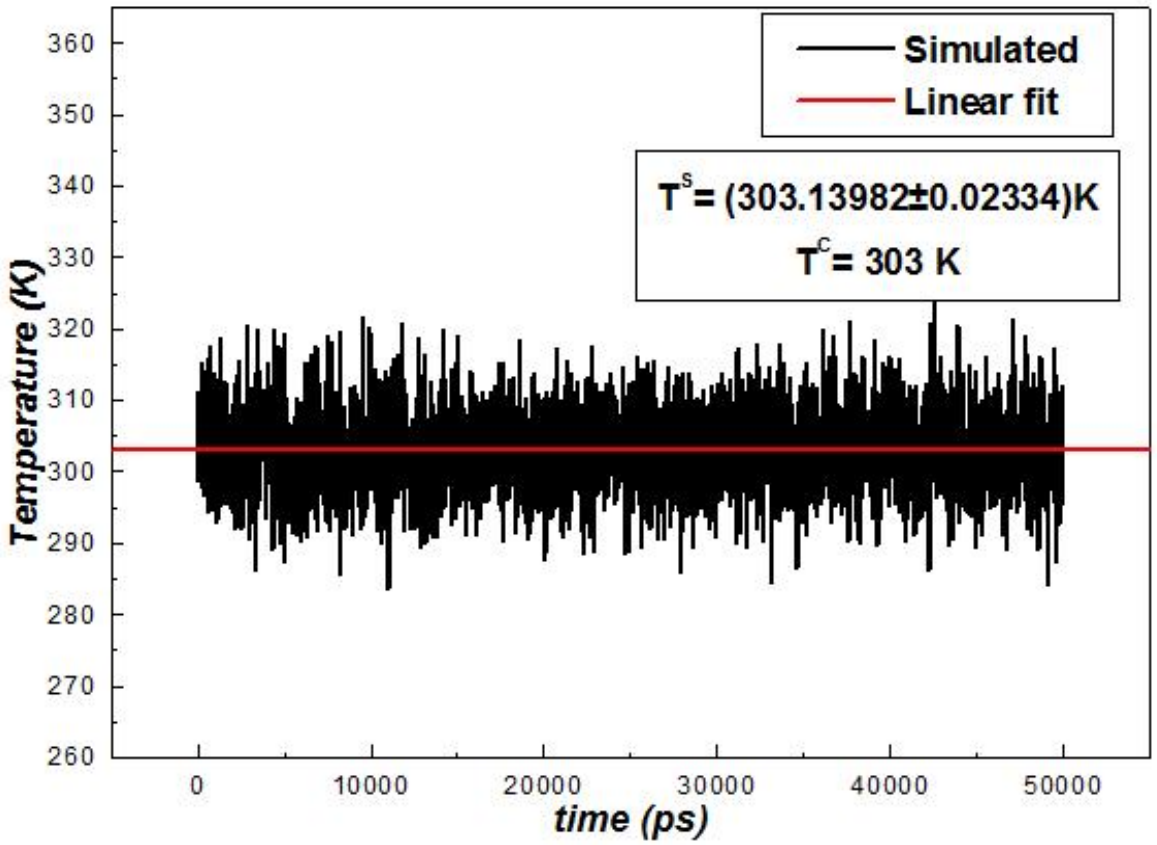

Figure 3.15: System temperature after equilibration period of 50 ns at 303 K using Berendsen thermostat.

Figure 3.15 is the variation of system temperature with time during equilibration. After equilibration of 50 ns, it is found that the system temperature fluctuates to the constant average value of 303.13982 K. The coupled temperature of the system is 303 K. This shows that the average system temperature is very close to the coupled temperature after equilibration.

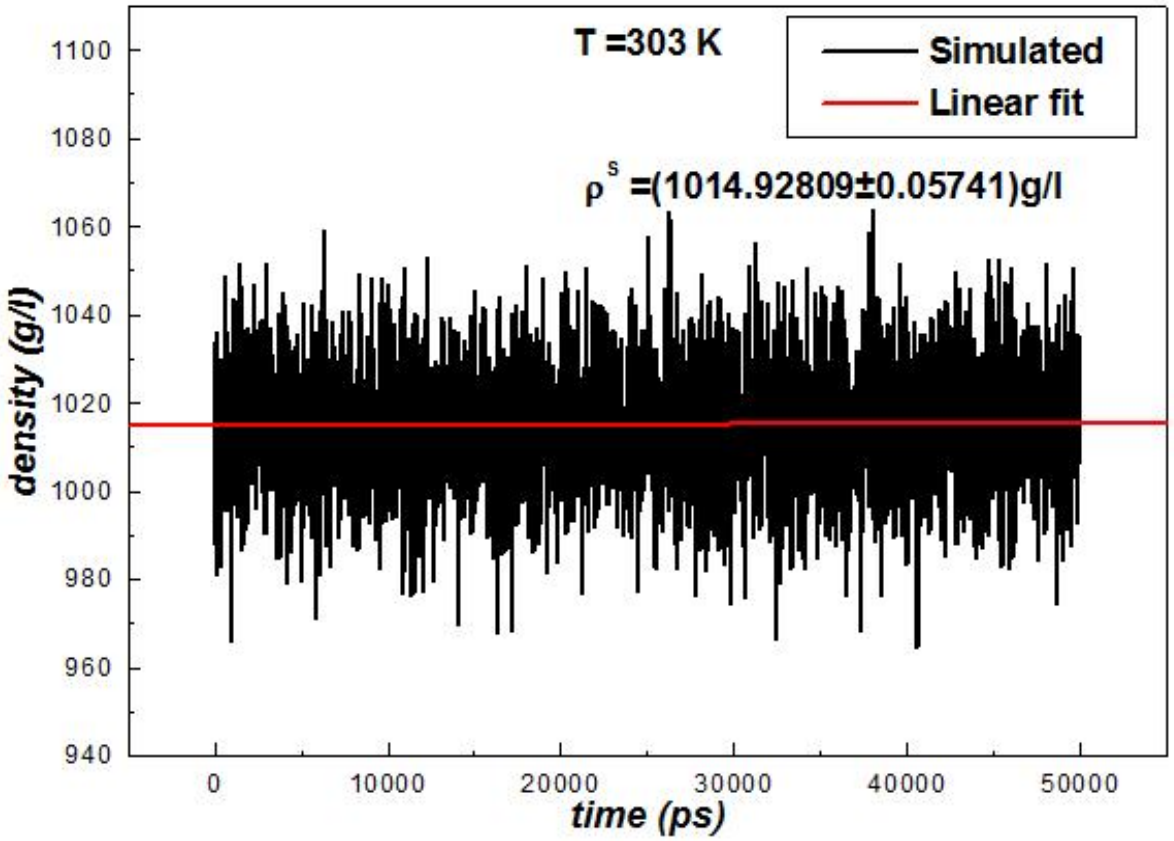

Figure 3.16: System density after equilibration period of 50 ns at 303 K using Berendsen thermostat and barostat.

Figure 3.16 shows the variation of the system density with time at the temperature of 303 K during equiibration. The equilibration is done for 50 ns using NPT ensemble. The simulated density of the system is obtained to be 1014.928 kg m^{-3} and experimental water density at this temperature is 995.651 kg m^{-3}. Again the average density of the system is close to the water density which is as desired for the system.

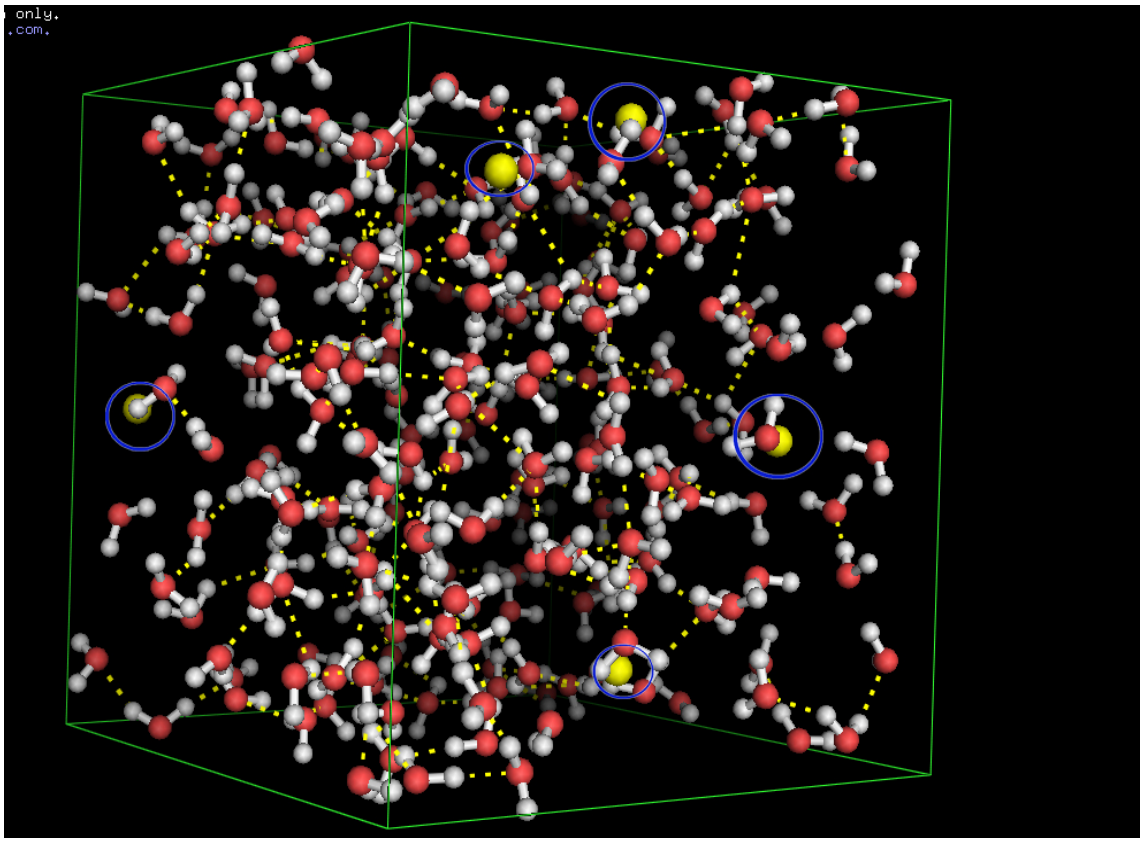

Figure 3.17: System structure at temperature 308 K and density 1011.380 kg m^{-3}.

Figure 3.17 shows the system structure at temperature 308 K and density 1011.380 kg m^{-3}. The water molecules are represented as ball and sticks where the encircled balls represent the argon atoms. The dotted lines represent the polar contact existing between the molecules. The figure is generated by using PYMOL.

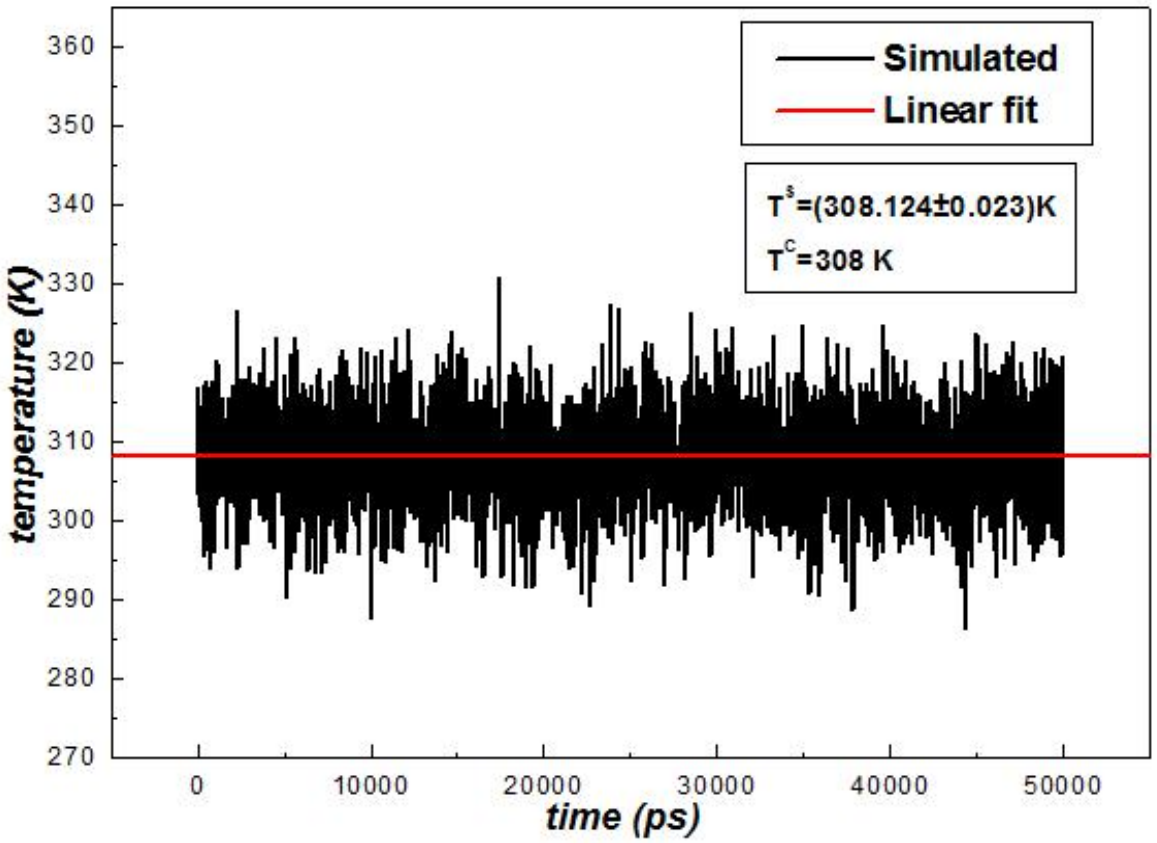

Figure 3.18: System temperature after equilibration period of 50 ns at 308 K using Berendsen thermostat.

Figure 3.18 shows the variation of system temperature with time during equilibration. After 50 ns of equilibration using NPT ensemble, the simulated temperature of the system attains approximately constant average value of 308.124 K. The coupled temperature of the system is 308 K. Thus the average value of the simulated temperature is close to the coupled temperature as desired for our system.

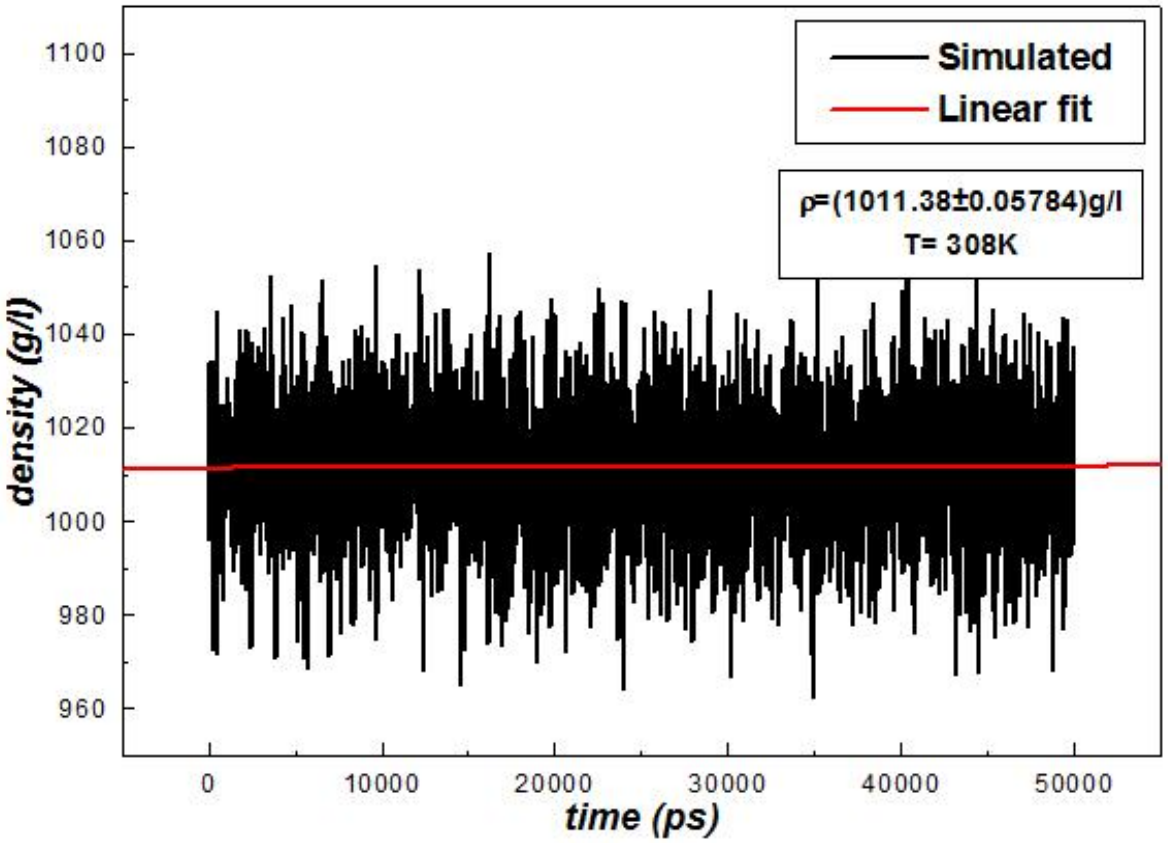

Figure 3.19: System density after equilibration period of 50 ns at 308 K using Berendsen thermostat.

Figure 3.19 shows the variation of the system density with time during equilibration at temperature 308 K. The simulated density of the system remain approximately constant to the value 1011.380 kg m^{-3} after equilibration of 50 ns. The experimental water density at this temperature is 994.035 kg m^{-3} which is again close to the average simulated density as required for our system [27].

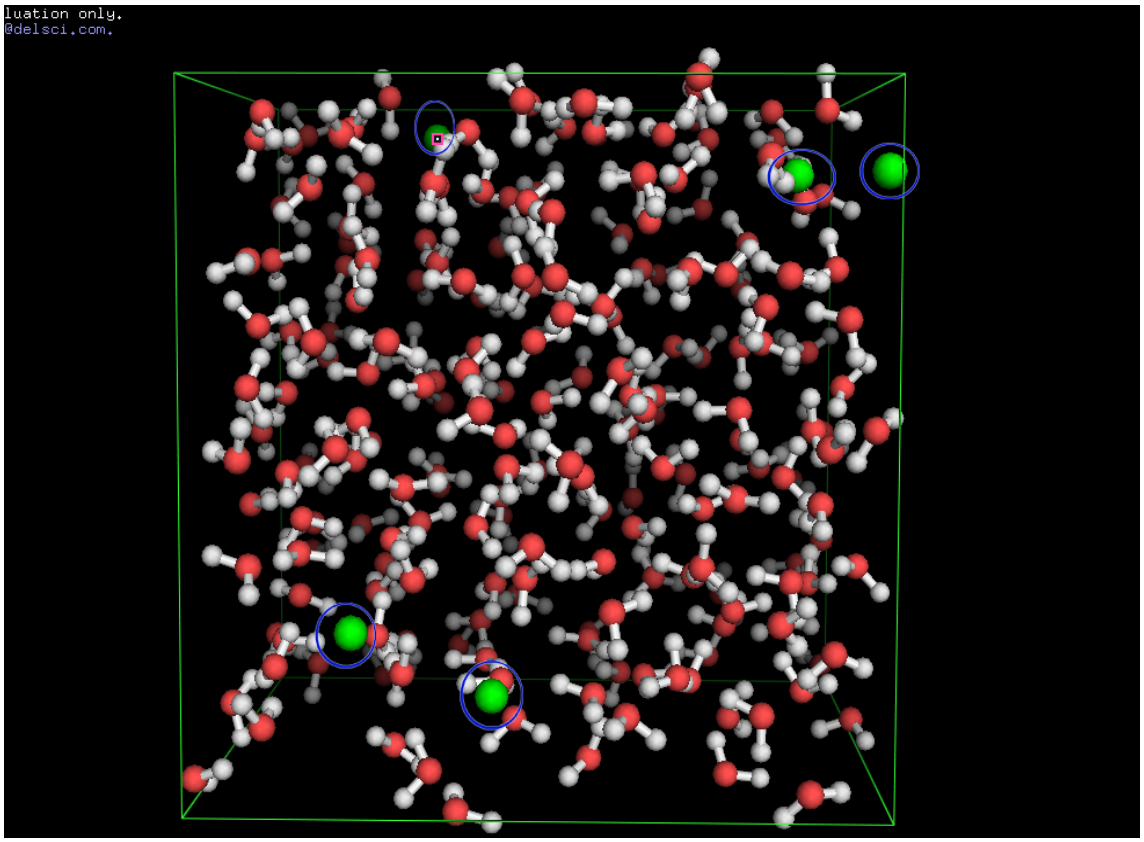

Figure 3.20: System structure at temperature 313 K and density 1008.070 kg m^{-3}.

Figure 3.20 shows the system structure at temperature 313 K and density 1008.070 kg m^{-3}. The water molecules are represented as ball and stick and the encircled balls are argon atoms. The figure is generated using PYMOL.

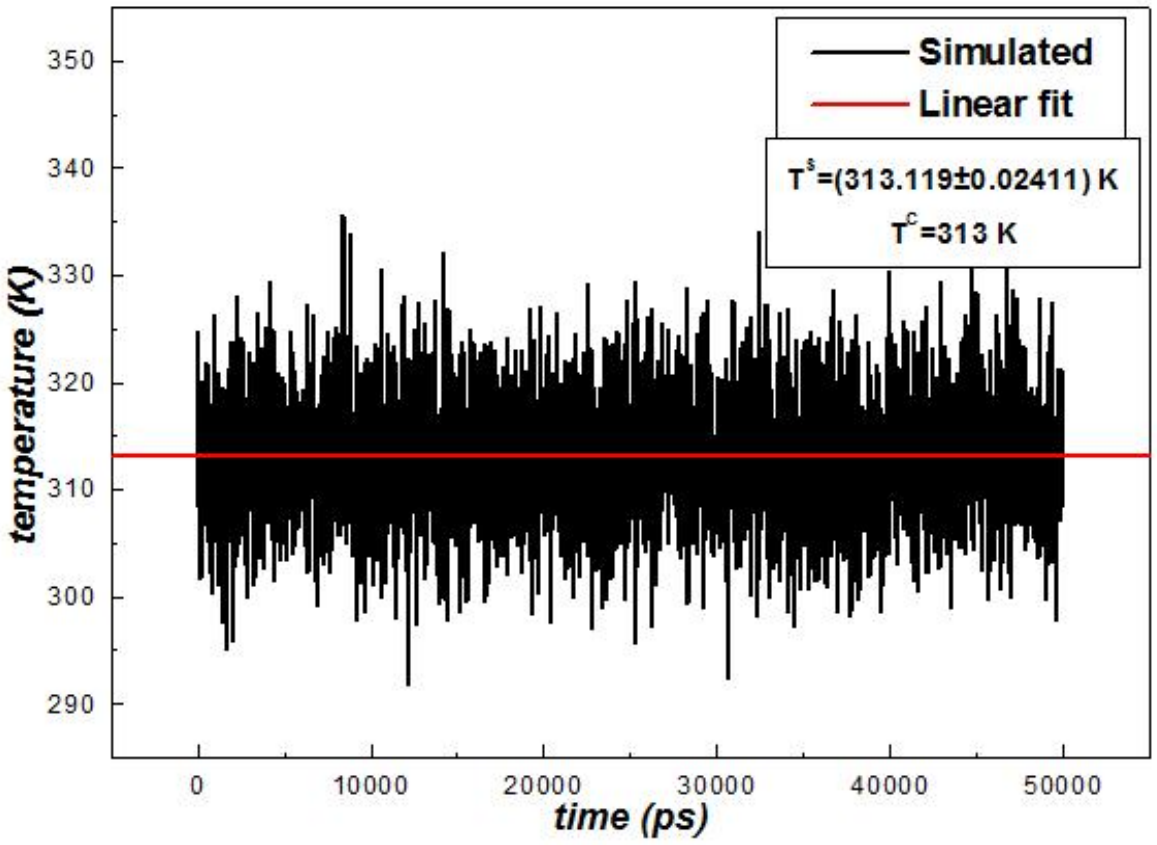

Figure 3.21: System temperature after equilibration period of 50 ns at 313 K using Berendsen thermostat.

Figure 3.21 is the variation of system temperature with time during equilibration. After the equilibration of 50 ns the simulated system temperature attains approximately the constant average value of 313.119 K. The coupled temperature is 313 K. Thus the average simulated temperature is nearly equal to the coupled temperature, which is desired for our system.

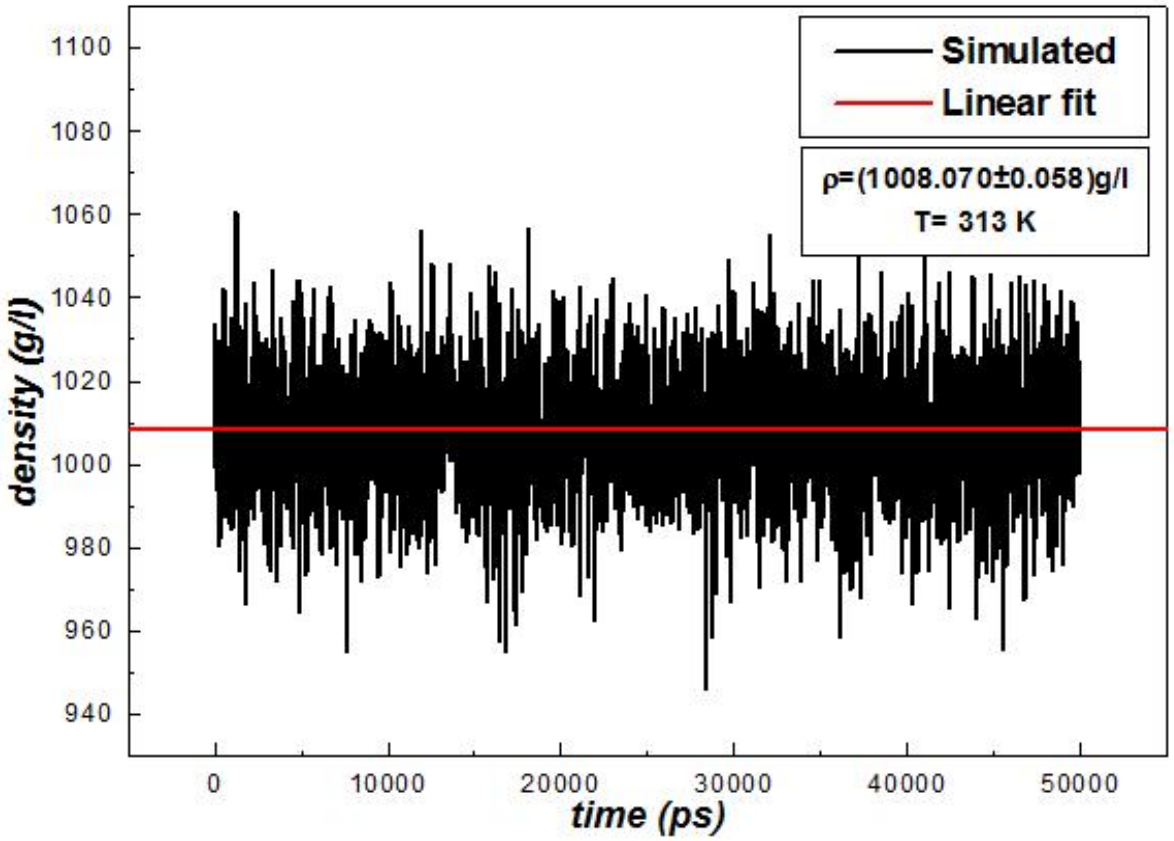

Figure 3.22: System density after equilibration period of 50 ns at 313 K using Berendsen thermostat and barostat.

Figure 3.22 shows the variation of system density with time during equilibration. After 50 ns of equilibration using NPT ensemble the density attains a constant average value of 1008.070 kg m^{-3}. The experimental water density at this temperature is 992.220 kg m^3 which is again close to the average value of the simulated system density [27].

3.1.7 Production

The production phase of run can begin once the equilibration is reached. In this phase of simulation no new programs but the two; viz. ***grompp*** and ***mdrun***, are used as in equilibration. The only difference is that now the system is in equilibrium and the simulation is conducted on NVT ensemble. The main purpose of production run is to derive dynamic non-equilibrium property called diffusion coefficient and static equilibrium property called radial distribution function. For the production run the structure file is taken as $afeq.gro$ which is the output of the equilibration phase. The new run input parameter file $feq.mdp$ is created for NVT ensemble by removing the pressure coupling. This keeps the box size fixed thereby making volume fixed. Since the simulation must continue with the velocities of the equilibration process, there is no initial generation of velocities. As in the case of equilibration, the program ***grompp*** preprocesses and the run is conducted by ***mdrun***. The contents of the run input parameter file $feq.mdp$ for the production run at a particular temperature of 298 K is presented in the figure 3.23 below.

```
title               =  MDP FOR ARGON
cpp                 =  /lib/cpp        ; C preprocessor
integrator          =  md              ; A Leap-Frog Algorithm
dt                  =  0.002           ; time step = 2 fs
nsteps              =  100000000       ; total time = 200 ns
nstcomm             =  1
nstxout             =  250             ; OUPUT CONTROL parameters
nstvout             =  1000
nstfout             =  0
nstlog              =  100
nstenergy           =  100
energygrps          =  system
nstlist             =  10              ; NEIGHBOUR SEARCHING parameters
ns_type             =  grid
rlist               =  0.9
rcoulomb            =  0.9             ; ELECTROSTATIC and VdW parameters.
rvdw                =  0.9
epsilon-r           =  1
Tcoupl              =  berendsen       ; BERENDSEN TEMPERATURE COUPLING is on
tc-grps             =  system
tau_t               =  0.01
ref_t               =  298
Pcoupl              =  no              ; PRESSURE COUPLING is off
;SIMULATED ANNEALING parameters are not specified.
gen_vel             =  no              ; No generation of velocity in this phase
gen_temp            =  298
```

Figure 3.23: Run input parameters for production phase

The simulations for different temperatures and different time durations can be performed by similar procedures mentioned above, only by making slight changes in the parameters. The time duration for each system is taken as 200 ns and different output files are generated which are then analyzed to find the diffusion coefficients of argon at different temperatures.

Chapter 4

Results and Discussion

4.1 General Consideration

Argon atoms are allowed to diffuse through the water molecules at different temperatures. The trajectory file obtained as output can be subjected to the different form of analysis. The results thus obtained are presented in this chapter. Initially, the structural analysis of the system at different temperatures and densities are presented in section 4.1. Then, in section 4.2 comes the energy profile of the system at different temperatures. Finally, the equilibrium dynamic property of the system, the diffusion coefficient, are presented in section 4.3. The overall discussion comes along with the results.

4.1.1 Structural Analysis

The radial distribution function (or RDF) is an example of a pair correlation function, which describes how the atoms in a system are radially packed around each other. The RDF is plotted as a function of the interatomic separation r. A typical RDF plot shows a number of important features. Firstly, at short separations, that is small r, the RDF is zero. This indicates that the atoms cannot approach any more closely than this width. Secondly, a number of peaks appear, which indicate that the atoms pack around each other in 'shells' of neighbors. The occurrence of peaks at long range indicates a high degree of ordering. Usually, at high temperature the peaks are broad, indicating thermal motion, while at low temperature they are sharp. At very long range every RDF tends to a value of 1, which happens because the RDF describes the average density at this range [28, 29]. Thus, the radial distribution function is the most common and an effective way of describing the average structure of disordered molecular systems such as liquids as discussed in section 2.2. To be precise, the shape of the radial distribution function determines the structure of the homogenous and isotropic fluid [15]. We have derived three different radial distribution functions, namely $g_{AR-AR}(r)$, $g_{AR-OW}(r)$, and $g_{ow-ow}(r)$. In GROMACS this is accomplished by the program ***g_rdf***. It calculates radial distribution functions in different ways. The normal method is around a (set of) particle(s), the other method is around the center of mass of a set of particles. In the system under study the RDF for atoms are computed which are in the index files. So for RDF in GROMACS index file plays a vital role [12]. The distribution of argon atoms within the simulation box as well as the interaction or correlation among

them is determined by the radial distribution function of argon atoms $g_{AR-AR}(r)$. On the other hand, $g_{ow-ow}(r)$ is the radial distribution function of the oxygen of the water molecules determining the structure of the solvent and the interaction between the solvent molecules. As mentioned before, the solvent we have used is SPC/E water model (see chapter 3, section 3.1.2). Similarly, $g_{AR-OW}(r)$ is the radial distribution function of argon atoms and water molecules. It provides the information regarding the distribution of water molecules around argon atoms and the interaction among them [14].

Figure 4.1-4.17 show the radial distribution functions, *g(r)*, as a function of separation distance for various temperatures and densities.

4.1.1.1 RDF for Solvent

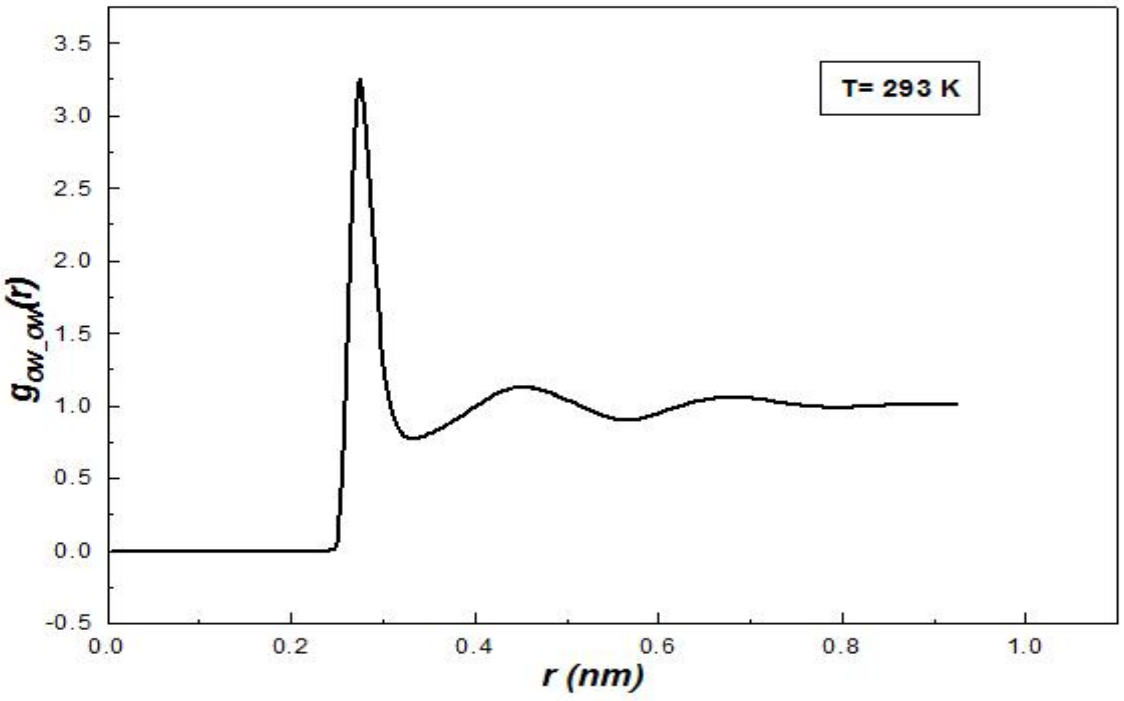

Figure 4.1: The radial distribution function of oxygen of water molecules, g_{ow_ow}(r), at temperature 293 K and density of system 1021.558 kgm^{-3}.

Figure 4.1 is a sketch of radial distribution function of solvent with respect to a solvent molecule $g_{ow\_ow}(r)$, as a function of separation between them. The temperature of a system

is 293 K and its density is 1021.558 kgm^{-3}. From the figure, it is seen that $g_{ow\_ow}(r)$ is zero up to the radial separation of 0.233 nm which implies that upto this separation the solvent molecules repel each other. The first peak occurs at 0.275 nm where $g_{ow\_ow}(r)$ is 3.25885 showing that the probability of finding molecules is highest at this point. Therefore, the nearest-neighbor separation for the solvent molecules obtained from simulation at this temperature is 0.275 nm which is less than the van der Waal's radius of SPC/E water molecule of 0.355 nm. A second and a third peaks occur at 0.453 nm and 0.673 nm at which $g_{ow\_ow}(r)$ is 1.127 and 1.055, respectively. The third peak is weak and beyond it no more peaks are obtained. The curve becomes almost constant with an average value of 1 after third minima. This constant region indicates that there is no more correlation between the solvent molecules where the local density equals the overall number density.

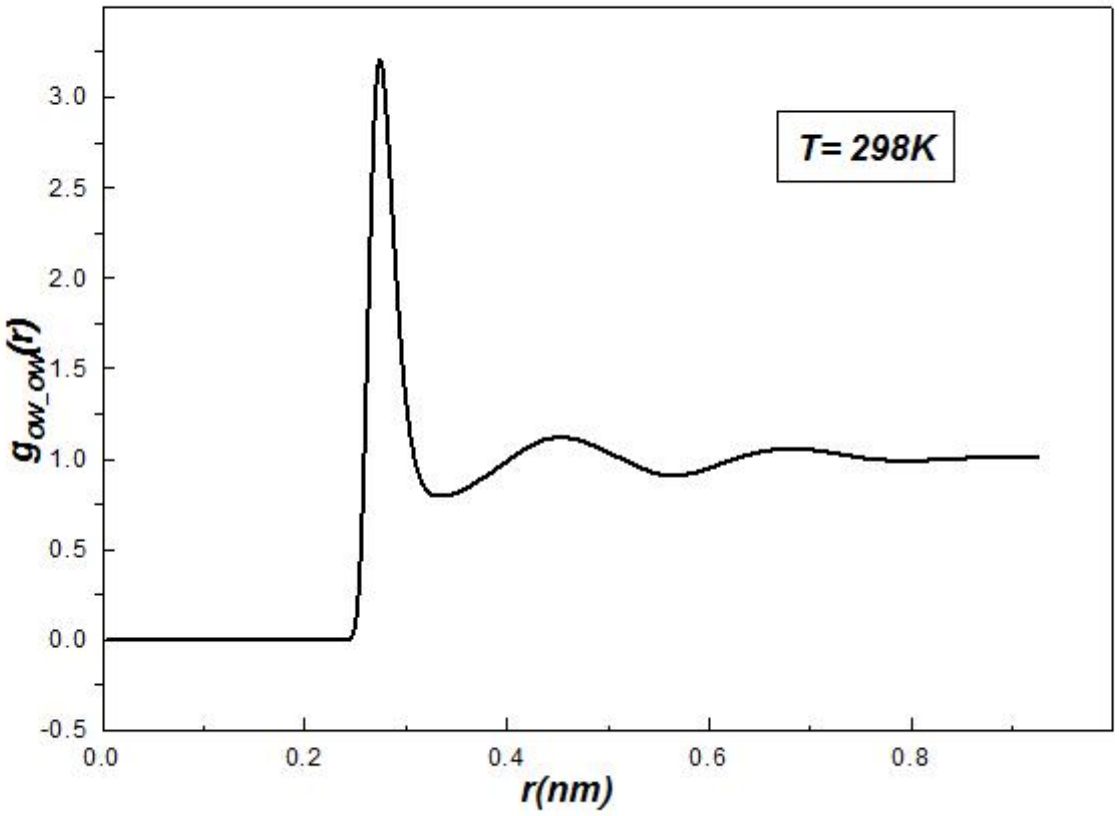

Figure 4.2: The radial distribution function of oxygen of water molecules, $g_{ow\_ow}(r)$, at temperature 298 K and density 1018.452 kgm^{-3} .

The variation of the radial distribution function of solvent molecule with respect to a solvent molecule with their radial separation, $g_{ow\_ow}(r)$, at temperature 298 K and density 1018.452 kgm^{-3} is presented in figure 4.2. From figure, it is observed that $g_{ow\_ow}(r)$ is zero upto the radial separation of 0.231 nm. The first peak occurs at 0.275 nm at which $g_{ow\_ow}(r)$ is 3.207. Thus, the nearest-neighbor separation at this temperature is 0.275 nm which is less than the van der Waal's radius of water model. The second peak occurs at 0.453 nm at which $g_{ow\_ow}(r)$ is 1.117. A very weak third peak occurs at 0.679 nm with the value of 1.053. The constant region of RDF with the approximate value of 1 extends beyond the third minima thereby showing no correlation between the solvent molecules.

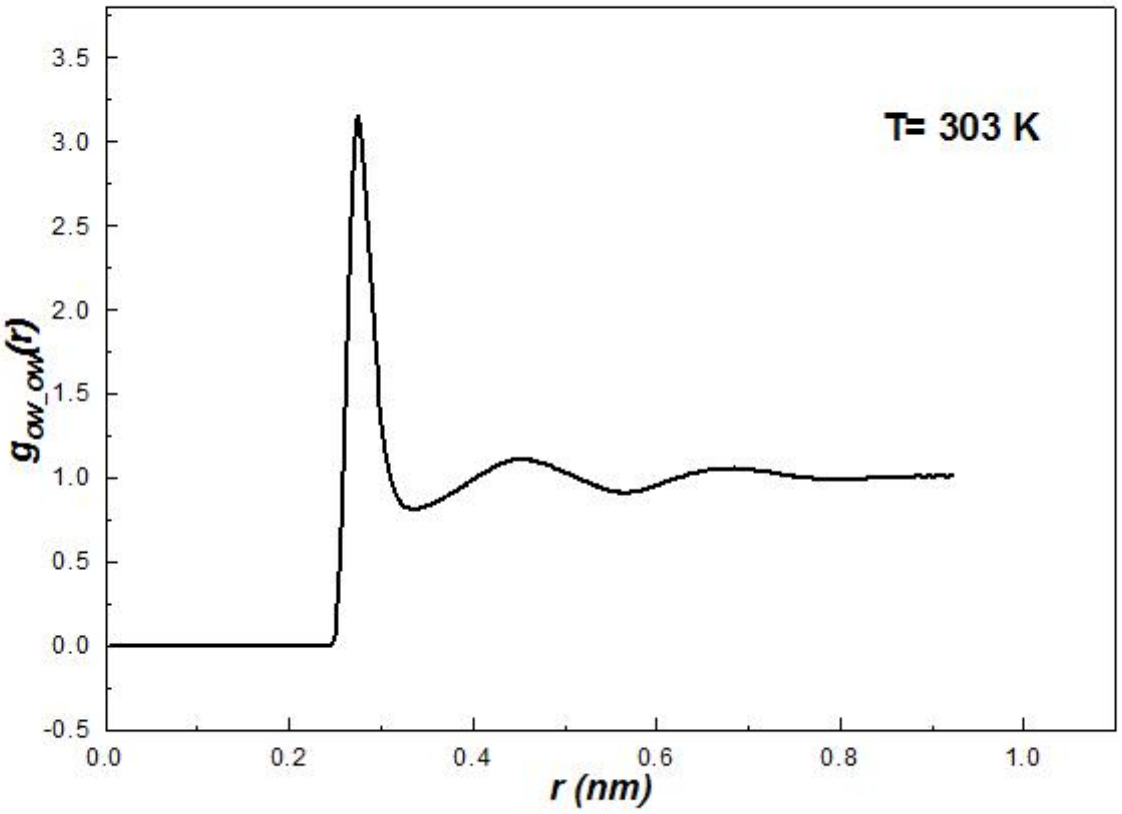

Figure 4.3: The radial distribution function of oxygen of water molecules, g_{ow_ow}(r), at temperature 303 K and density 1014.928 kgm^{-3}.

A plot of radial distribution function of solvent with respect to a solvent molecule, $g_{ow\_ow}(r)$, as a function of the distance between them is shown in figure 4.3. The temperature of the system is 303 K and the density is 1014.928 kgm^{-3}. At this temperature $g_{ow\_ow}(r)$ is zero upto 0.233 nm. The first peak again occurs at 0.275 nm at which $g_{ow\_ow}(r)$ is 3.160, showing the nearest-neighbor separation as 0.275 nm which is less than the van der Waal's radius of water molecule 0.355 nm. The second peak occurs at 0.453 nm at which $g_{ow\_ow}(r)$ is 1.107. The weak third peak is obtained at 0.685 nm with a value of 1.054. Beyond third minima $g_{ow\_ow}(r)$ is again constant with an average value of 1 thereby showing no correlation.

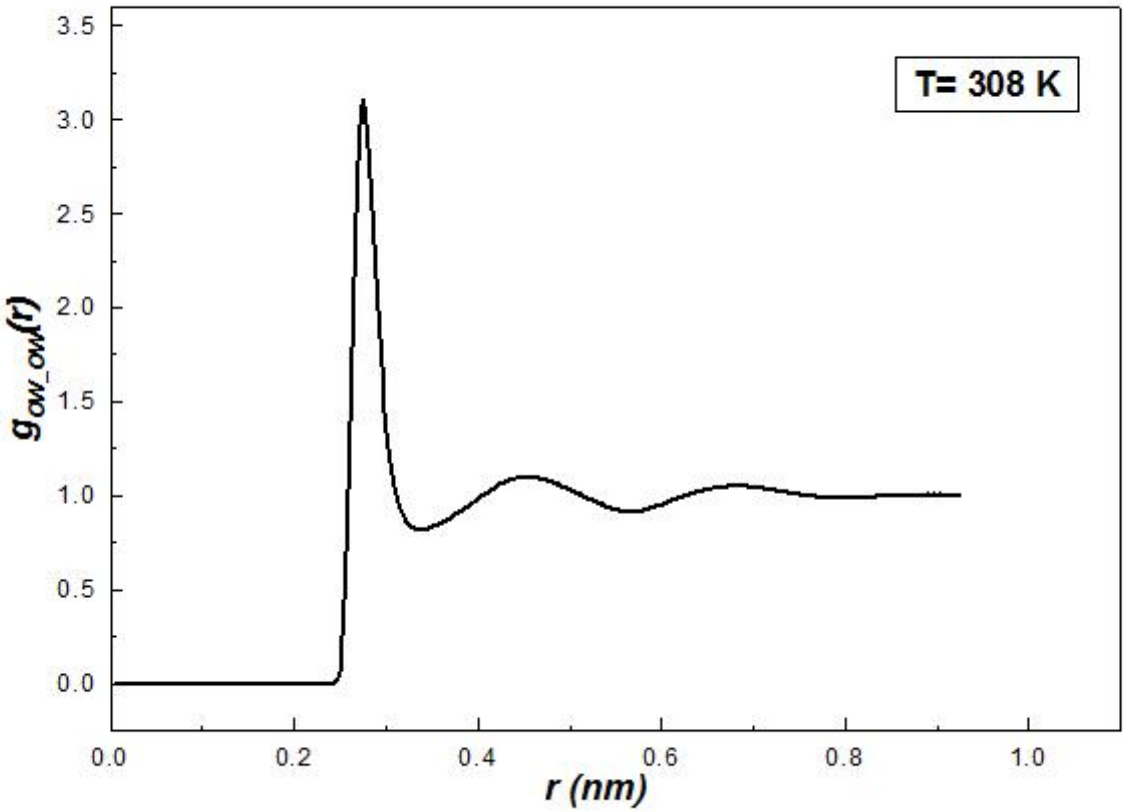

Figure 4.4: The radial distribution function of oxygen of water molecules, g_{ow_ow}(r), at temperature 308 K and density 1011.380 kgm^{-3}.

Figure 4.4 is a plot of radial distribution function of solvent $g_{ow\_ow}(r)$ as a function of distance between them, at the system temperature 308 K and density 1011.380 kgm^{-3}. At this temperature $g_{ow\_ow}(r)$ is zero upto the radial separation of 0.233 nm. From the figure, it is obtained that the excluded region for solvent molecules is within 0.233 nm where the radial distribution function is zero. The first peak occurs at 0.275 nm at which $g_{ow\_ow}(r)$ is 3.110. Therefore, the nearest-neighbor separation is 0.275 nm which is less than the van der Waal's radius of the model water molecule. The second peak occurs at 0.451 nm at which $g_{ow\_ow}(r)$ is 1.098. The weak third peak is observed at 0.681 nm with a value 1.047. Beyond the third minima, the RDF again attains a constant value of 1 showing no long range correlation.

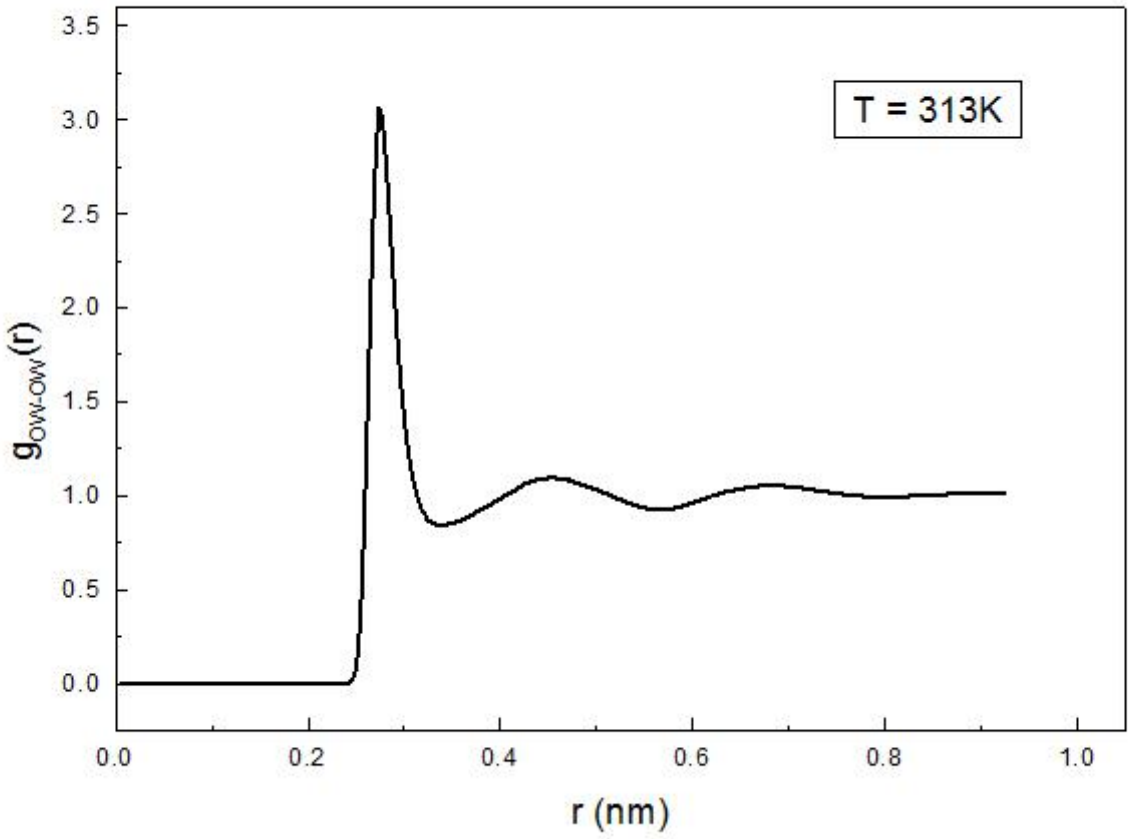

Figure 4.5: The radial distribution function of oxygen of water molecules, g_{ow_ow}(r), at temperature 313 K and density 1008.070 kgm^{-3}.

The radial distribution function of solvent $g_{ow\_ow}(r)$, as a function of their separation, at temperature 313 K and density 1008.070 kgm^{-3} is shown in figure 4.5. In this case, as shown in the figure, $g_{ow\_ow}(r)$ is zero upto 0.233 nm while the first peak is obtained at 0.275 nm with the value of 3.067. So, the nearest-neighbor separation is 0.275 nm which is less than the van der Waal's radius of water molecule 0.3552 nm. The second peak occurs at 0.455 nm at which $g_{ow\_ow}(r)$ is 1.090. The weak third peak is observed at 0.681 nm carrying a value of 1.049. Beyond third minima the RDF attains an almost constant value of 1, indicating that there is no long range correlation.

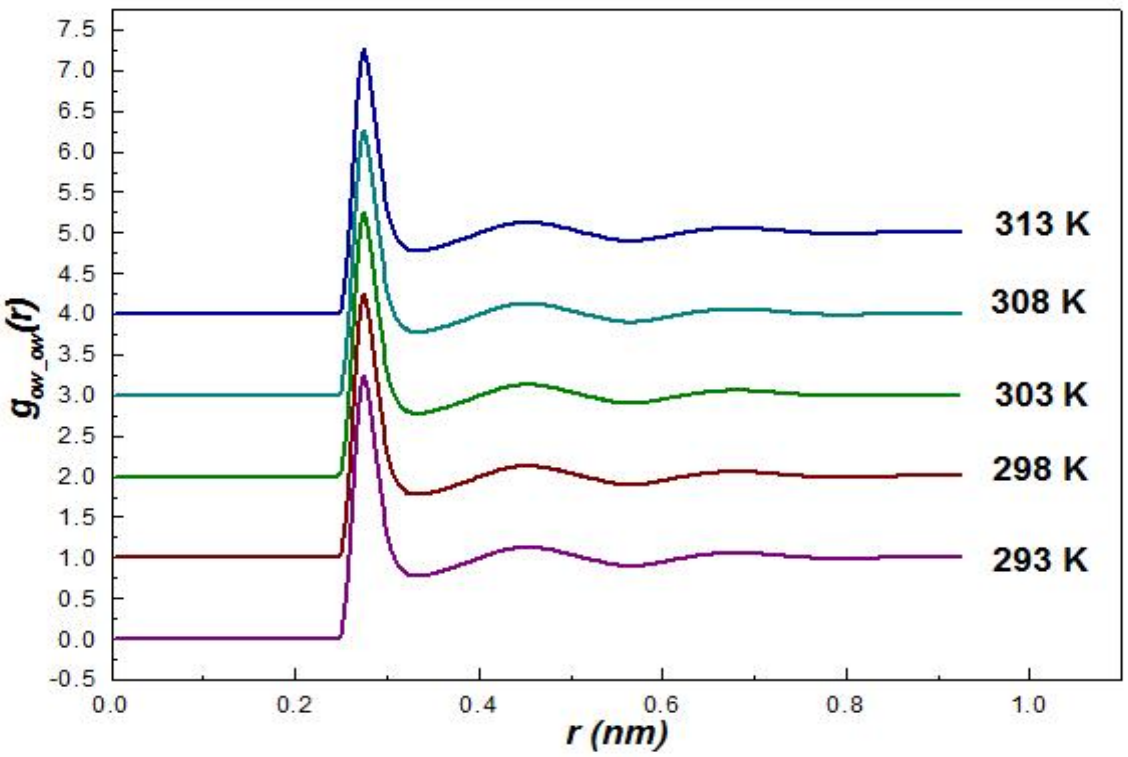

Figure 4.6: The radial distribution functions of oxygen of water molecules, $g_{ow\_ow}(r)$, at different temperatures and corresponding densities.

For the comparative analysis of RDF the radial distribution functions at all temperatures and their corresponding densities are plotted in a single graph which is shown in figure 4.6. It can be seen that the g_{ow_ow} is zero for the radial separation of 0.233 nm for almost all temperatures. Also, the positions of the first peaks for all temperatures are obtained to be at 0.275 nm. But the positions of second peaks are found to fluctuate, especially at higher temperatures. Also it is observed that the heights of the first and second peaks are found to decrease with increasing temperature. However, some fluctuations are observed in the heights of third peaks. Moreover, it is observed in the figure that with the rise in temperature the width of the peaks are increased by very small amount which is primarily due to thermal agitation. The details are summarized in table 4.1. Also for comparison, experimental values at 298 K are presented in the table [14]. This concludes that the simulated values agree well with the experimental values within 5% at maximum.

Simulated values at T(K)	FPP(nm)	FPV	SPP(nm)	SPV	TPP(nm)	TPV
293	0.275	3.258	0.453	1.127	0.673	1.055
298	0.275	3.207	0.453	1.117	0.679	1.053
303	0.275	3.160	0.453	1.107	0.685	1.054
308	0.275	3.110	0.451	1.098	0.681	1.047
313	0.275	3.067	0.455	1.090	0.681	1.049
Experimental values at 298K [14]	0.288	3.090	0.450	1.140	0.673	1.070

Table 4.1: Details of RDF, g_{ow_ow}, at different temperatures and densities.

FPP: First peak position
FPV: First peak value
SPP: Second peak position
SPV: Second peak value
TPP: Third peak position
TPV: Third peak value

4.1.1.2 RDF for Argon

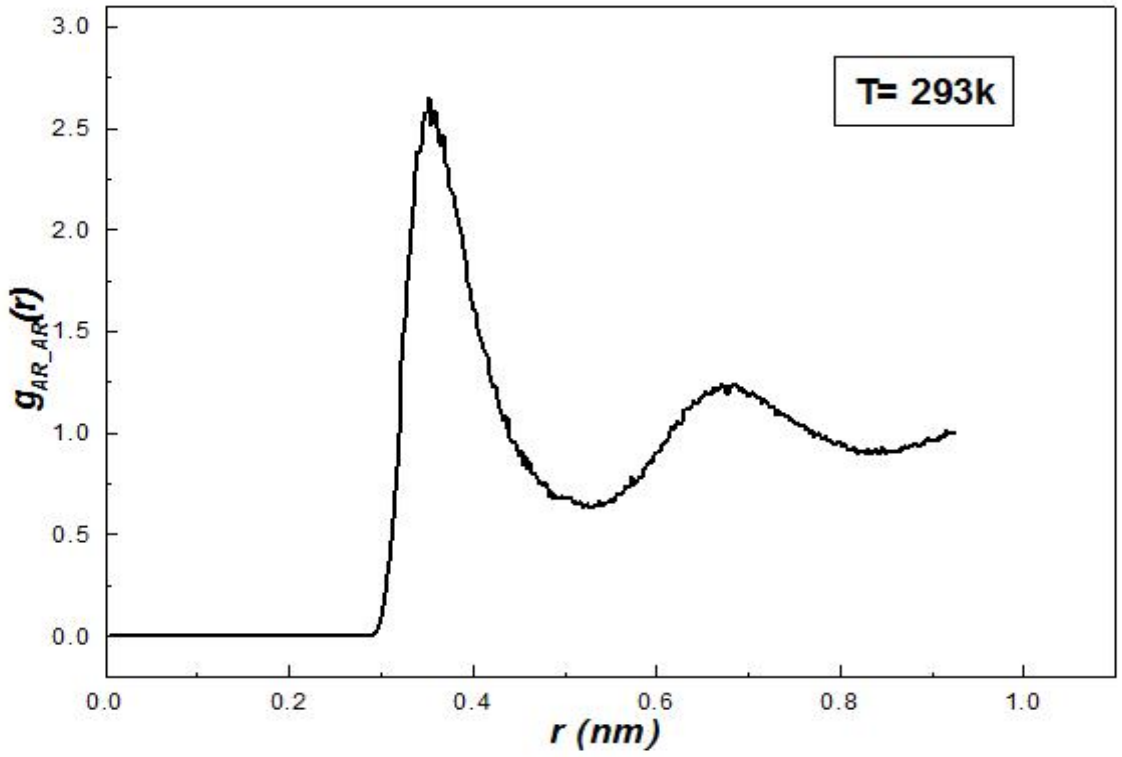

Figure 4.7: The radial distribution function of argon atoms, g_{AR_AR}(r), at temperature 293 K and density 1021.558 kgm^{-3}.

Figure 4.7 is a plot of radial distribution function of argon atoms, $g_{AR\_AR}(r)$, as a function of distance between them. The temperature of the system is 293 K and its density is 1021.558 kgm^{-3}. From the figure, it is obtained that $g_{AR\_AR}(r)$ is zero upto the radial separation of 0.281 nm. The first peak occurs at 0.353 nm at which $g_{AR\_AR}(r)$ is 2.656. So, the nearest-neighbor separation is 0.353 nm which is less than 0.397 nm, the van der Waals radius of argon atom. The second peak occurs at 0.671 nm at which the value of radial distribution function is 1.248. There is no third peak, instead the curve terminates by rising through small value after second minima. The RDF curve is not that smooth as in case of water. The roughness in the curve is due to insufficient statistics caused by a few number of argon atoms in our system.

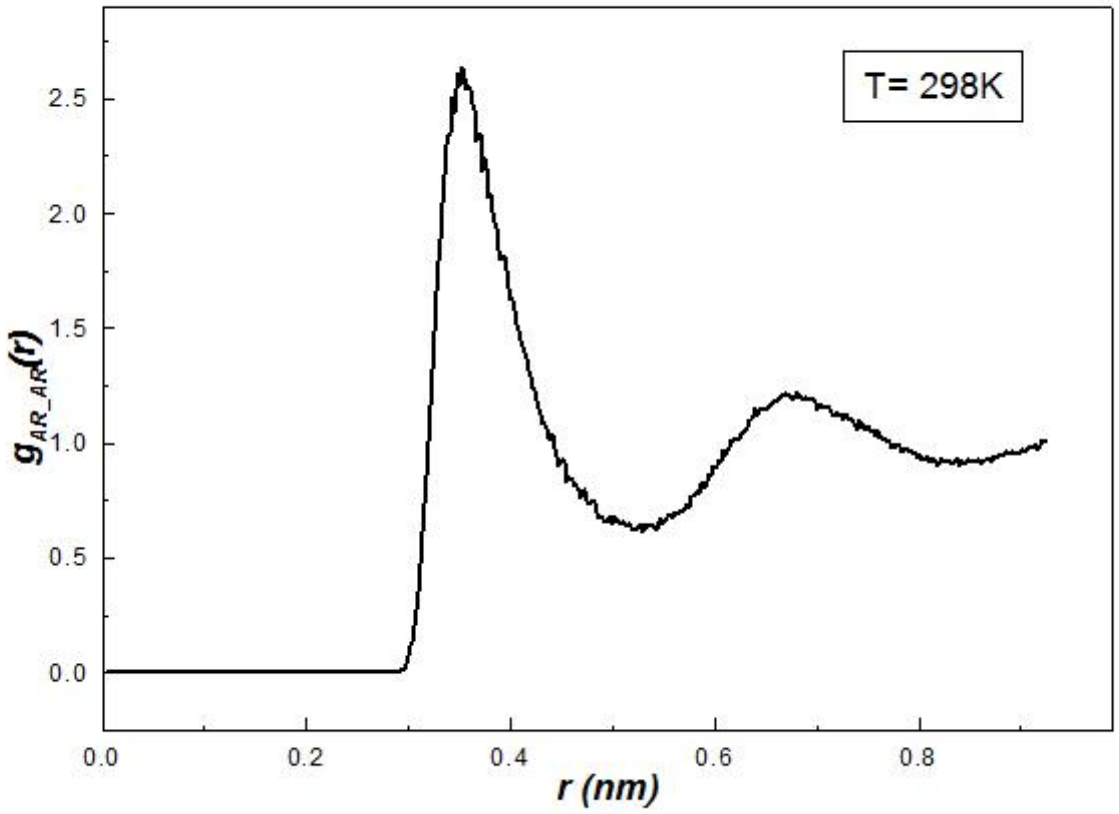

Figure 4.8: The radial distribution function of argon atoms, $g_{AR\_AR}(r)$, at temperature 298 K and density 1018.452 kgm^{-3}.

Figure 4.8 is a variation of radial distribution function of argon atoms, $g_{AR\_AR}(r)$, with the distance between them. The temperature of the system is 298 K and and its density is 1018.452 kgm^{-3}. From the figure, $g_{AR\_AR}(r)$ is zero upto the radial separation of 0.285nm. The first peak occurs at 0.353 nm at which $g_{AR\_AR}(r)$ is 2.63777 nm. So, the nearest-neighbor separation is 0.353 nm which is less than the van der Waals radius of argon atom 0.397 nm. The second peak occurs at 0.681 nm at which $g_{AR\_AR}(r)$ is 1.221. There is no third peak, instead the curve elevates upto a small value beyond the second minima and truncates. This indicates that there is no correlation beyond the second minima.

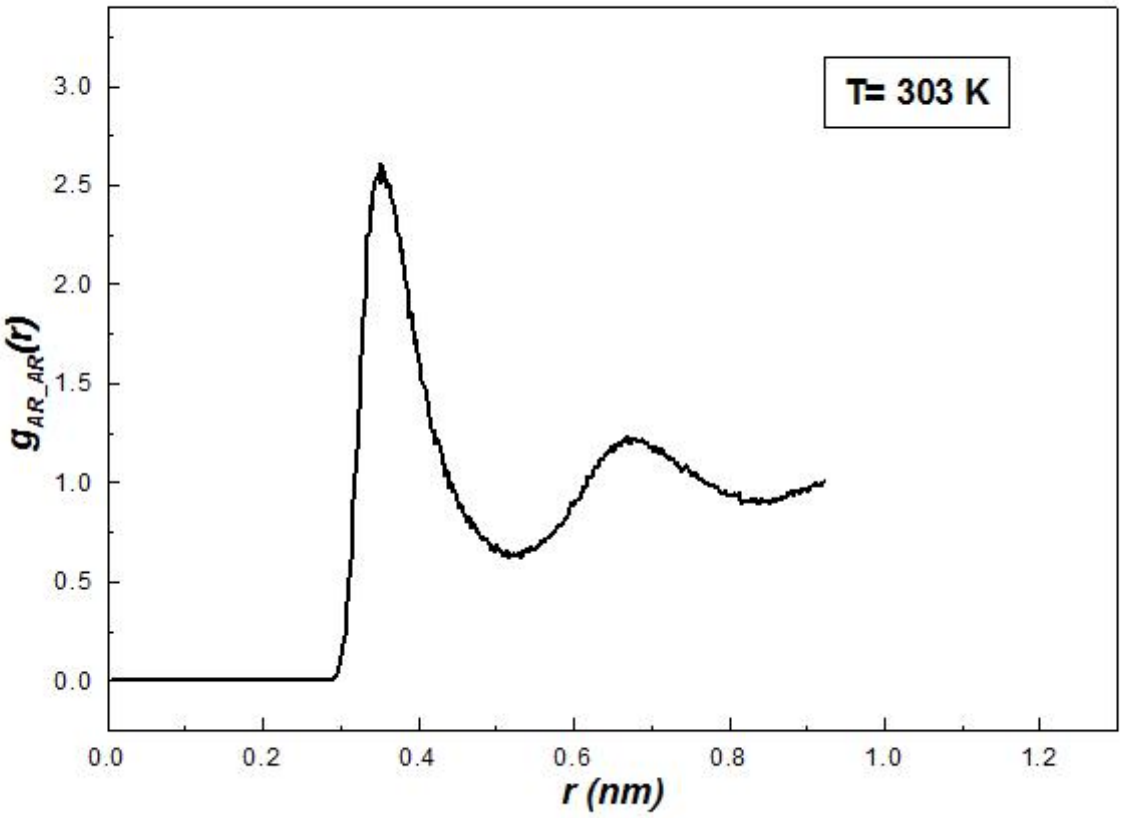

Figure 4.9: The radial distribution function of argon atoms, $g_{AR\_AR}(r)$, at temperature 303 K and density 1014.928 kgm^{-3}.

The variation of radial distribution function of argon atoms, $g_{AR\_AR}(r)$, with the radial separation between them is shown in figure 4.9. The system temperature in this case is 303 K and its density is 1014.928 kgm^{-3}. From the figure, it is obtained that the value of $g_{AR\_AR}(r)$ is zero upto the radial separation of 0.281 nm. The first peak occurs at 0.353 nm at which $g_{AR\_AR}(r)$ is 2.608. Therefore, the nearest-neighbor separation is 0.353 nm less than the van der Waals radius 0.397 nm. The second peak occurs at 0.699 nm at which $g_{AR\_AR}(r)$ is 1.238. The third peak is absent. Beyond the second minima the RDF elevates up to a small value and is truncated. This indicates that there is no correlation beyond the second minima.

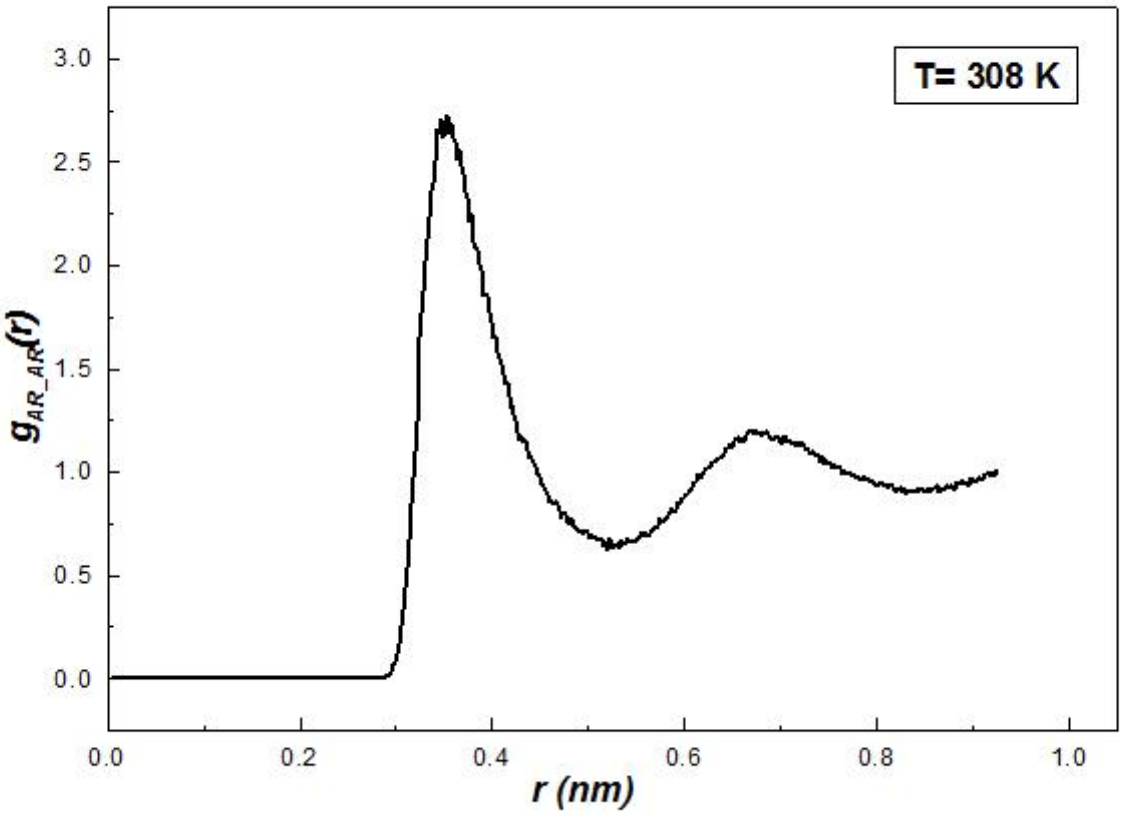

Figure 4.10: The radial distribution function of argon atoms, $g_{AR\_AR}(r)$, at temperature 308 K and density 1011.380 kgm^{-3}.

A sketch of radial distribution function of argon atoms, $g_{AR\_AR}(r)$, as a function of distance between them is shown in the figure 4.10. The system temperature is 308 K and density is 1011.380 kgm^{-3}. The figure shows that $g_{AR\_AR}(r)$ is zero upto the separation of 0.283 nm. The first peak occurs at 0.353 nm at which $g_{AR\_AR}(r)$ is 2.729. Therefore, the nearest-neighbor separation is 0.353 nm which is less than the van der Waals radius of the model argon atom. The second peak occurs at 0.675 nm at which $g_{AR\_AR}(r)$ is 1.208. Again, the third peak is absent and the curve elevates up to a small value beyond the second minima. Then the RDF is truncated, showing no correlation beyond the second minima.

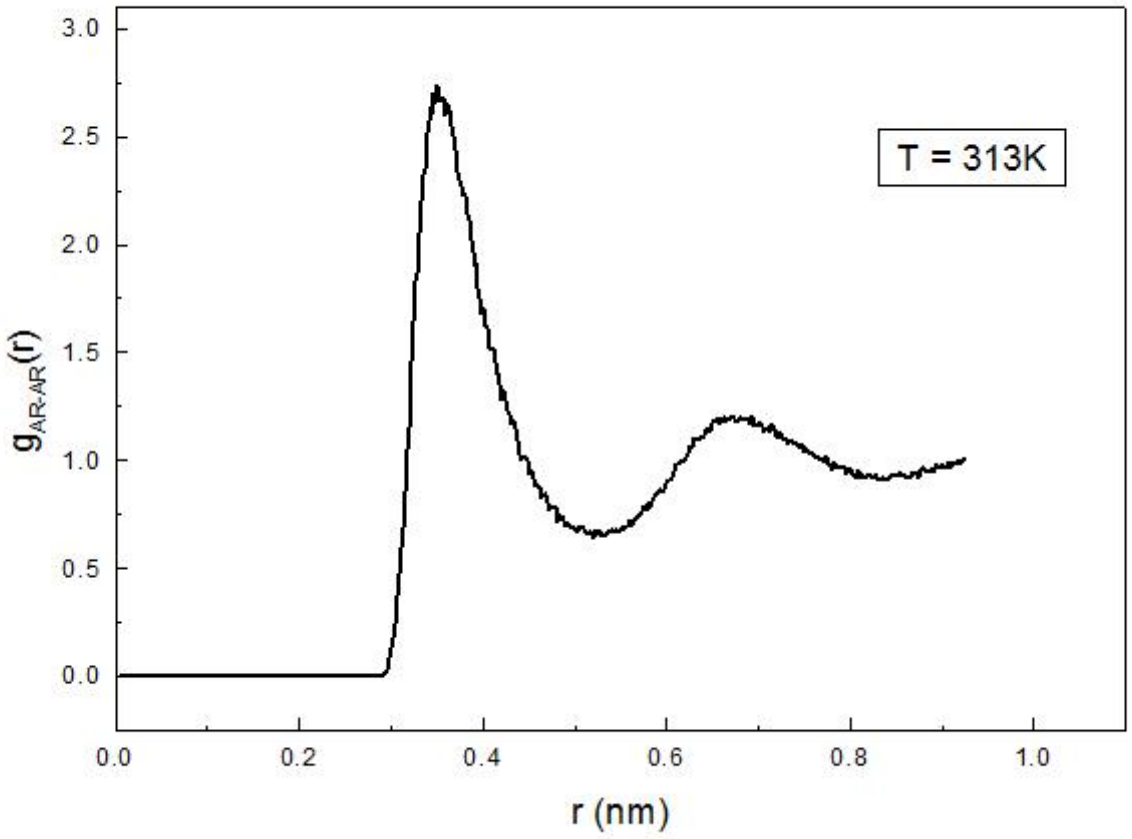

Figure 4.11: The radial distribution function of argon atoms, $g_{AR\_AR}(r)$, at temperature 313 K and density 1008.070 kgm^{-3}.

Figure 4.11 is a plot of radial distribution function of argon atoms, $g_{AR\_AR}(r)$, as a function of separation between them. The temperature of the system is 313 K with the density of 1008.070 kgm^{-3}. The nature of the RDF is same as in other temperatures. It can be seen from the figure that $g_{AR\_AR}(r)$ is zero upto the radial separation of 0.283 nm. The first peak occurs at 0.351 nm at which $g_{AR\_AR}(r)$ is 2.741, so the nearest-neighbor separation is 0.351 nm which is less than the van der Waal's radius of our model argon atom. The second peak occurs at 0.671 nm at which $g_{AR\_AR}(r)$ is 1.205. The curve again elevates by a small value and truncates beyond the second minima. This indicates that beyond the second minima there is no correlation.

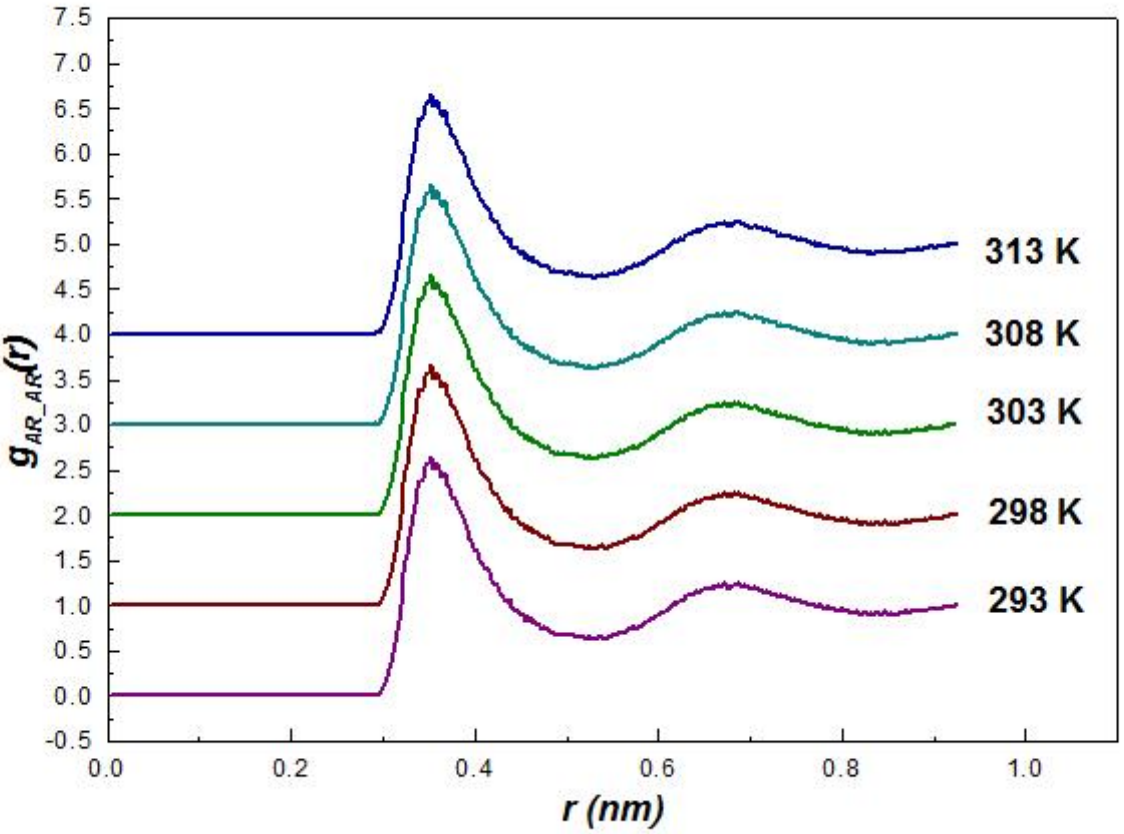

Figure 4.12: The radial distribution functions of argon atoms, $g_{AR\_AR}(r)$, at different temperatures and densities.

For the comparative study of radial distribution function of argon atom at different temperatures and corresponding densities figure 4.12 is referred. As seen from the figure, the radial distance upto which the RDF remains zero for all temperatures is not same but fluctuates by small value around 0.283 nm. The main cause for this fluctuation is due to the lack of smoothness in the curve. The position of first peak for the temperatures 293 K, 298 K, 303 K and 308 K is obtained as 0.353 nm but for 313 K, it is 0.351 nm. The values of first peak decrease with the increase in temperature initially. But, for temperatures 308 K and 313 K this height is found to fluctuate because of the increase in randomness with temperature which is obtained in the form of more irregularity in the RDF. The position of second peak is found to fluctuate while its height is found to decrease with the increase in temperature except at 303 K. The details have been presented in table 4.2. It is also observed that the

T(K)	FPP(nm)	FPV	SPP(nm)	SPV
293	0.353	2.656	0.671	1.248
298	0.353	2.637	0.681	1.221
303	0.353	2.608	0.699	1.238
308	0.353	2.729	0.675	1.208
313	0.351	2.741	0.671	1.205

Table 4.2: Details of the radial distribution function of argon atom, $g_{AR\_AR}(r)$, at different temperatures and densities.

widths of the first and the second peaks increase as the temperature is raised which is basically due to the random thermal motion at higher temperatures. This indicates that as the temperature increases, the argon atoms scatter and become less structured. The radial distribution function of argon calculated above signifies that the argon atoms don't move independently and are correlated to some extent. Although our system contains 5 argon atoms in 212 water molecules, the system cannot be considered to be infinitely dilute.

4.1.1.3 RDF for Water-Argon

This section comprises of the radial distribution functions of solvent with respect to argon atoms g_{AR_OW}(r) at different system temperatures and corresponding system densities.

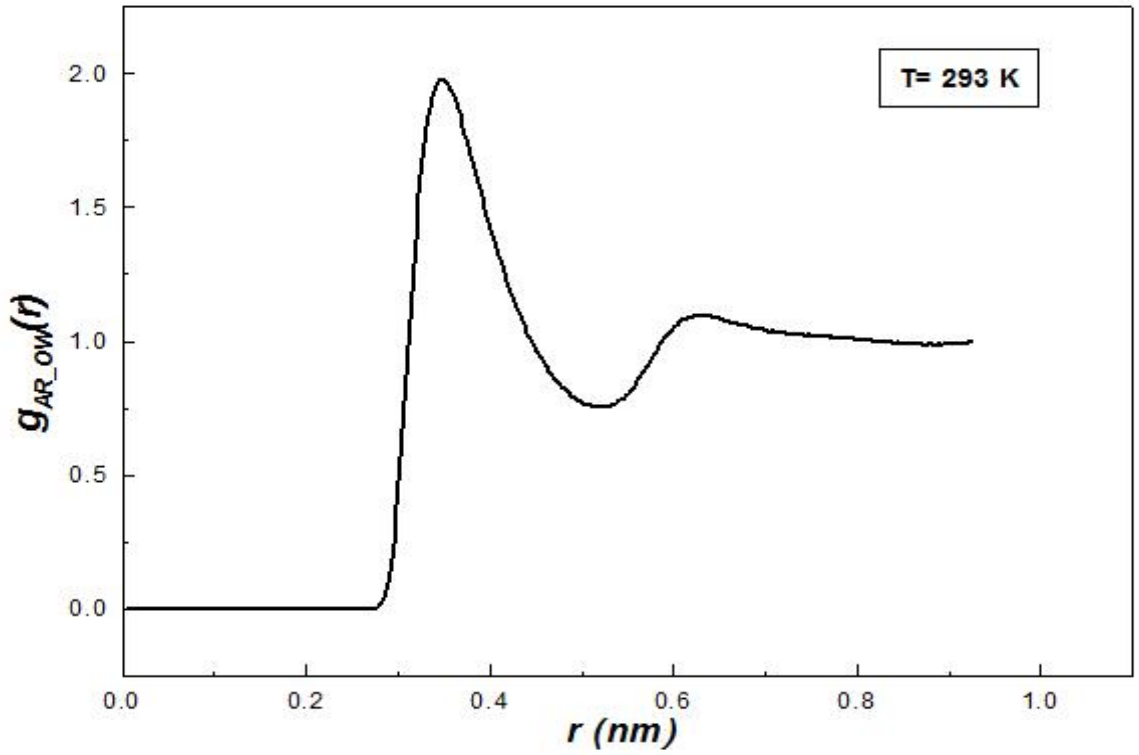

Figure 4.13: The radial distribution function of water molecules with respect to the argon atoms, g_{AR_OW}(r), at temperature 293 K and density 1021.558 kgm^{-3}.

Figure 4.13 is a variation of radial distribution function of water molecules with respect to the argon atoms, g_{AR_OW}(r), with the radial distance between them. The system temperature is 293 K and its density is 1021.558 kgm^{-3}. The value of g_{AR_OW}(r) is zero upto the separation of 0.263 nm. The first peak occurs at 0.347 nm at which g_{AR_OW}(r) is 1.98121. So, the nearest-neighbor separation is 0.347 nm which is less than 0.376 nm, the van der Waals radius of argon-water combination. The second peak occurs at 0.631 nm at which g_{AR_OW}(r) is 1.094. In this case the second peak is weakly defined. The RDF falls shortly after second peak,thereby attaining an almost constant value of 1 . This implies that there is no long range correlation between the argon and solvent molecules.

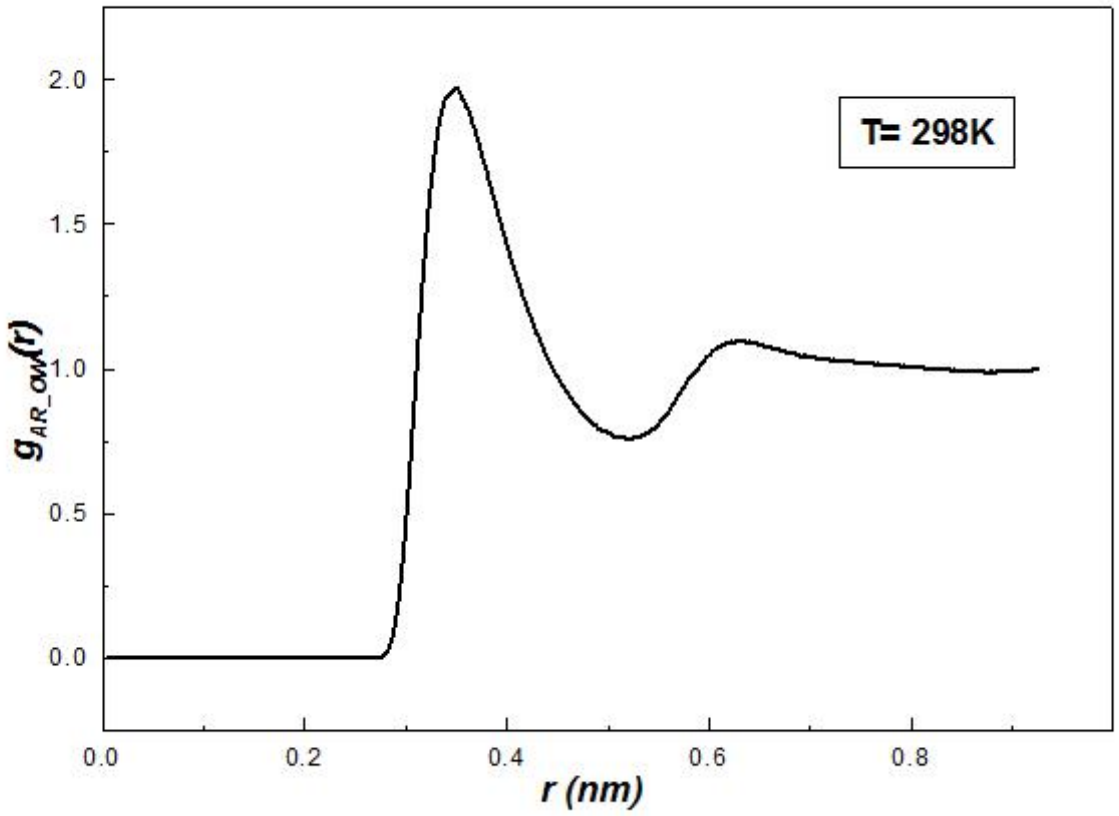

Figure 4.14: The radial distribution function of water molecules with respect to the argon atoms, g_{AR_OW}(r), at temperature 298 K and density 1018.452 kgm^{-3}.

Figure 4.14 is a plot of radial distribution function, g_{AR_OW}(r), as a function of radial separation at temperature 298 K and density 1018.452 kgm^{-3}. In this case, the value of g_{AR_OW}(r) is zero upto the separation of 0.261 nm. The first peak occurs at 0.347 nm at which g_{AR_OW}(r) is 1.967. So, the nearest-neighbor separation is 0.347 nm which is less than the van der Waals radius. The second peak occurs at 0.629 nm at which g_{AR_OW}(r) is 1.092. In this case too, the RDF falls shortly after second peak, thereby attaining an approximately constant value of 1 indicating no long range correlations between argon and water.

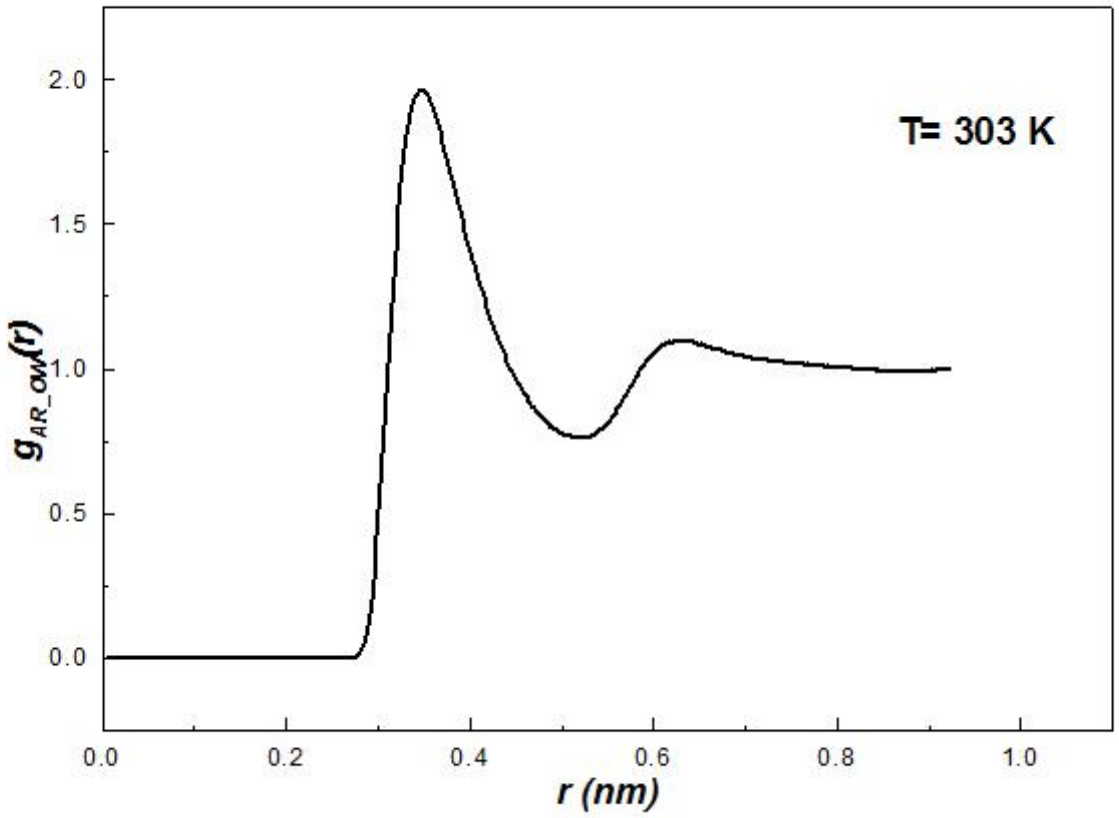

Figure 4.15: The radial distribution function of water molecules with respect to the argon atoms, g_{AR_OW}(r), at temperature 303 K and density 1014.928 kgm^{-3}.

Figure 4.15 is a plot of radial distribution function, g_{AR_OW}(r), as a function of radial separation at temperature 303 K and density 1014.928 kgm^{-3}. From the figure, the value of $g_{AR-OW}(r)$ is zero upto the radial separation of 0.263 nm. The first peak occurs at 0.347 nm at which g_{AR_OW}(r) is 1.968. Therefore, the nearest-neighbor separation is 0.347 nm which is less than the van der Waals radius. The second peak occurs at 0.631 nm at which g_{AR_OW}(r) is 1.097. Again after second peak, the RDF falls shortly, attaining approximately the constant average value of 1. This indicates that there is no long range correlation.

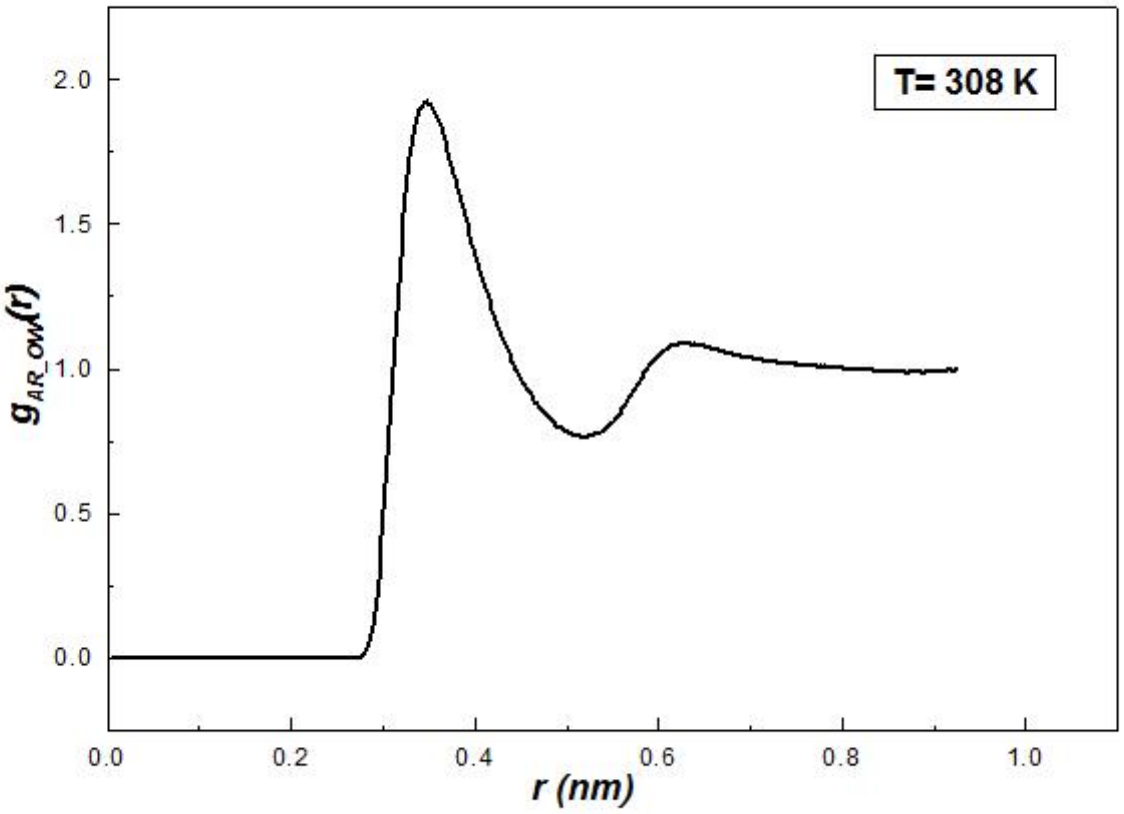

Figure 4.16: The radial distribution function of water molecules with respect to the argon atoms, g_{AR_OW}(r), at temperature 308 K and density 1011.380 kgm^{-3}.

Figure 4.16 is a variation of radial distribution function, g_{AR_OW}(r), with the separation between the argon atoms and water molecules at temperature 308 K and density 1011.380 kgm^{-3}. The value of The excluded region for argon atoms is confined within 0.261 nm where g_{AR_OW}(r) is obtained as zero upto the radial separation of 0.261 nm. The first peak in this case occurs at 0.349 nm at which g_{AR_OW}(r) is 1.924. So, the nearest-neighbor separation is 0.349 nm which is less than the van der Waal's radius taken in the model. The second peak occurs at 0.629 nm at which $g_{AR-OW}(r)$ is 1.086. After second peak the RDF falls shortly, thereby attaining an approximately constant value of 1. The constant value indicates that there is no long range correlation.

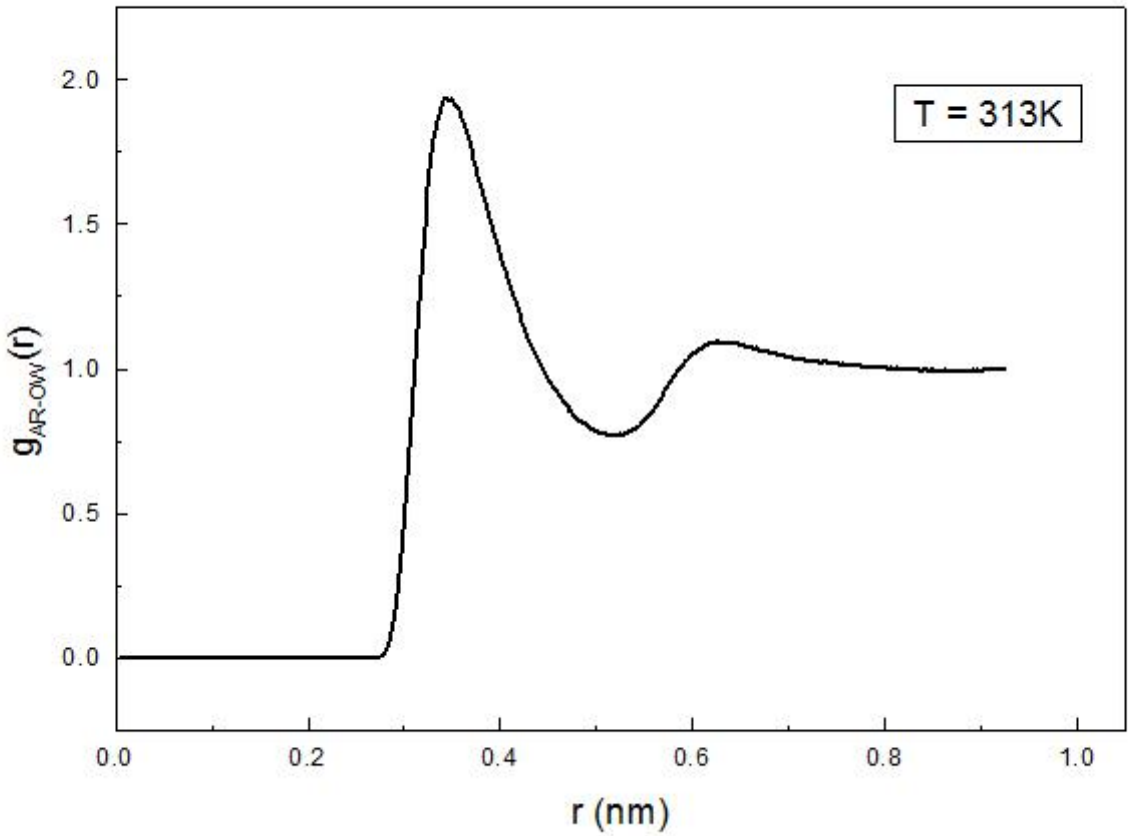

Figure 4.17: The radial distribution function of water molecules with respect to the argon atoms, g_{AR_OW}(r), at temperature 313 K and density 1008.070 kgm^{-3}.

Figure 4.17 is a plot of radial distribution function, g_{AR_OW}(r), as a function of radial separation at temperature 313 K and density 1008.070 kgm^{-3}. The value of g_{AR_OW}(r) is found to be zero upto the radial separation of 0.261 nm. The first peak occurs at 0.343 nm at which $g_{AR-OW}(r)$ is 1.936. So, the nearest-neighbor separation is 0.343 nm which is less than the van der Waals radius. The second peak occurs at 0.625 nm at which g_{AR_OW}(r) is 1.093. Also in this case, the RDF falls shortly after second peak and quickly attains almost constant value of 1, thereby indicating the absence of long range correlations as before. The

radial distribution functions at different temperatures and densities is shown in figure 4.18 for their comparative analysis. From the figure it is seen that the value of RDF remains

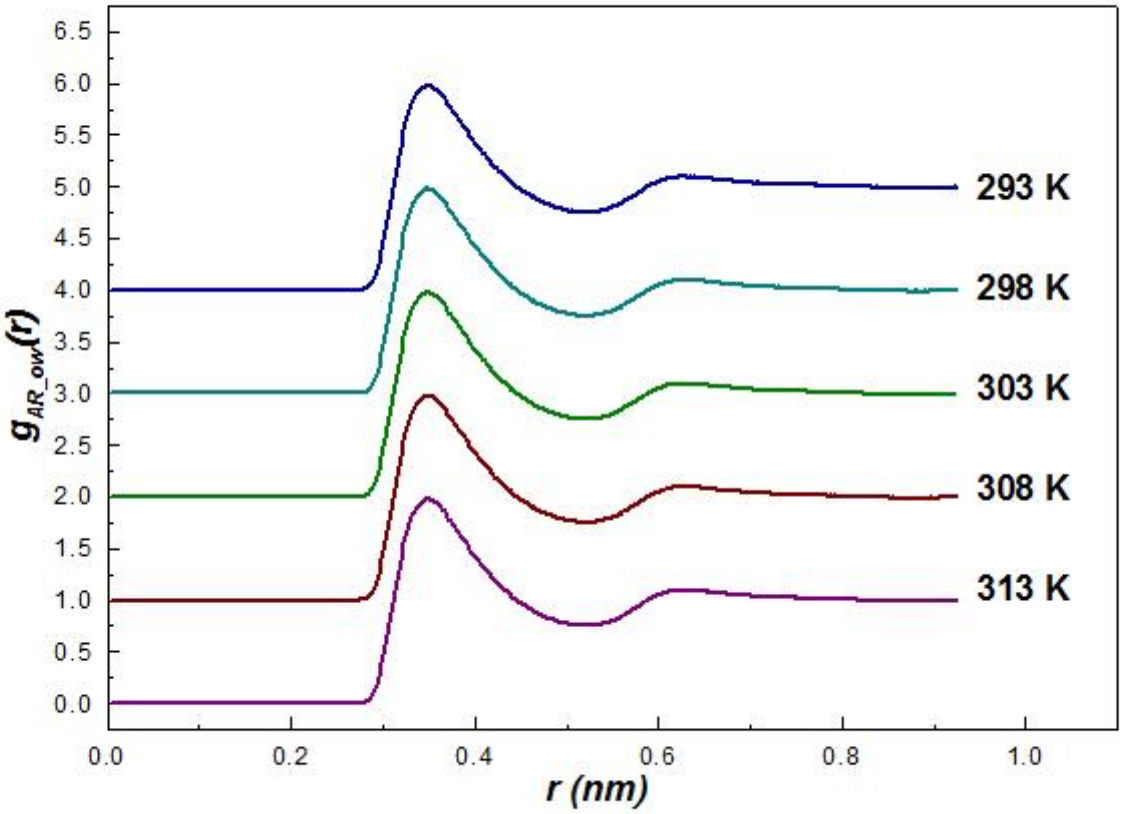

Figure 4.18: The radial distribution functions of water molecules with respect to the argon atoms, g_{AR_OW}(r), at different temperatures and densities.

zero at all temperatures within the radial separation of 0.263 nm. The position of first peak for the temperatures 293 K, 298 K, and 303 K is 0.347 nm but for 308 K and 313 K, it fluctuates. The position of second peak as well as the heights of both the first and second peaks fluctuate in this case. The fluctuations can arise due to the non uniform interaction between the argon atoms and water molecules, lack of statistics and the random thermal motion of the atoms and molecules. The details of the analysis of RDF's are presented in the table 4.3.

T(K)	FPP(nm)	FPV	SPP(nm)	SPV
293	0.347	1.981	0.631	1.094
298	0.347	1.967	0.629	1.092
303	0.347	1.968	0.631	1.097
308	0.349	1.924	0.629	1.086
313	0.343	1.936	0.625	1.093

Table 4.3: Details of the radial distribution function of solvent molecules with respect to argon atoms, g_{AR_OW}(r), at different temperatures and densities.

Moreover, it is observed that the width of the peaks increase as the temperature increases. This is basically due to the random thermal motion of the atoms and molecules at higher temperatures. This also signifies that the correlation between argon and water molecules decreases as temperature is increased.

4.1.2 Energy Profile

In this section, various energy of the system at different temperatures are calculated and analyzed. The energies comprise of Lennard-Jones, Couomb, Potential, Kinetic and the Total energy of the system. All these energies are evaluated after the production run. The program used by the GROMACS for the energy calculation is *g_energy*. This program extracts energy components or distance restraint data from an energy file the energy terms can be selected as desired. It uses the file *ener.edr* as input and gives *energy.xvg* as output. The total potential energy is the sum of the Lennard-Jones energy and the Coulomb potential energy. As we have used cutoff Lennard-Jones and Coulomb potential, the atoms and molecules will experience only short-range interaction. Therefore, the calculated potential energy from the simulation data contains only short range contribution. Besides, it is also analyzed how the energies vary with temperatures. The variations in energy with time is plotted for different temperatures using the computer software ORIGIN50 and the results are analyzed from the graphs thus obtained.

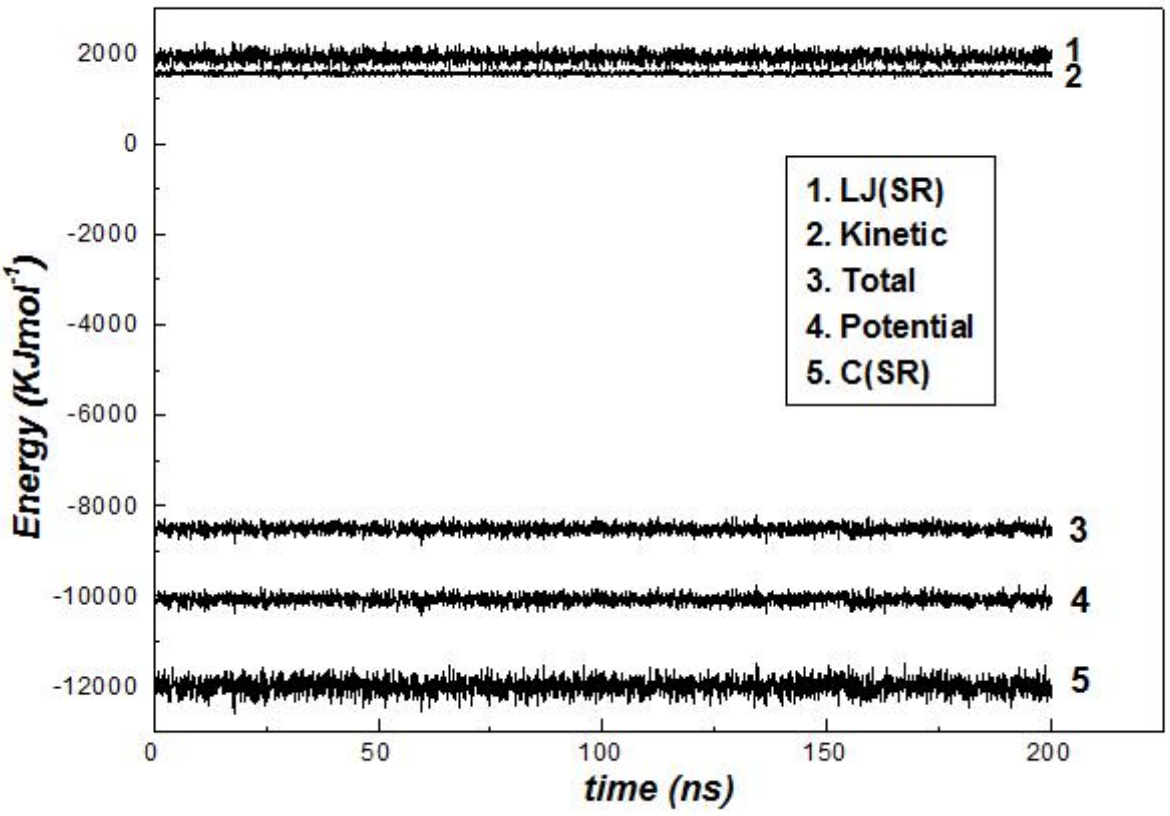

Figure 4.19: Energy profile for the system at temperature 293 K.

Figure 4.19 is the variation of different energies of the system in kJmol^{-1} with time in ns. The system temperature is 293 K. From the figure, it is seen that the LJ energy is positive with an average of 1917.749±0.212 kJmol^{-1}. The Coulomb energy is negative with an average value of -11995.976±0.326 kJmol^{-1}. Therefore, the total potential energy is -10078.227±0.184 kJmol^{-1}. The average kinetic energy at this temperature is obtained as 1564.864±0.061 kJmol^{-1}. The average total energy is -8513.363±0.175 kJmol^{-1}. The total energy in negative signifies that the system is stable.

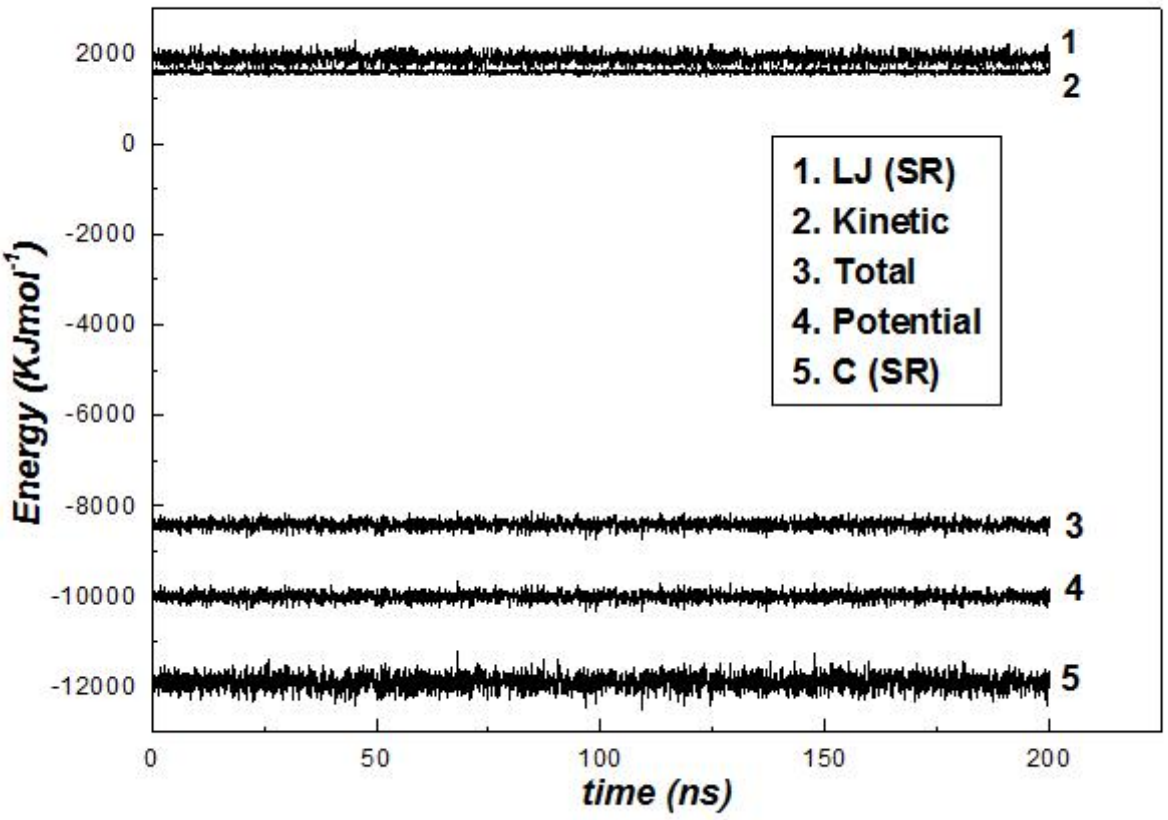

Figure 4.20: Energy profile for the system at temperature 298 K.

Figure 4.20 is the variation of different energies of the system in kJmol^{-1} with time in ns. The system temperature is 298 K. From the figure, it is seen that the LJ energy is positive with an average value of 1894.818±0.212 kJmol^{-1}. The Coulomb energy is negative with an average value of -11905.504±0.327 kJmol^{-1}. Therefore, the total potential energy is -10010.686±0.185 kJmol^{-1}. The average kinetic energy at this temperature is obtained as 1591.639±0.062 kJmol^{-1}. The average total energy is -8419.046±0.176 kJmol^{-1}. The total energy is negative which signifies that the system is stable.

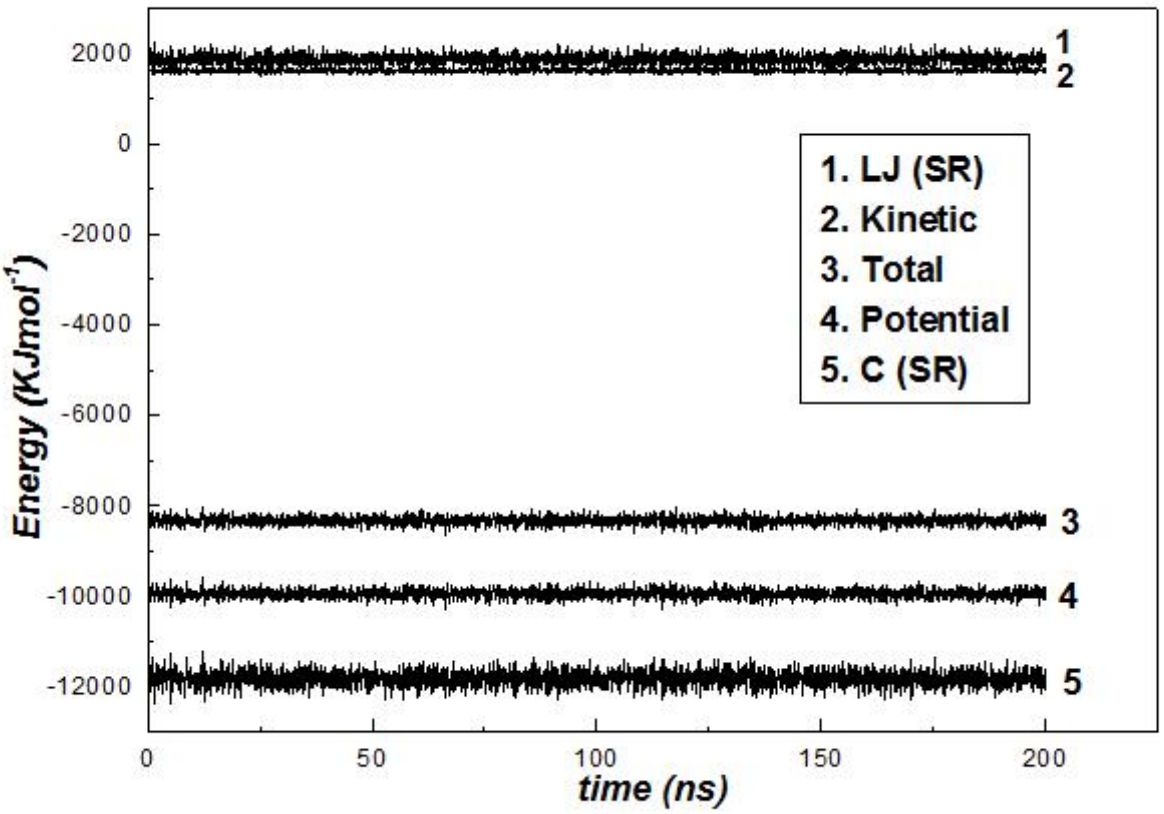

Figure 4.21: Energy profile for the system at temperature 303 K.

Figure 4.21 is the variation of different energies of the system in kJmol^{-1} with time in ns. The system temperature is 303 K. From the figure, it is seen that the LJ energy is positive with an average value of 1877.368±0.213 kJmol^{-1}. The Coulomb energy is negative with an average value of -11828.342±0.327 kJmol^{-1}. Therefore, the total potential energy is -9950.973±0.185 kJmol^{-1}, which is also negative. The kinetic energy at this temperature is 1618.401±0.062 kJmol^{-1} which is positive. The average total energy is -8332.571±0.176 kJmol^{-1}. The negative total energy therefore signifies that the system is stable.

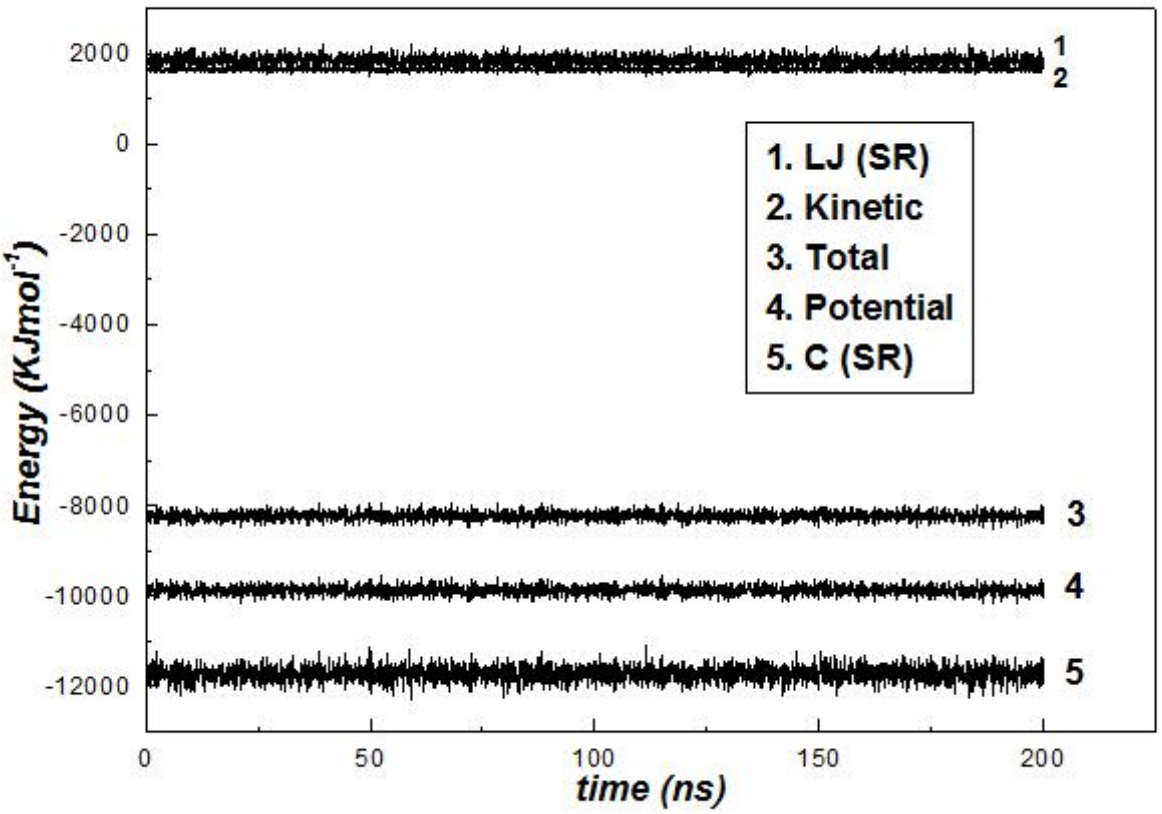

Figure 4.22: Energy profile for the system at temperature 308 K.

Figure 4.22 is the variation of different energies of the system in kJmol^{-1} with time in ns. The system temperature is 308 K. From the figure, it is seen that the LJ energy is positive with an average value of 1847.337±0.213 kJmol^{-1}. The Coulomb energy is negative with an average value of -11724.102±0.328 kJmol^{-1}. Therefore, the total potential energy is -9876.764±0.186 kJmol^{-1} which is negative as well. The average kinetic energy at this temperature is 1645.042±0.064 kJmol^{-1}. The average total energy is -8231.721±0.177 kJmol^{-1}. The negative total energy signifies that the system is stable.

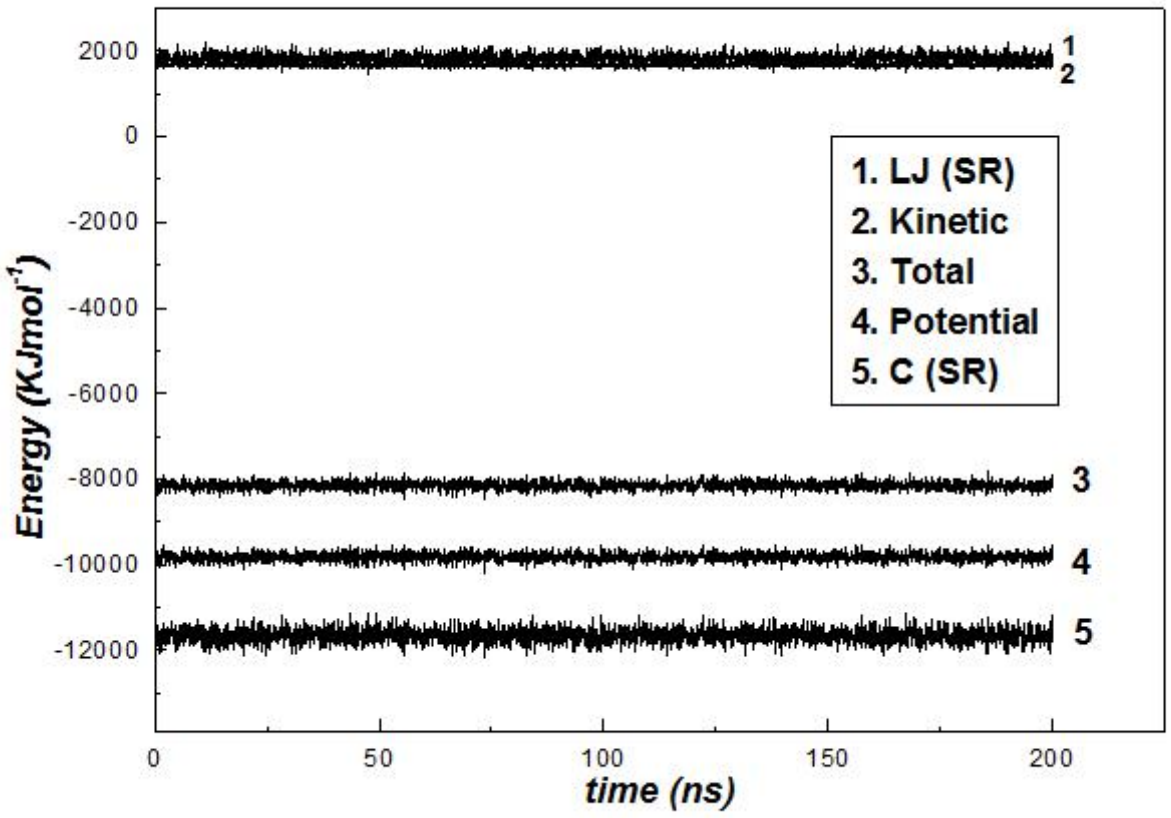

Figure 4.23: Energy profile for the system at temperature 313 K.

Figure 4.23 is the variation of different energies of the system in kJmol^{-1} with time in ns. The system temperature is 313 K. From the figure, it is seen that the LJ energy is positive with an average value of 1833.535±0.214 kJmol^{-1}. The Coulomb energy is negative with an average value of -11655.965±0.328 kJmol^{-1}. Therefore, the total potential energy is -9822.429±0.187 kJmol^{-1} which is negative. The average kinetic energy at this temperature is 1671.760±0.065 kJmol^{-1}. The average total energy is -8150.668±0.177 kJmol^{-1}. The total energy is negative which signifies that the system is stable.

It can be concluded from the above results that as the temperature increases the Lennard-Jones energy decreases while the Coulomb increases (decreases in negative). The potential energy is also found to decrease in negative with the rise in temperature. The kinetic energy increases with the rise in temperture which is quite obvious. The total energy is found to decrease in negative.

4.1.3 Diffusion Coefficients

In this section, the self-diffusion coefficient of solvent (water) and argon gas are estimated separately by using Einstein's relation (see chapter 2, section 2.1.22). This relation can be restated as:

$$D_\alpha = \lim_{t\to\infty} \frac{< (r_\alpha(t+t_i) - r_\alpha(t_i))^2 >}{6t}. \tag{4.1}$$

where α denotes the type of the component (solvent or argon), t_i is any time origin. The angled brackets $< ... >$ indicate that an ensemble average has been taken. The ensemble average is over all atoms of the component α in the simulation and all time origins [14]. In GROMACS, the program ***g_msd*** is used to calulate the self diffusion coefficient of argon and water separately. This program produces a data file of average mean-squared displacement as a function of time, *msd.xvg*. The time steps taken for the calculation of MSD is 10 ps. The production run time in our case is 200 ns for all temperatures. But for argon, the better statistics is obtained only within 2.5 ns. So, the data is truncated for 2.5 ns and then plotted by using ORIGIN50 to obtain a straight line. The self diffusion coefficients are then given by the slope of the linear fit of MSD versus time graph.

The self diffusion coefficients thus obtained are used to calculate the mutual diffusion coefficients of argon in water by invoking Darken's relation (see chapter 2, section 2.1.22). Also the temperature dependence of the diffusion coefficients are analysed. The results have been shown in figures 4.25-4.35.

4.1.4 Self-diffusion Coefficient of Argon

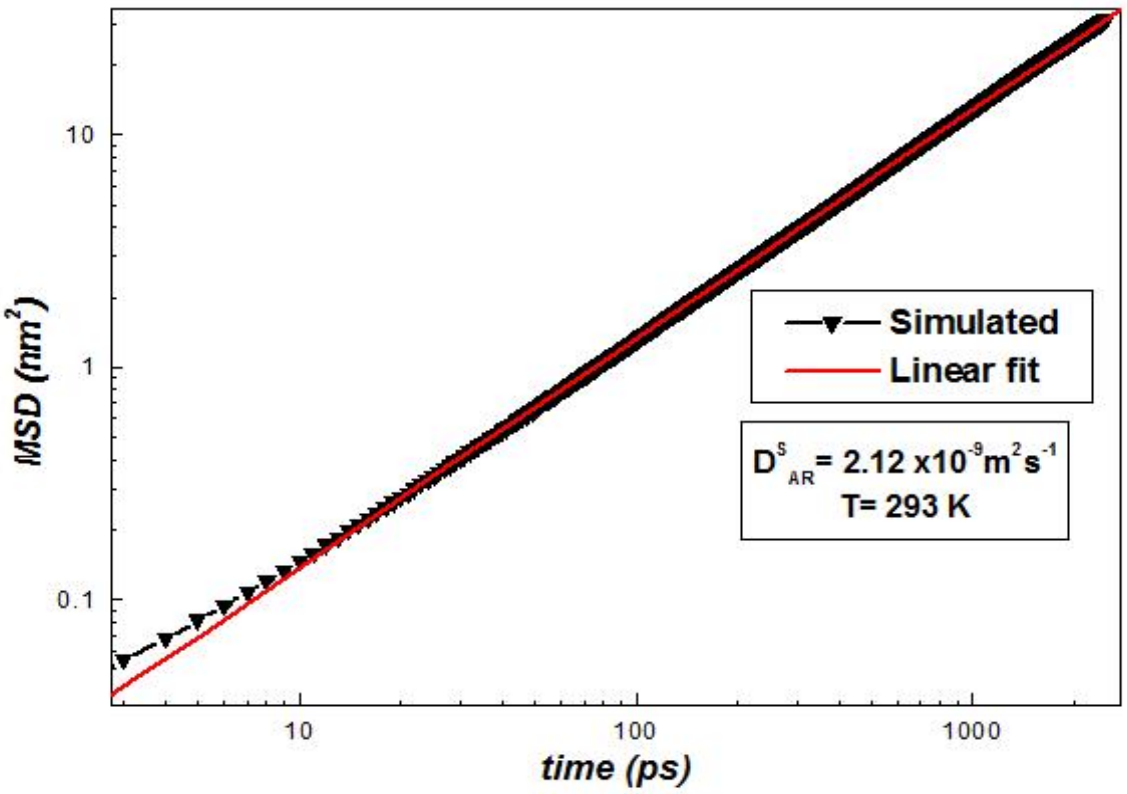

Figure 4.24: Mean-squared displacement of argon atoms as a function of time at temperature 293 K.

The time dependence of MSD for argon at temperature 293 K is plotted in figure 4.24 which is double logarithmic plot. For short times, less than 9 ps, it is seen that the MSD varies with the square of the time. This increment of MSD with time is due to the ballistic motion of atoms, that is, the atom flies in a straight line with constant speed before collisions with the water molecules, slow it down and randomize its direction. The ballistic motion is dominated by the inertia of the particle and its surrounding fluid. For longer times, the values of MSD are in proportion to time. The atomic motion in this case becomes diffusive. In the diffusive regime, all inertia effects die out and the motion is completely random. The diffusive regime where MSD is linear function of time, starts beyond 9 ps and extends up to 2.5 ns. The self-diffusion coefficient is calculated by fitting a straight line in the diffusive regime. The calculated value of self-diffusion coefficient, D^S_{AR}, is 2.12×10^{-9} m^2s^{-1}. The error obtained is insignificant.

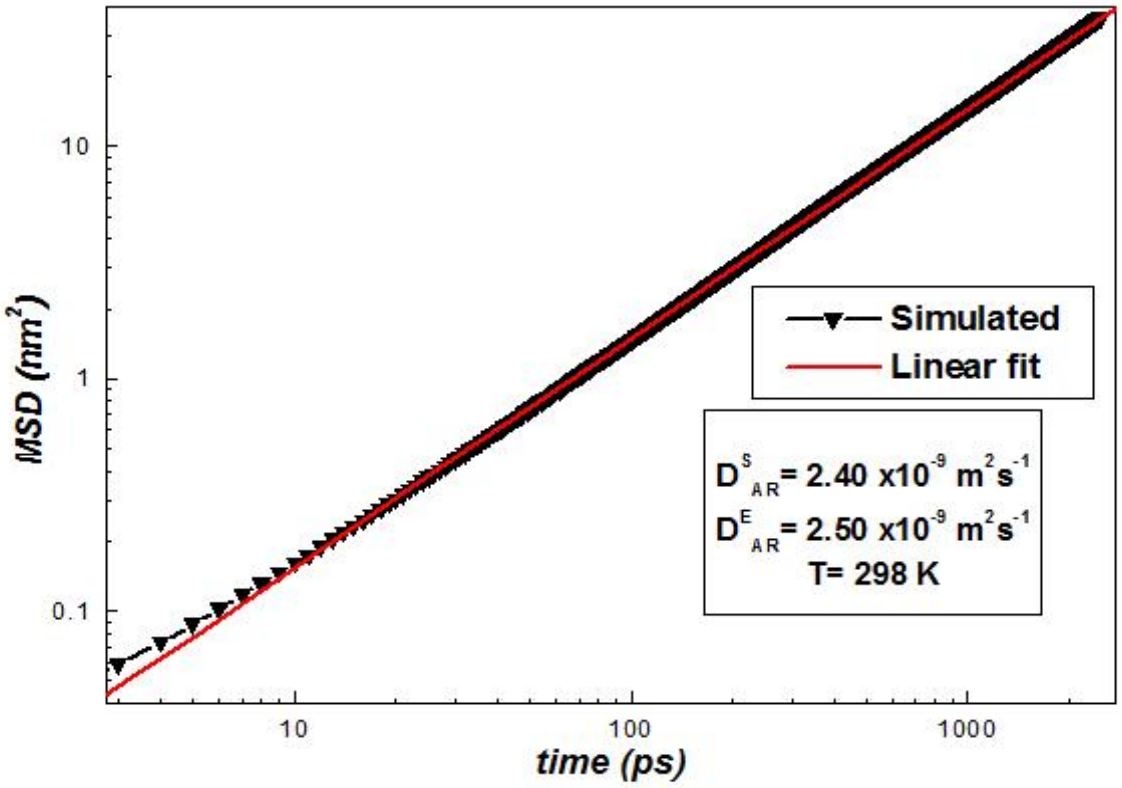

Figure 4.25: Mean-squared displacement for argon atoms as a function of time at temperature 298 K.

The time dependence of MSD for argon at temperature 298 K is plotted in figure 4.25 which is double logarithmic plot. For short times, less than 9 ps, there is a ballistic regime. Beyond that the MSD varies linearly with time and is diffusive regime which extends to 2.5 ns. The calculated value of self-diffusion coefficient, D^S_{AR}, is 2.40×10^{-9} m^2s^{-1} and that from the experiment, D^E_{AR} is $(2.50\pm0.01)\times10^{-9}$ m^2s^{-1}. The error in simulated value is insignificant. Also the simulated value agrees the experimental value within 4%.

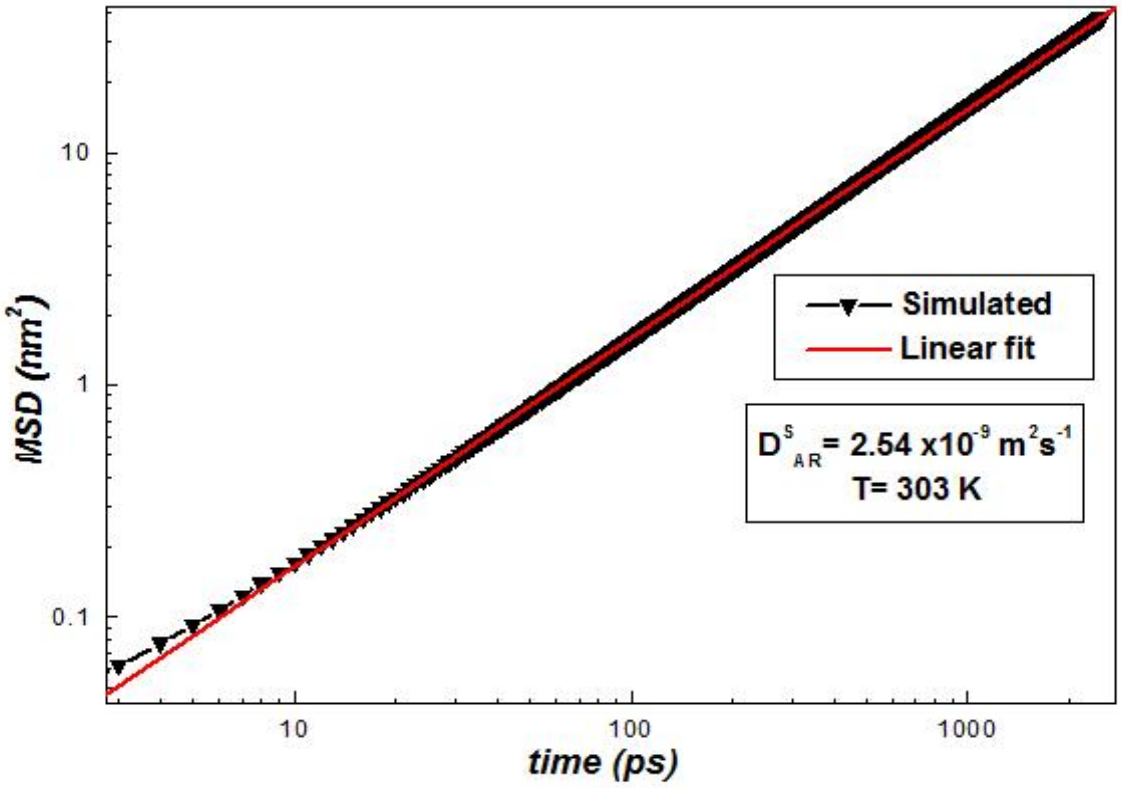

Figure 4.26: Mean-squared displacement for argon atoms as a function of time at temperature 303 K.

The time dependence of MSD for argon at temperature 303 K is plotted in figure 4.26 which is double logarithmic plot. As seen in the figure, the curve has parabolic nature in around and below 9 ps. This attributes to the ballistic motion of the atoms. The diffusive motion starts beyond that and extends to 2.5 ns. The calculated value of self-diffusion coefficient, D^S_{AR}, is 2.54×10^{-9} m^2s^{-1}. The error is insignificant.

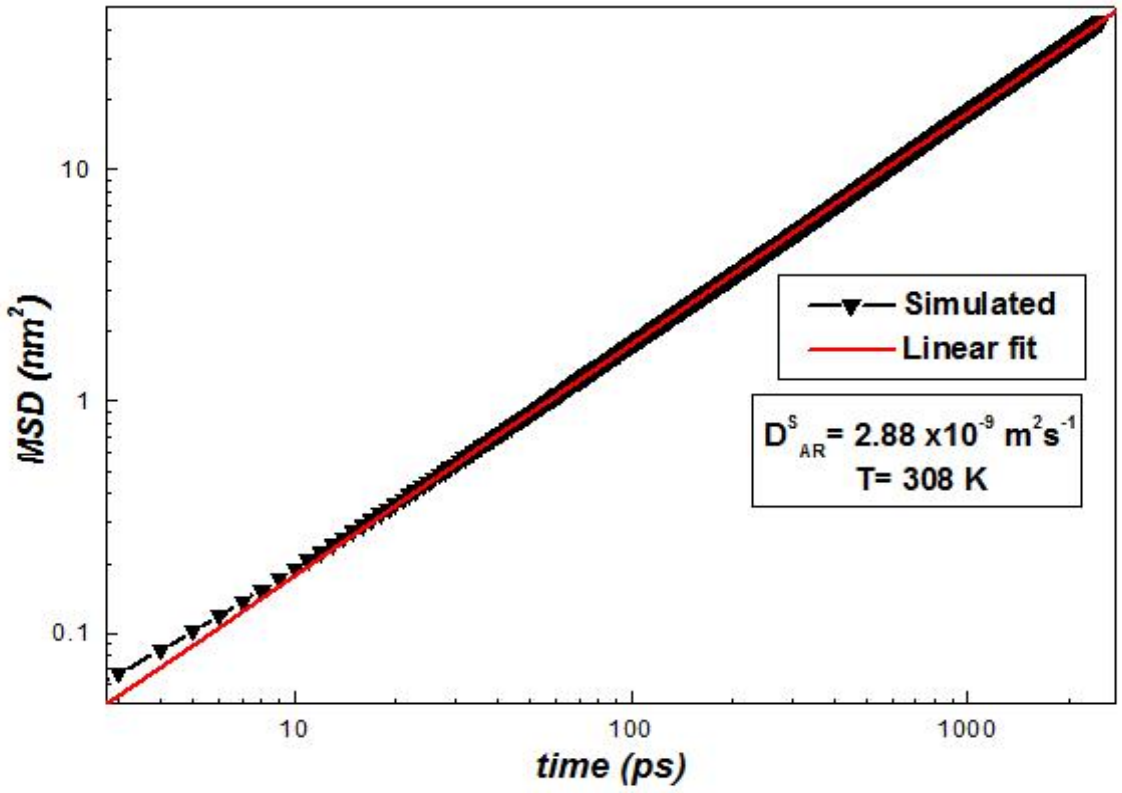

Figure 4.27: Mean-squared displacement for argon atoms as a function of time at temperature 308 K.

The time dependence of MSD for argon at temperature 308 K is plotted in figure 4.27 which is double logarithmic plot. For short times, less than 9 ps, there is again a ballistic regime. Beyond that the MSD varies linearly with time and is known as diffusive regime which extends to 2.5 ns. The calculated value of self-diffusion coefficient, D^S_{AR}, is 2.88×10^{-9} m^2s^{-1}. The error is insignificant.

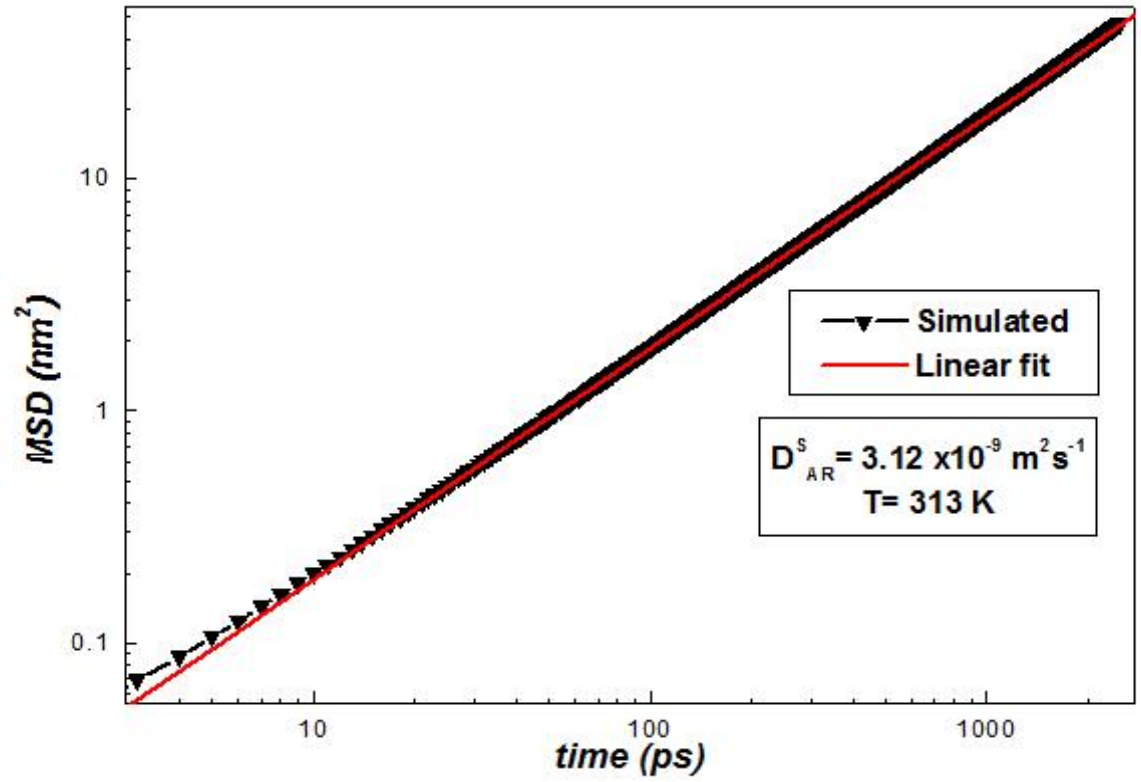

Figure 4.28: Mean-squared displacement for argon atoms as a function of time at temperature 313 K.

The time dependence of MSD for argon at temperature 313 K is plotted in figure 4.28 which is double logarithmic plot. For short times in and around 9 ps, there is a ballistic regime. Beyond that the MSD varies linearly with time and is known as diffusive regime which extends to 2.5 ns. The calculated value of self-diffusion coefficient, D^S_{AR}, is 3.12×10^{-9} m^2s^{-1}. The error obtained in the simulated value is insignificant.

T(K)	$D^S_{AR}(10^{-9}m^2s^{-1})$	$D^E_{AR}(10^{-9}m^2s^{-1})$[27]	% ERROR
293	2.12	–	–
298	2.40	2.50±0.01	3.88
303	2.54	–	–
308	2.88	–	–
313	3.12	–	–

Table 4.4: Details of the self-diffusion coefficients of argon at different temperatures and corresponding densities.

The self diffusion coefficients thus obtained from the simulation at different temperatures along with the experimental values (if available) are presented in table 4.4. From the table it can be seen that the self-diffusion coefficient at 298 K from simulation has a good agreement with the experimental value within 3.88% [27]. It can also be seen that the self diffusion coefficient increases with the rise in temperature. The reason behind it is that, the generated velocities of the argon atoms increase as the temperature increases. Because of these, the mean-squared displacement increases and according to the Einstein's relation self diffusion coefficient also increases. This variation is also consistent with the increase in width of the radial distribution function g_{AR_OW}(r) with the rise in temperature. Therefore, when the width increases, the second maxima becomes less defined increasing the diffusion coefficient [14].

4.1.5 Self-diffusion Coefficient of Water

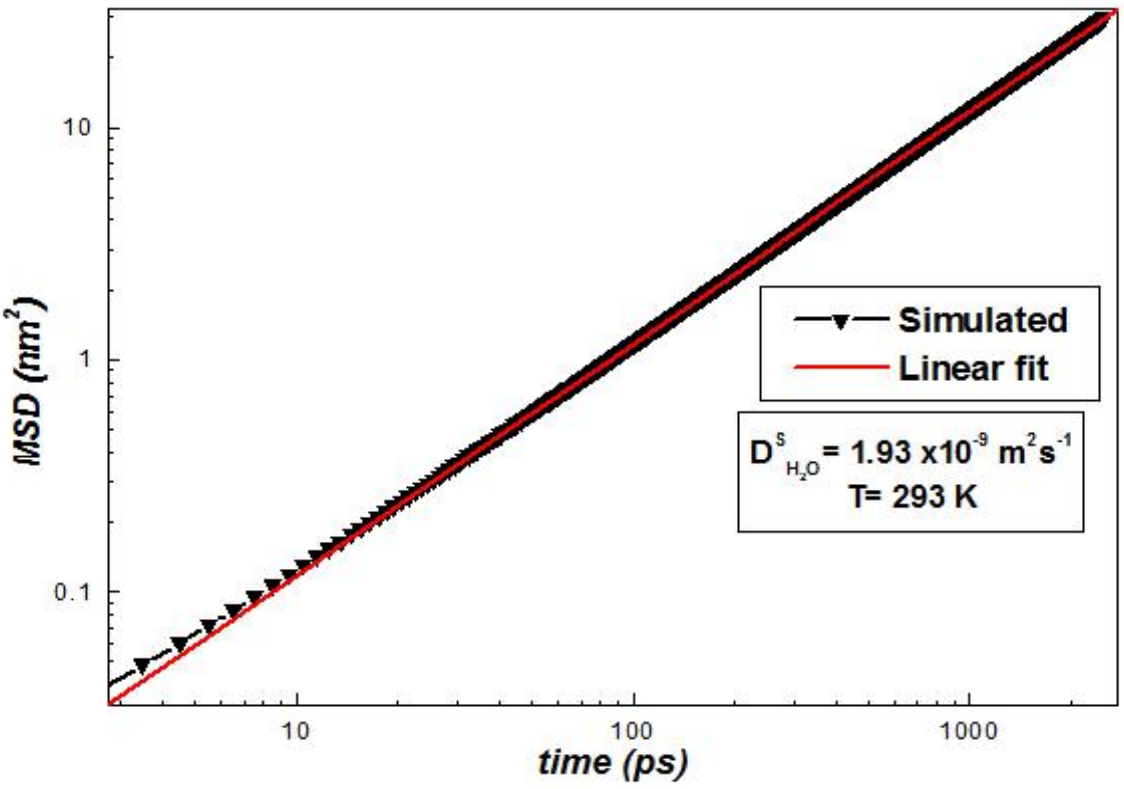

Figure 4.29: Mean-squared displacement for liquid water as a function of time at temperature 293 K.

The time dependence of MSD for water at temperature 293 K is plotted in figure 4.29 which is double logarithmic plot. For short times, less than 8 ps, it is seen that the MSD varies with the square of the time. This increment of MSD with time is due to the ballistic motion of molecules. The diffusive regime where MSD is linear function of time, starts beyond 8 ps and extends up to 2.5 ns. The self-diffusion coefficient is calculated by fitting the diffusive regime. The calculated value of self-diffusion coefficient, $D^S_{H_2O}$, is 1.93×10^{-9} m^2s^{-1} and that from the experiment, $D^E_{H_2O}$, is $(2.02\pm0.001)\times10^{-9}$ m^2s^{-1}. Hence, the result of present work agree within 5% of the experimental result. The error in the calculated value is insignificant.

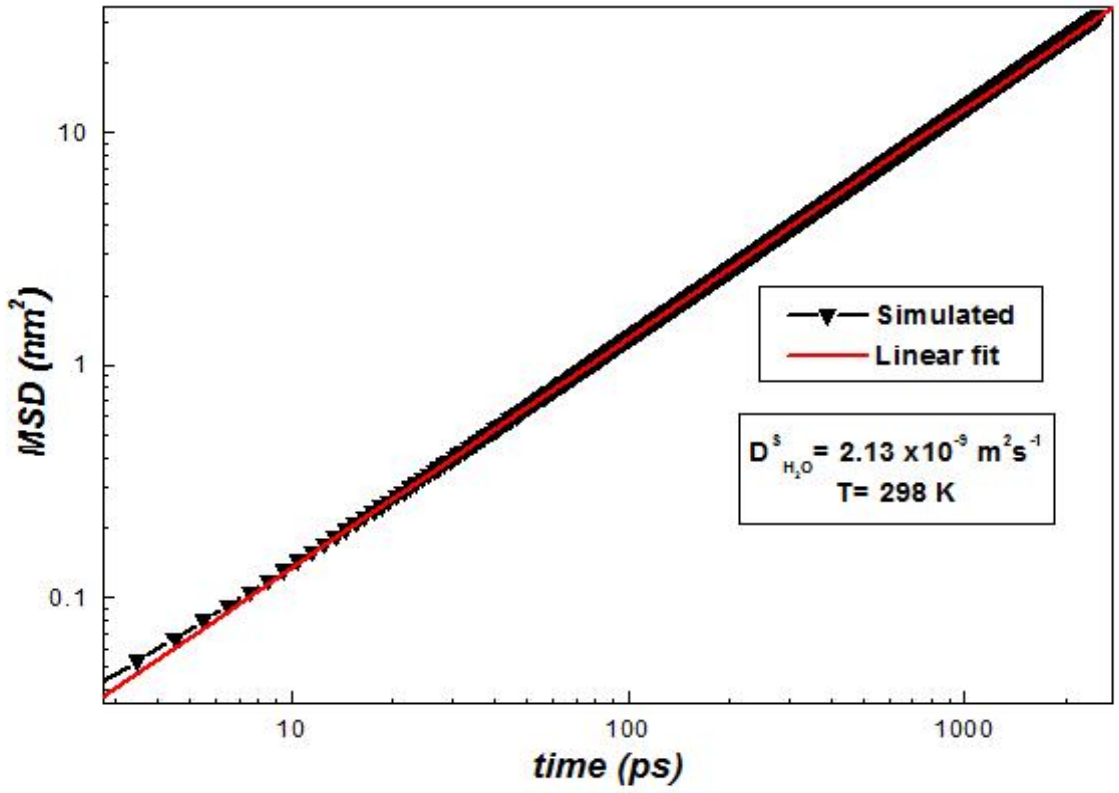

Figure 4.30: Mean-squared displacement for liquid water as a function of time at temperature 298 K.

The time dependence of MSD for water at temperature 298 K is plotted in figure 4.30 which is double logarithmic plot. For short times, less than 8 ps, there is again a ballastic regime. Beyond that the MSD is linear function of time and extends up to 2.5 ns. The self-diffusion coefficient is calculated by fitting the diffusive regime. The calculated value of self-diffusion coefficient, $D^S_{H_2O}$, is 2.13×10^{-9} m^{2}s^{-1} and that from the experiment, $D^E_{H_2O}$, is $(2.29\pm0.001)\times10^{-9}$ m^{2}s^{-1}. Hence, the result of present work agree within 7% of the experimental result. The error in the calculated value is insignificant.

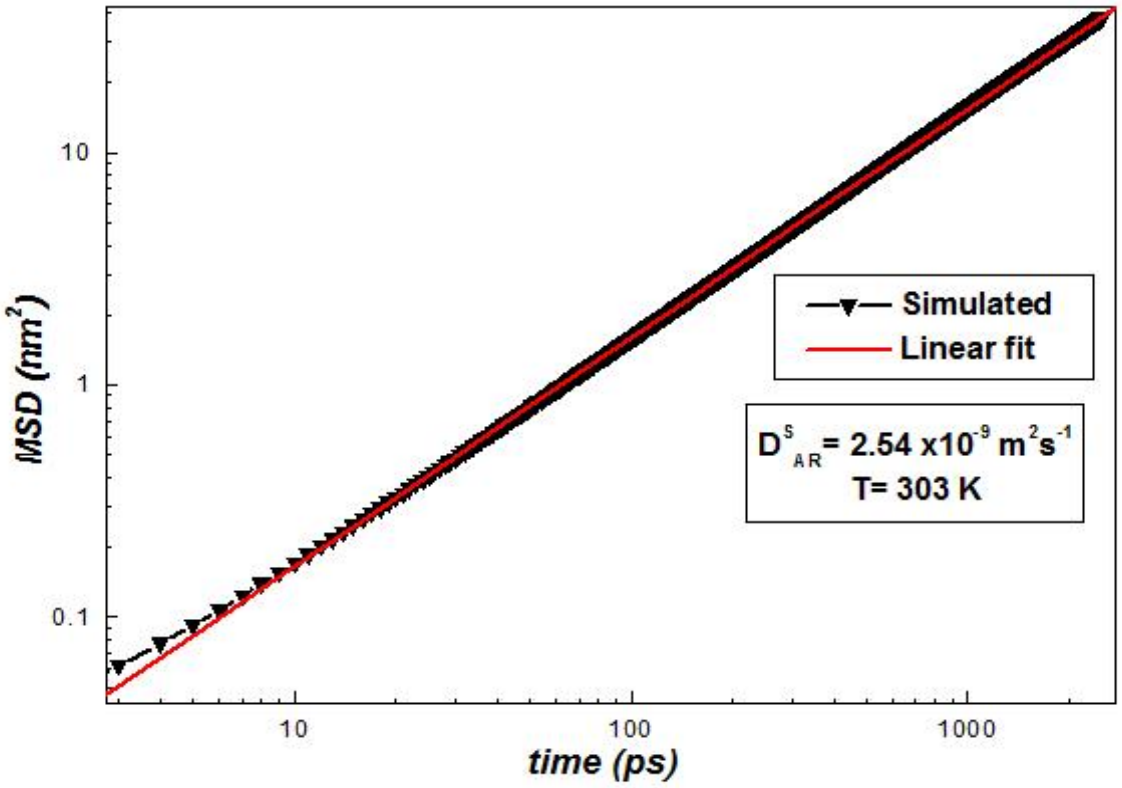

Figure 4.31: Mean-squared displacement for liquid water as a function of time at temperature 303 K.

The time dependence of MSD for water at temperature 303 K is plotted in figure 4.31 which is double logarithmic plot. Is can be seen from the figure that for short times, less than 8 ps, the curve has parabolic nature showing the ballastic regime. Beyond that the MSD is linear function of time and extends up to 2.5 ns. The self-diffusion coefficient is calculated by fitting the diffusive regime. The calculated value of self-diffusion coefficient, $D^S_{H_2O}$, is 2.30×10^{-9} m^{2}s^{-1}. The error in the calculated value is insignificant.

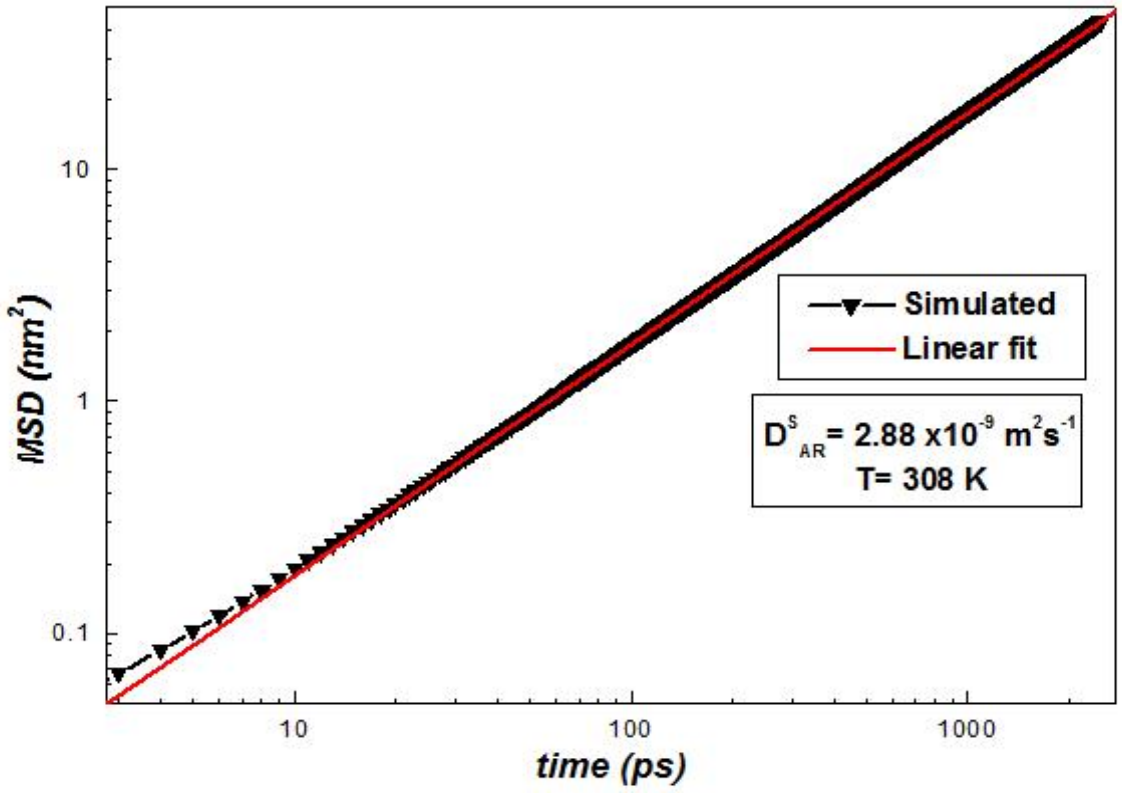

Figure 4.32: Mean-squared displacement for liquid water as a function of time at temperature 308 K.

The time dependence of MSD for water at temperature 308 K is plotted in figure 4.32 which is double logarithmic plot. For short times, less than 8 ps, there is again a ballastic regime shown by the parabolic nature of the curve. Beyond that the MSD is linear function of time and extends up to 2.5 ns. The self-diffusion coefficient is calculated by fitting the diffusive regime. The calculated value of self-diffusion coefficient, $D^S_{H_2O}$, is 2.61×10^{-9} m^2s^{-1}. The error in the calculated value is insignificant.

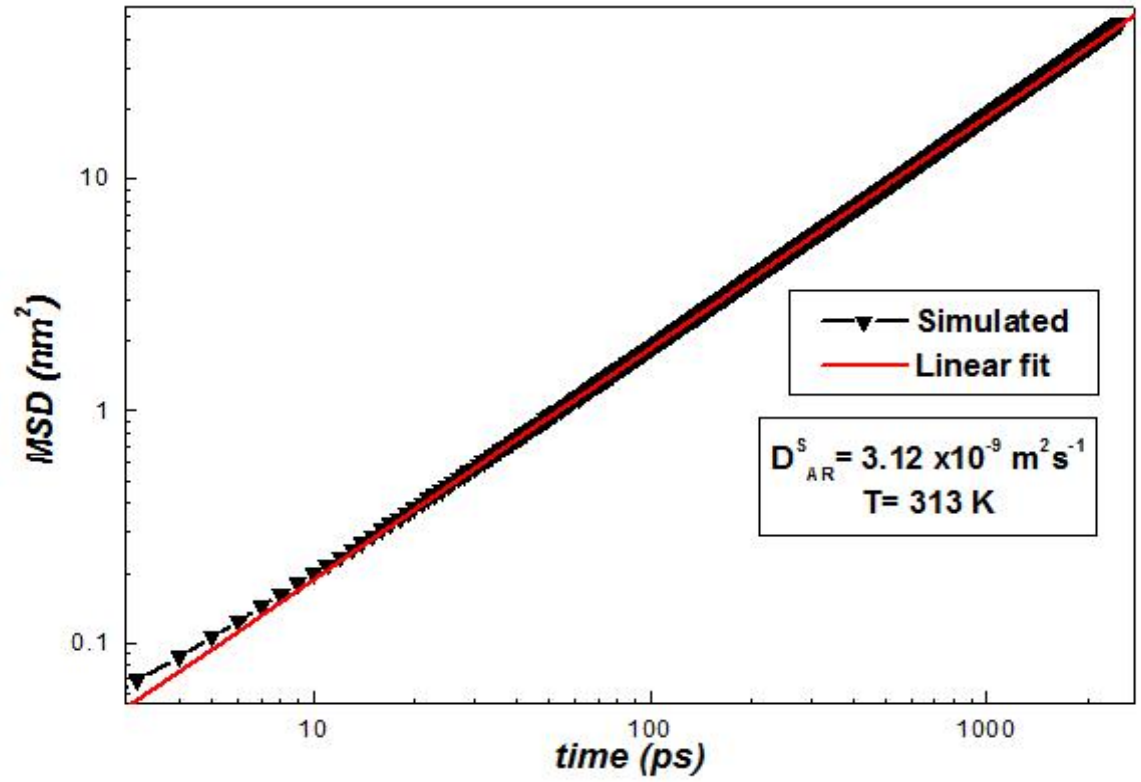

Figure 4.33: Mean-squared displacement for liquid water as a function of time at temperature 313 K.

The time dependence of MSD for water at temperature 313 K is plotted in figure 4.33 which is double logarithmic plot. For short times, less than 8 ps, the MSD varies with t^2 which is due to the ballistic motion of the molecules. Beyond that the MSD is linear function of time and extends up to 2.5 ns. The self-diffusion coefficient is calculated by fitting the diffusive regime. The calculated value of self-diffusion coefficient, $D^S_{H_2O}$, is 2.84×10^{-9} m^2s^{-1}. The error in the calculated value is insignificant.

T(K)	$D^{S}_{H_2O}(10^{-9}m^2s^{-1})$	$D^{E}_{H_2O}(10^{-9}m^2s^{-1})$[12]	% ERROR
293	1.93	2.02±0.01	4.45
298	2.13	2.29±0.01	6.98
303	2.30	–	–
308	2.61	–	–
313	2.84	–	–

Table 4.5: Details of the self-diffusion coefficients of water (solvent) at different temperatures and corresponding densities.

The self diffusion coefficients of water thus obtained from the simulation at different temperatures along with the experimental values (if available) are presented in table 4.5. This table is very much useful for the comparative analysis of the self diffusion coefficients of water. From the table it can be seen that the self-diffusion coefficients are in better agreement with the experimental value within about 6.98% at maximum [27]. Therefore, the SPC/E water model can be taken as an appropriate model from the perspective of diffusion coefficient. It can also be seen that the self diffusion coefficient increases with the rise in temperature. The reason behind it is that, the generated velocities of the water molecules increase as the temperature increases. Also, the density of the system decreases increasing volume of free space available for the water molecules to execute random-walk. Because of these, the mean-squared displacement increases and according to the Einstein's relation self diffusion coefficient also increases. This variation is also consistent with the increase in width of the radial distribution function g_{ow-ow} with the rise in temperature. Therefore, when the width increases, the second maxima becomes less defined increasing the self-diffusion coefficient [14].

4.1.6 Mutual Diffusion Coefficient of Argon

The mutual diffusion coefficient of argon in water, D_{AB}, where A is for argon and B is for water, is calculated using the Darken's relation

$$D_{AB} = N_B D_A + N_A D_B. \tag{4.2}$$

In our system, there are 5 argon atoms and 212 water molecules. Therefore, the mole fraction for argon, N_A, is 0.023 and that for water, N_B, is 0.977. The radial distribution function $g_{AR-AR}(r)$ (see section 4.3) indicates that there exists a some correlation between the argon atoms, though the argon atoms are few in number compared to the water molecules. The binary mixture of argon and water, therefore, doesn't satisfy the infinite-dilution condition because of which we need to invoke Darken's relation. The calculated values of mutual diffusion coefficient from the simulation have been presented in table 4.6.

T(K)	$D_A^S(10^{-9}m^2s^{-1})$	$D_B^S(10^{-9}m^2s^{-1})$	$D_{AB}^S(10^{-9}m^2s^{-1})$
293	2.12	1.93	2.11
298	2.40	2.13	2.39
303	2.54	2.30	2.53
308	2.88	2.61	2.88
313	3.12	2.84	3.11

Table 4.6: Details of the mutual diffusion coefficient of argon water, D_{AB}^S at different temperatures and corresponding densities.

From the table, it can be seen that the mutual diffusion coefficient of argon in water is slightly less than the self diffusion coefficient of argon. It is because of the correlation of the argon atoms with the water molecules, as shown by the radial distribution function g_{AR-OW}(r).

4.1.7 Temperature dependence of diffusion coefficients

Diffusion coefficients are found to vary considerably with temperature. This variation can often be expressed in terms of the Arrhenius equation, D= $D_o$exp(-E/$N_A k_B$T), where N_A is Avogadro's number, k_B is the Boltzmann constant, T is the temperature in Kelvin, and D_o is a constant term referred to as the pre-exponential factor. The term E is called the activation energy of diffusion. A plot of lnD versus 1/T gives Arrhenius plot. The variation of self diffusion coefficients of argon and water with temperature has been shown in figures 4.34 and 4.35 respectively and the variation of mutual diffusion coefficients of argon in water with temperature has been shown in figure 4.36.
The variation of self-diffusion coefficient of argon with temperature is shown in figure 4.34.

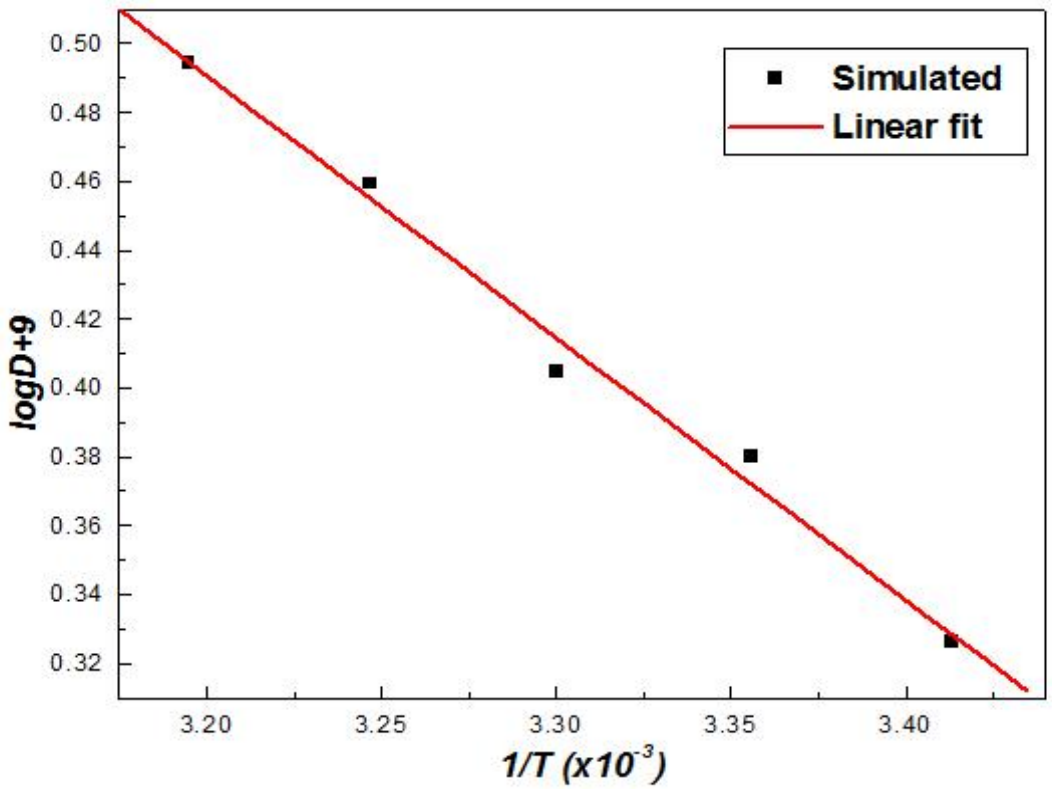

Figure 4.34: Temperature dependence of self-diffusion coefficient of argon.

As shown in the figure, it is a Arrhenius plot which have been followed well by the simulated values of the self diffusion coefficients. Therefore, it can be inferred that self-diffusion coefficient has an Arrhenius dependence on temperature[33]. The activation energy estimated from the slope of the plot is (14.708±0.86) kJmol^{-1}.

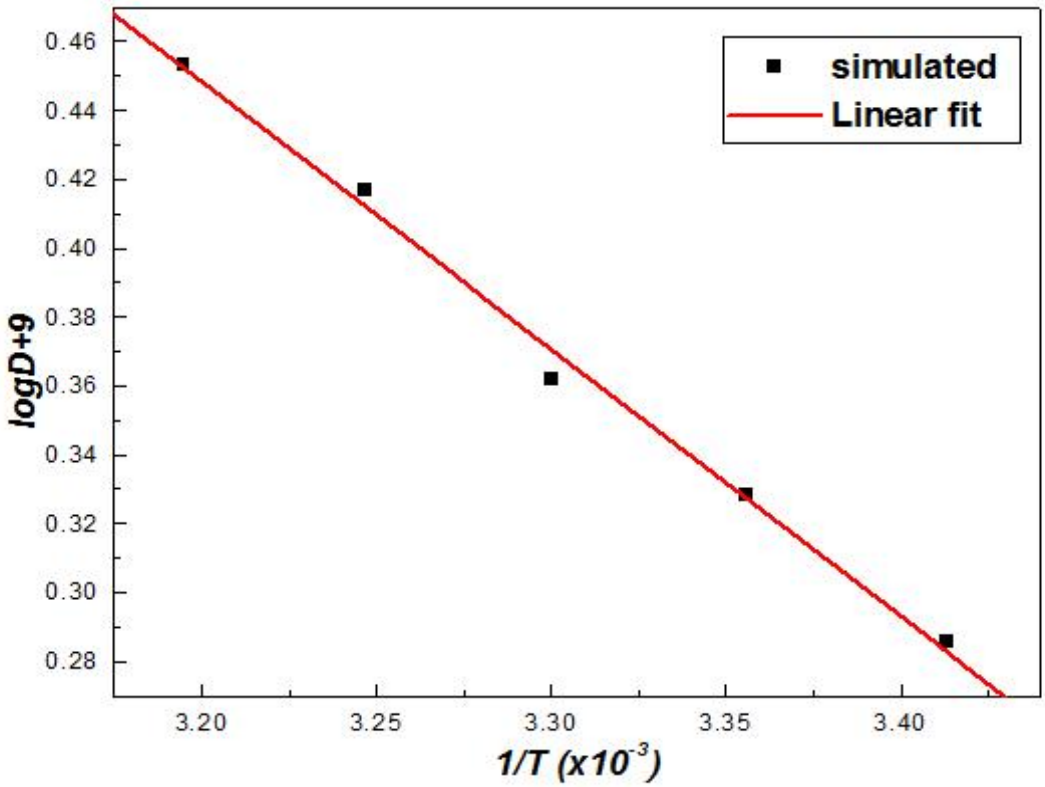

Figure 4.35: Temperature dependence of self-diffusion coefficient of water.

The variation of self diffusion coefficient of water with temperature is shown in the figure 4.35. It is a Arrhenius plot which have been followed well by the simulated values of the self diffusion coefficients. This variation is in good agreement with that for the experimental values. Therefore, it can be inferred that self diffusion coefficient of SPC/E water has an Arrhenius dependence on temperature. The estimated value of the activation energy from the slope of the plot is (14.820±0.90) kJmol^{-1}.

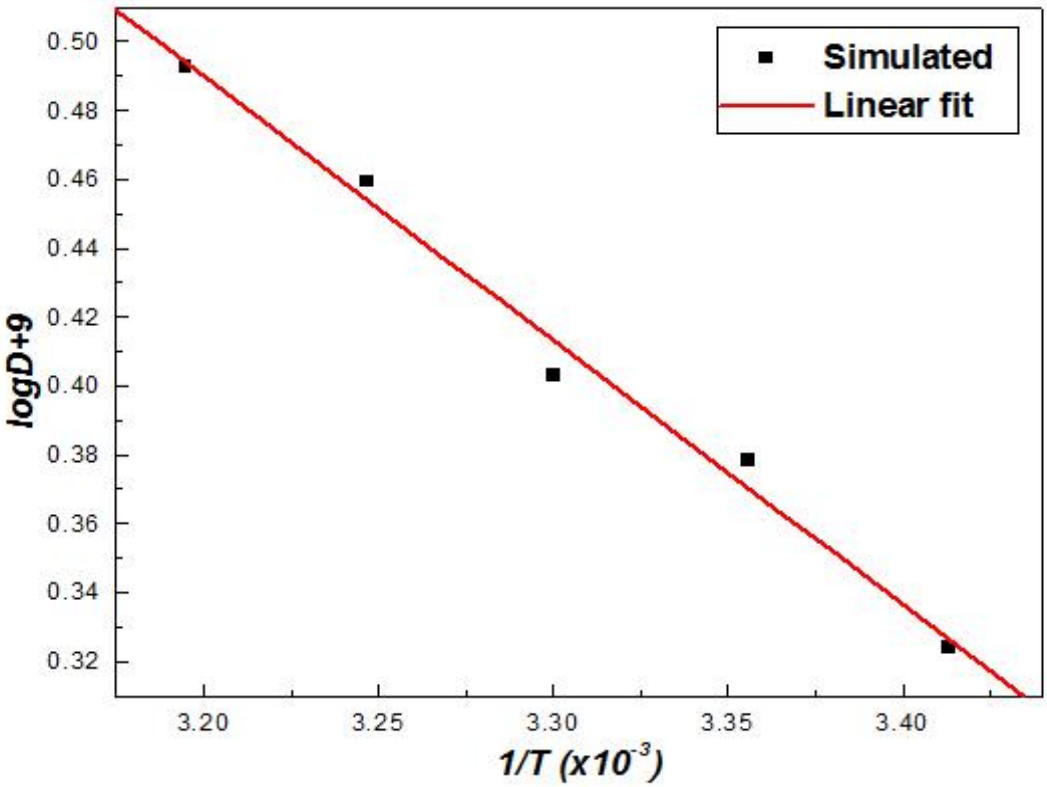

Figure 4.36: Temperature dependence of mutual diffusion coefficient of argon in water.

The variation of mutual diffusion coefficient of argon in water with temperature is shown in the figure 4.36. It is also a Arrhenius plot. Thus, the mutual diffusion of argon in water has an Arrhenius dependence on temperature. The activation energy estimated from the slope of the plot is (15.015±0.66)kJmol^{-1}.

Chapter 5

Conclusion and Concluding Remarks

5.1 Conclusions and Concluding Remarks

A molecular dynamics study of a binary fluid system containing 212 SPC/E water molecules and 5 argon atoms were performed at temperatures 293 K, 298 K, 303 K, 308 K, and 313 K. The simulation software GROMACS 3.3.1 was used for the purpose. The parameters were defined by taking into consideration that our system model resembles very much close to the real experiment. Only short-range non-bonded interactions within 0.9 nm were taken. The energy minimization performed using the steepest descent algorithm was found to converge well. The minimized system was subjected to the equilibration run of 50 ns using NPT ensemble. The temperature was quickly equilibrated while it took some time to equilibrate the pressure around 1 bar due to fluctuations. The pressure coupling was done in order to attain constant average density at 1 bar pressure. The long time production run of 200 ns with the time steps of 2 fs was then performed on the system using NVT ensemble. Berendsen coupling methods were used to attain constant temperature and constant pressure conditions. The total effective simulation time for the production run was 1000 ns for five different temperatures. The coordinates, velocities, and energies were written at various rates to produce results with good statistics. As the number of water molecules in the system dominated the number of argon atoms, the system density was very much close to the density of water at respective temperatures. The scaling of velocities to maintain a constant temperature in the NVT and the NPT ensembles produced small fluctuations in the energies. Also the choice of the time step of 2 fs, large number of time steps as well as due to short range and non-bonded interactions, there were drifts in the energies. Then, the structural properties and dynamical properties have been studied.

The structural analysis at different temperatures and for both the components was done by calculating the corresponding partial radial distribution functions, viz. $g_{AR-AR}(r)$, $g_{ow-ow}(r)$, and $g_{AR-OW}(r)$ without employing any long-range corrections. These distribution functions described the fluid structure with only slight disagreement with the experimental results. This may be attributed to the exclusion of the long-range Coulomb and van der Waal's corrections. The roughness of the radial distribution function $g_{AR-OW}(r)$ is due to insufficient statistics taken over only 5 atoms.

The self diffusion coefficients as equilibrium dynamical property of the system were studied. The self-diffusion coefficients both for argon and water were separately calculated. The results are in agreement with the experimental values within 7%. The mutual diffusion coefficients of argon in water were calculated using Darken's relation. The self diffusion coefficients as well as the mutual diffusion coefficients follow the linear Arrhenius behavior, thereby showing Arrhenius dependence on temperature. The activation energies are estimated from the slope of Arrhenius plots.

From this study, we conclude that molecular dynamics can be used as a reliable method to study the equilibrium structure and dynamic properties of fluid mixture. The molecular dynamics, being computational research, is devoid of any experimental competence and hazards. As gas-liquid diffusion coefficients are difficult to measure, and large differences are found between values obtained by different authors and through different experimental methods, the calculated values of the diffusion coefficient may be used as a crude reference for any further fluid studies. Besides, the MD simulations are cost efficient and easily accessible.

This study can be extended in several ways in the future. The diffusion coefficient can also be obtained from velocity autocorrelation function using Green-Kubo relation [16, 17]. We can also find the equivalence between the Green-Kubo and the Einstein's relation including the long-range corrections in the Coulomb energy and van der Waals energy. Also other transport properties such as thermal conductivity can be evaluaten from the MD simulations. We can also calculate the self diffusion coefficient by varying the concentration of argon at same temperature or even by forming a system that comprises of only argon atoms. We can also change the Berendsen temperature and pressure coupling schemes to Nose-Hoover and observe the changes in fluctuations and drifts in the energies. We can extend this study to study the diffusion of argon in supercritical water. One can study the diffusion coefficient of other gases such as Nitrogen (N_2), Xenon (Xe) as well as carbondioxide (CO_2) which has important applications in regular life.

Bibliography

[1] Lee, Song Hi, *Molecular Dynamics Simulation Study of the Transport Properties of Liquid Argon: The Green-Kubo Formula Revisited*,Bull. Korean Chem. Soc., vol.28, 1371-1374, 2007.

[2] Vergeles, Maxim, Szame, Grzegorz, *A theory for self-diffusion in liquids*, Journal of Chemical Physics, vol. 110, 3009-3022, 1999.

[3] Balbuena,Perla B.,Seminario,Jorge M., ed.;*Molecular Dynamics:From Classical to Quantum Methods*, Elsevier, New York 1999.

[4] Boerboom, A.J.H., Kleyn, G., *Diffusion Coefficients of Noble Gases in water*, The Journal of Chemical Physics, vol.50, 1086-1088, 1969.

[5] Osburn, James O., Stitzell, John A., Peterson, R.E.; *Diffusion of argon, krypton and xenon in olive oil*, Journal of Applied Physiology, vol.27, 624-629, 1969.

[6] Cox, P.A., *The Elements - Their origin, abundance and distribution*, Oxford University Press, Oxford 1991.

[7] Crank, J.,*The Mathematics of Diffusion* $2^n d$ ed.; Oxford University Press; Oxford 1975.

[8] Cussler,E.L.;*Diffusion:Mass Transfer in Fluid System* $2nd$ edition, Cambridge University Press, Cambridge 1997.

[9] Haile,J.M.,*Molecular Dynamics Simulation:Elementary Methods*, John Wiley and Sons, New York 1992.

[10] Van Buvren, A.R., Marrnik, S.J, Berendsen,H.J.C., *A molecular dynamics study of the decane/water interface*, Journal of Physical Chemistry, vol.97, 9206-9212, 1993.

[11] Bergethon,Peter R.,*The Physical Basis of Biochemistry: The Foundation of Molecular Biophysics*, Springer, New York 1998.

[12] van der Spoel, D.; Lindahl, E.; Hess, B.; Kutzner, C.; van Buuren, A.R.; Apol, E.; Meulenhoff, D.P.; Sijbers, A. L.T.M.; Feenstra, K. A.; van Drunen, R.; van D. R.; Berendsen, H.J.C.; *Gromacs User Manual Version 4.0*, www.gromacs.org, 2005.

[13] Smit, B., *Phase diagrams of Lennard-Jones fluids*, J. Chem. Phys., vol. 96, 8639, 1992.

[14] Thapa, S.K., *Molecular Dynamics Study of Diffusion of Oxygen in Water at Different Temperatures*, A M.Sc Dissertation, Kirtipur, Kathmandu 2010.

[15] Allen, M. P.; Tildesley, D.J. *Computer Simulations of Liquids*; Clarendon Press; Oxford 1987.

[16] Frenkel, D.; Smit, B.; *Understanding Molecular Simulation From Algorithms to Applications*; Academic Press; New York 2002.

[17] Rapport,D.C.;*The Art of Molecular Dynamics Simulation*; 2^{nd}edition, Cambridge University Press, Cambridge 2004.

[18] www.pdb.org

[19] B.Guillot, *A reappraisal of what we have learnt during three decades of computer simulations on water*, J. Mol. Liq., vol.101, 219-260, 2002.

[20] H. J. C. Berendsen; J.P.M. Postma, W.F. van Gunsteren, J. Hermans, *In Intermolecular Forces, Reidel, Dordrecht*, Elsevier, New York, 1981

[21] H. J. C. Berendsen; J. R. Grigera; T. P. Straatsma, *The Missing Term in Effective Pair Potentials*, J. Phys. Chem, vol.91, 6269-6271, 1987.

[22] Jorgensen, W. L.; Chandrasekhar, J.; Madura, J. D.; Impey, R. W.; Klein, M. L., *Comparison of Simple Potential Functions for Simulating Liquid Water*, J. Chem. Phys, vol.79, 926-935, 1983.

[23] Jorgensen, W. L.; Madura, J.D.; *Mol. Phys. An International Journal at the Interface Between Chemistry and Physics*, vol.56, 1381, 1985.

[24] Jorgensen, W. L.; Mahoney, M. W.; *A five-site model for liquid water and the reproduction of the density anomaly by right nonpolarizable function*, J. Chem. Phys, vol.112, 20-22, 2000.

[25] H. Yu, W. F. van Gunsteren, *Accounting for polarization in molecular simulation*, Comput. Phys. Comm., vol.172, 69-85, 2005.

[26] Maaren, Paul J., van der Spoel D., *Molecular Dynamics Simulations of Water with Novel Shell-Model Potentials*, J. Phys. Chem., vol. 105 , 2618-2626, 2002.

[27] Lide, David R., Haynes, W.M."Mickey" , ed., *CRC Handbook of Physics and Chemistry*, 90^{th}Edition, CRC Press, Florida 2009.

[28] Hansen, J.P., Mc Donald, I.R.; *Theory of Simple Liquids* 3^{rd} edition; Elsevier, New York, 2006.

[29] Mc Quarrie, Donald A., *Statistical Mechanics*, University Science Books, New York 2000.

[30] Heitjans, P., Krager, J.; *Diffusion in Condensed Matter: Methods, Materials, Models* Springer, New York 2009.

[31] Krishna, R., van Baten, J.M., *The Darken Relation for Multicomponent Diffusion in Liquid Mixtures of Linear Alkanes: An Investigation Using Molecular Dynamics (MD) Simulations*, American Chemical Society, vol.44, 69396947, 2005.

[32] Hartley, G.S.,Crank, J.; *Trans. Faraday Soc.*, vol.45, 801, 1949.

[33] Leipzig; *Diffusion Fundamentals*, Springer, Berlin 2005